PHYSICOCHEMICAL CHARACTERISTICS OF METAL OXIDE ASHES DERIVED FROM USED WALL FLOW DIESEL PARTICULATE FILTER

SATTATAD RODVANNA

A THESIS REPORT SUBMITTED IN PARTIAL FULFILLMENT
OF THE REQUIREMENTS FOR THE DEGREE OF
MASTER OF ENGINEERING IN AUTOMOTIVE ENGINEERING
SCHOOL OF ENGINEERING
KING MONGKUT'S INSTITUTE OF TECHNOLOGY LADKRABANG
2021

KMITL-2021-EN-M-037-045

THESIS TITLE	Physicochemical Characteristics of Metal Oxide Ashes Derived from Used Wall Flow Diesel Particulate Filter
STUDENT	Mr. Sattatad Rodvanna
STUDENT ID	60610026
DEGREE	Master of Engineering
YEAR	2021
PROGRAM	Automotive Engineering (International Program)
ADVISOR	Assoc. Prof. Dr. Preechar Karin
CO-ADVISOR	Dr. Nuwong Chollacoop
CO-ADVISOR	Prof. Dr. Katsunori Hanamura

Abstract

The investigation of physicochemical characteristics of metal oxide ashes deposited on diesel particulate filter (DPF) operating on a diesel passenger car were conducted utilizing an electron microscopy, energy dispersive spectroscopy, X-Ray Fluorescence, and X-Ray Diffractometer. The macroscale analysis reveals a deposition of ash particles mainly took place at the end plug with various deposited length depending on channels, while the microscale analysis reveals Fe is the main component of deposited ash on the SiC DPF. The majority of ash components consisted of elements such as Fe, Si, Ca, Cu, S, P, Zn, Al and minor Cr, Ni, Mn. These components are products of engine wear metal, exhaust corrosion, as well as lubricant additives. In addition, the influence of metal oxide ash on soot oxidation were successfully investigated utilizing thermogravimetric analysis (TGA). It was clarified that this metal oxide ash has catalytic effect that contributed to an enhancement of PMs oxidation.

Keywords: Diesel engine; Particulate filter; Metal oxide ash; Fuel additives; Engine wear, TGA

Acknowledgement

First, I would like to express my deep and sincere gratitude to my supervisor, Assoc. Prof. Dr. Preechar Karin, who gave me a great opportunity to study in this excellence institute and wonderful laboratory. His fruitful suggestion, dynamism, vision and motivation have deeply inspired me to achieve such a great research. It was a great privilege and honor to work and study under his guidance. In addition, I would like to thanks to my thesis Co-Advisor Dr. Nuwong Chollacoop, and Prof. Dr. Katsunori Hanamura who advised me a research and all useful discussions.

I would like to thank all members in KMITL laboratory, Undergraduate students and other friends in DPF research group who advised me a research and all useful discussions. Special thanks to Swe Zin and Veerayut for your support of all documents, paper works and assistance for laboratory equipment.

Beside the people mention above, I would like to express my sincere appreciation to all technical support from all staff members in FOCUSLAB Ltd, the National Science and Technology Development Agency (NSTDA) and National Nanotechnology Center (NANOTEC) for your support and advice of fuel, lubricating oil analysis, analysis using electron microscope, TGA, and other instruments.

Finally, thanks to my parent and other relatives for giving encouragement, motivation and invaluable assistance to me.

RODVANNA Sattatad

Table of Contents

Chapters **Page**

LIST OF TABLES

Figures **Page**

LIST OF FIGURES

Figures **Page**

CHAPTER 1

INTRODUCTION

1.1 Research Background

Recently, automotive trends are focusing to the future of the vehicles, for example, autonomous vehicle, Plug-in Hybrid Electric Vehicle (PHEV), and the most popular one Electric vehicles (EV). These future developments require a revolutionized of the infrastructure in which only a few countries are well-prepared. Therefore, internal combustion engines will continue to be used as a main power source for transportation. Among the engines, diesel engine is widely used [1] due to its highest thermal efficiency among others [2]. However, the diesel exhaust gas contains high amount of particulate matter (PM), which is harmful for our body and environment. A solid fraction of diesel PM composed of soot formed by an incomplete combustion, and ash which mainly derived from fuel or engine oil additives [3].

Diesel Particulate Filter (DPF) was introduced as the most effective way to mitigate this emission because the PM removal efficiency is more than 98% [4]. DPF generally made of ceramic materials, such as cordierite ($2MgO{\cdot}2Al_2O_3{\cdot}5SiO_2$) or silicon carbide (SiC) which have high heat resistance (1,000°C or more) and thermal shock resistance, as shown in figure 1.1 The structure is comprised of many rectangular channels with alternate channels blocked with cement at each end [5].

A B

Figure 1.1 SiC (A), and cordierite filter (B).

The exhaust gas is forced to flow through a numerous gas-permeable microscale porous walls that trap the diesel particulate matter. This process called Trapping process. A direct consequence of soot accumulation in the filter is increased flow restriction and a corresponding rise in exhaust backpressure, resulting in a fuel economy penalty. Therefore, the collected particulate matter must be oxidized to regenerate the DPF and reduce the back pressure on the diesel engine through the regeneration or oxidation process. Unlike to soot particles, an incombustible metal oxide ash cannot be removed from DPF by regeneration or oxidation process. There are two types of ash deposition: wall ash [6] and plug ash [7], as shown in figure 1.2 wall ash covers the DPF wall and performs as a membrane filter resulting in a high filtration efficiency, but too much deposition can restrict the channel diameter. On the other hand, plug ash completely fills the channel and reduces the effective length of the filter [8] causing a large pressure drop and reducing the efficiency of Diesel engines. To maintain a high working performance of DPF, the investigations on the ash physico-chemical property and the ash formation process inside the actual operated DPF, will be helpful to solve the abovementioned issues.

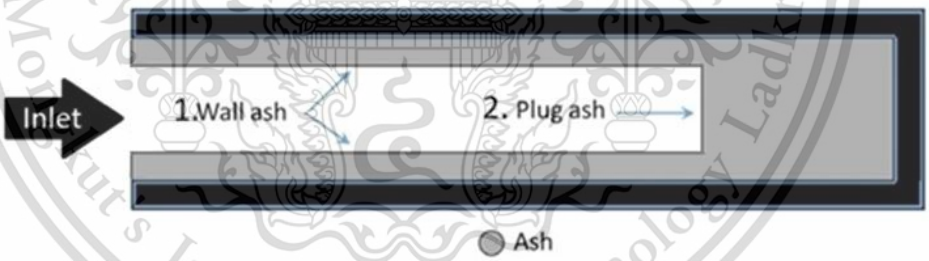

Figure 1.2 types of ash deposition in DPF

1.2 Objectives

1. To investigate the physicochemical characteristics of metal oxide ash derived from passenger cars' diesel particulate filter (DPF)
2. To analyze the influence of metal oxide ash on PMs oxidation

1.3 Scope of Works

In the first part of this study, the actual operated DPF obtained diesel passenger cars were disassembled for the investigation of macro and microscale analysis of deposited metal oxide ash. The macroscale analysis reveals the characteristics of accumulation, as well as distribution pattern of ash in DPF. In addition, a mechanical removal of ash from the filter also performed as the microscale analysis to clarify chemical components of ash particles utilizing X-Ray Fluorescence (XRF), and X-Ray Diffractometer (XRD) methods. A field emission scanning electron microscope (FE-SEM) equipped with an energy dispersive X-Ray spectroscopy (EDX), and a transmission electron microscope (TEM) were utilized for the microscopic investigations. In addition, diesel fuels and lubricating oil were also analyzed their elemental compositions utilizing ICP-AES technique.

For the second part, the effect of an incombustible ash on soot oxidation were investigated. Two differences PMs sample, soot and soot contained ash, were analyzed their oxidation behavior utilizing thermogravimetric analysis (TGA) and evaluation of reaction rate was also conducted and described by the Arrhenius expression.

CHAPTER 2

LITERATURE REVIEWS

2.1 Diesel Engine

Diesel engines have gained more popularity among internal combustion engines due to the highest thermal efficiency and low fuel consumption. In addition, because of their high output torque compare with the same size gasoline engines, diesel engines are widely used in commercial vehicles such as buses, construction vehicles, and heavy-duty trucks. However, particulate matter (PM) must be removed from exhaust gases emitted from diesel engines to protect environment and human health. J.B. Heywood [2] was clearly described a formation of diesel emission. In a diesel engine or compression-ignition (CI) engine, soot or black smoke strongly depends on uniformity of air-fuel mixture. The fuel is injected by the fuel-injection system into the engine cylinder toward the end of the compression stroke, just before the combustion starts. Therefore, the combustion mixture is non-uniform due to a shortage of premixing time. In addition, there are problems with air utilization during combustion lead to the formation of excessive soot that cannot be burned up prior to exhaust due to an increasing of fuel injected per cycle. As a result, diesel engines are an important source of particulate emissions which consist primary of soot with some additional absorbed hydrocarbon material.

2.2 Particulate matter

Diesel particulate matters are composed of solid, liquid fraction and sulphates with water [9]. The solid fraction is composed primarily of elemental carbon. This carbon, not chemically bound with other elements, is the finely dispersed carbon black or soot substance responsible for black smoke emission. Another important component of the solid fraction of PM is metal oxide ashes. The metal oxide ashes are incombustible material mainly derived from lubricant additives. The role of these lubricant additives [10] are to improve a performance of engine oil such as rust and corrosion inhibitors, anti-oxidants, anti-wear, and viscosity index modifiers. A liquid fraction usually refers to a soluble and volatile organic fraction, SOF and VOF [11]. In addition, the concepts of diluted and cooled diesel PM also reported by M.M. Maricq., as shown in figure 2.1 [12]. It consists of two main particles. First, soot which is primary

particles imbedded with metallic ash, and coated with condensed organic compounds and sulfate. Second is nucleation particles consist of condensed HCs and sulfate. Morphology and chemical compositions of particulate matters are varied by the engine operating conditions, also depended on fuel properties and usage of lubricating oil [13,14].

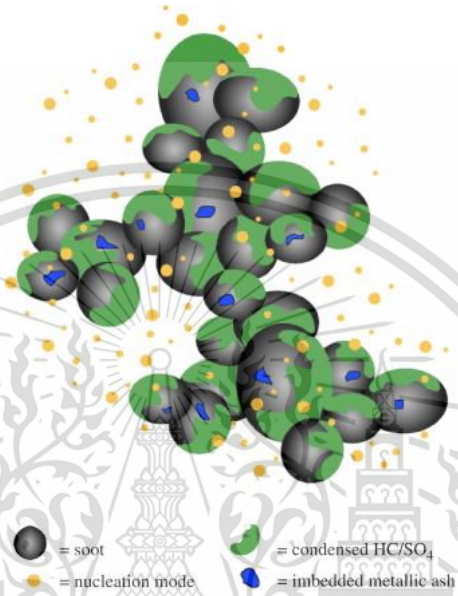

Figure 2.1 Artist's conception of diesel PM [12].

2.3 Diesel particulate filters

Figure 2.2 presents schematic of diesel engine equipped with DPF. The exhaust gas, consists of PM, is forced to flow through a channel wall having numerous micron-scale pores that trap the diesel particulate matter. The trapped particles perform as an additional membrane filter resulting in a high filtration efficiency as the PMs are loaded. A direct consequence of soot accumulation in the filter is increased flow restriction corresponding to a rise in exhaust backpressure which reduce the efficiency of Diesel engines. Therefore, the collected particulate matter must be oxidized to regenerate the DPFs and reduce the back pressure of the diesel engine. There are two methods of DPF regeneration: active and passive (continuous regeneration). Active regeneration utilizes burner or electric heater to burn trapped PMs effectively. This system can increase the exhaust gas temperature higher than 600℃. However, mass of PM loaded in the DPFs before active regeneration must be controlled to prevent an excessive amount of heat that cause damage to DPF. Active

regeneration is suitable for city-driving since exhaust gas temperature is not sufficiently high to oxidize collected PMs. In passive regeneration, catalytic additives are coated on the filter wall to reduce the overall activation energy for PMs oxidation. As a result, oxidation occurs at a lower temperature than active regeneration.

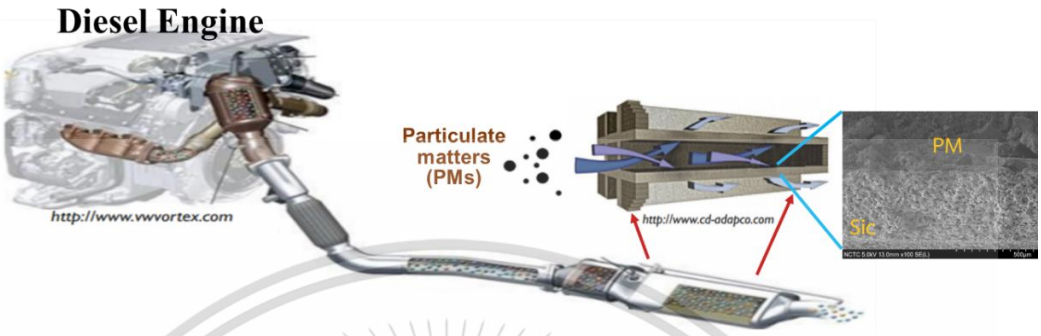

Figure 2.2 diesel engine equipped with DPF.

DPFs are the most effective way to reduce the emission of PM. Soot can be trapped with high filtration efficiency and burnt through the regeneration process. However, the unburned metal oxide ashes will remain and deposit along the filter length causing a high engine back pressure. Therefore, a performance relates to filtration efficiency and pressure drop depend on amount of ash deposition.

2.4 Ash in Diesel Particulate Filter

2.4.1 Ash sources

Ash is one component of solid fraction in particulate matter that cannot be removed from DPF during regeneration process. It is an incombustible material come from difference sources such as diesel fuel, engine wear, and chemical contaminants from the exhaust. The majority of ash, however, come from lubricant additives [15]. These additives are commonly calcium (Ca), zinc (Zn) and magnesium (Mg) based which presents in the form of phosphates, sulphates and oxides [16]. In order to reduce amount of ash introduced to aftertreatment systems, some limit of chemical contents in lubricant was placed. The CJ-4, oils use in high-speed four-stroke cycle diesel engines, described the acceptable level of sulfated ash content (1.0%), phosphorous content (0.12%), sulfur content (0.4%) and maximum volatility (13%) [17].

The amount of ash loading to the DPF is depending on engine oil consumption. Ash compounds from the lubricating oil transfer to the DPF through

the combustion in cylinder. During a combustion process, a small layer of oil is swept up by the piston rings and pass through the cylinder where it is oxidized and can be entrained in the exhaust flow. This is also the major cause of oil consumption in the engine [18].

2.4.2 Ash Transport

Figure 2.3 presents ash transport in diesel particulate filter. Ash enters the DPF with the soot particles as small precursors with various in diameter size, all significantly smaller than soot [15,19]. They are mainly layer on the DPF wall ash show in figure 2.3 (a). During regeneration, these ash precursors are gathered together to form primary particles, diameter ranges from 0.5-2 μm.[20]. Over time these primary particles continuously to agglomerate and produce large-scale ash particles as large as 5-50 μm. deposited on the wall of DPF (wall ash) [20]. When there is a proper amount of deposited wall ash, it can be removed by the fluid-dynamical shear force and accumulated at the end of DPF channel as the plug ash [21], figure 2.3 (b), (c). There are two parameters resulting in a transportation of wall to plug ash: regeneration reduced transport and flow induced transport. For the regeneration reduced transport, soot oxidation initiates from the greatest contact area between the catalyst coated DPF wall and the bottom of soot cake layer. As a result, the remaining soot cake layer can be easily removed by the exhaust flow and transported to the end plug. Flow induced transport is the result of high speed of exhaust that increase the fluid-dynamical shear force beyond the forces that holding the particle in place [7]. In addition, it is expected that a thin PM layer can adhere to the surface of DPF rather than a thicker soot cake layer. Therefore, a thick soot cake layer may result in a large deposition of plug ash [7].

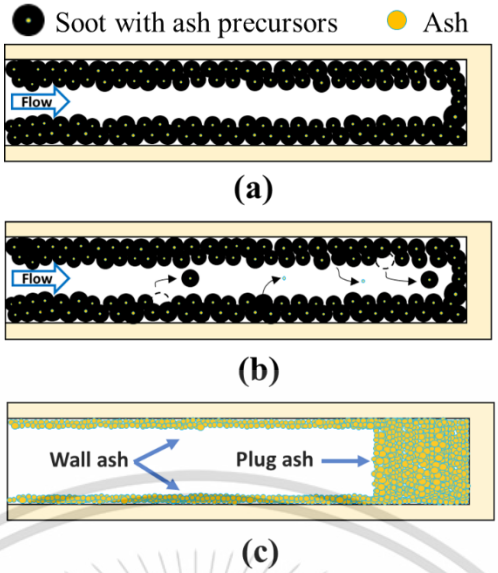

Figure 2.3 ash transport in diesel particulate filter.

In addition, previous research [22] also suggested that the mechanism of ash distribution process depended on the DPF regenerative way. By using active regeneration ash tends to accumulate at the end of the channel as plug ash, while wall ash was formed by the passive regeneration. In addition, the ash formation can be influenced by the attractive forces between particles. Based on the previous results of in-situ optical system [23], revealed that wall ash can be removed and accumulated at the end plug as the plug ash through the process of soot oxidizing at 600°C. This process can occur even in the absence of any flow through the channel due to the presence of substantial cohesive. Although the different mechanisms of the ash distribution process were proposed, the debate about the complex ash formation, accumulation, as well as fundamental mechanisms of ash property, are still ongoing without firm evidence.

2.4.3 Effect of ash on DPF pressure drop

The pressure drop through a porous medium can be described by Darcy's law as shown in the following equation.

$$\Delta P = -\frac{\mu}{kA} Q$$

where,

$$\Delta P = \text{pressure drop across DPF}$$
$$\mu = \text{Fluid viscosity}$$
$$k = \text{Permeability}$$
$$A = \text{filter area}$$
$$Q = \text{Volume flow rate}$$

Wall ash block surface pores which reducing the permeability (k) of the DPF, while plug ash reducing the filter area (A). As a result, the pressure drop across the filter increase. The ash deposition can both increase and decrease the pressure drop across the DPF depending on the amount loading [15]. Figure 2.4 presents effect of ash loading on DPF pressure drop. At 12.5 g/L ash loading, the pressure drop from soot loading is less than that of the clean DPF. This is due to the ash particles that already created a bridging structure inside surface pores instead of soot. Since ash composed of larger agglomerate particles which has a higher porosity and lower packing density than soot, therefore, filling up surface pores with ash resulting in a reduction of pressure drop. However, the pressure drop drastically increased at higher ash loading, 33g/L and 42 g/L, due to too high layer of wall and plug ash. Therefore, it's important to optimize the amount of ash layer to utilize its benefits of the reduction of pressure drop.

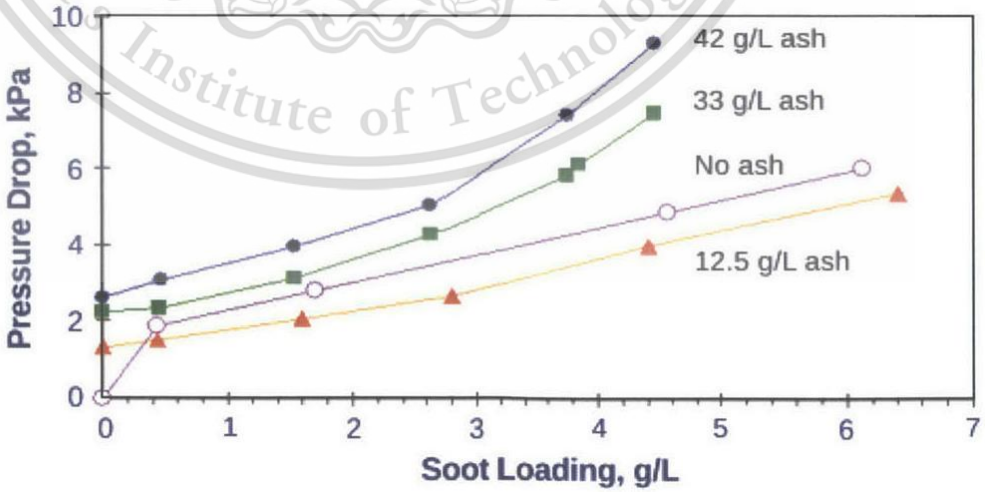

Figure 2.4 presents effect of ash loading on DPF pressure drop [15].

2.4.4 Mechanisms of oxidation enhancement by metal oxide ash

There have been excellent reviews and numerous works carried out concerning research on catalytic soot oxidation since a research and development of DPFs started in 1980. Catalysts are necessary when using DPFs to increase the oxidation rate, reduce soot oxidation temperature, as well as reduce a frequency of active regeneration process. A good catalyst necessary to have high reversibility or high redox properties of the oxidation states. For instance, V_2O_5 and Ce^{3+} are assumed to release bulk lattice & surface oxygen to carbon surfaces by recycling between different redox states [24], as follow:

$$v_2o_5 \leftrightarrow v_6o_{13}$$
$$Ce^{3+} \leftrightarrow Ce^{3+}$$

Other transition metal compounds such as Cr_2O_3, Mo and Cu, also have high redox properties, and exhibit high carbon oxidation activity. Another important key factor to determine the capability of catalysts on low temperature soot oxidation is oxygen storage capacity (OSC) and the delivering of active oxygen species, such as $peroxide\ O_2^{2-}$, $superoxide\ O_2^-$, and o^- onto soot particles [25]. According to previous studies [26], these active oxygen species obtain either from O_2 working gas (surface spillover), or from diffusion of bulk lattice oxygen. Iron oxide (Fe_2O_3) is commonly used as ferric oxide catalysts due to its ultrahigh bulk oxygen capacity and very low cost. A schematic diagram describes mechanism of oxidation enhancement by Fe_2O_3 is shown in figure 2.5.

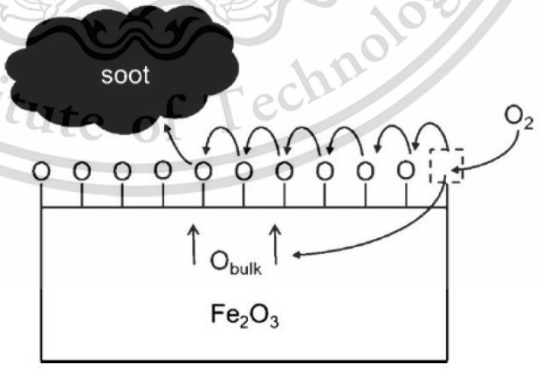

Figure 2.5 Mechanisms of oxidation enhancement by Fe_2O_3 [26]

From this scheme, oxygen is transferred from Fe_2O_3 catalyst surface to soot by physical contact points. Then, the oxygen vacancies on the surface can be refilled by migration of surface oxygen, and diffusing from catalyst lattice. The oxygen

deficiency of the lattice is balanced by migration of oxygen from the surface or re-oxidation by gaseous O_2. In addition, it is well known that some of Alkaline (Li, Na, K, Rb, Cs, Fr) and alkaline-earth metal (Be, Mg, Ca, Sr, Ba, Ba) promote soot oxidation [27]. However, these metal groups do not seem to have high redox properties (oxidation-reduction reaction) because they have only one stable ionic valency, +1 and +2, respectively. A previous studied on Effect of Different Aging Conditions on the Soot Oxidation by Thermogravimetric Analysis [28], suggested that adding $CaSO_4$ into carbon black (Printex-U, PU) didn't effect the changing of activation energy (reduce) compare with the sample contained only pure PU. The pure PU sample, PU mix with CeO_2, and CaSO4, at the weight ratio of 1:5 and 1:1 respectively, were used in this analysis as show in figure 2.6. Since only a small part of ash usually exists in soot, so the mass ratio of PU/CaSO4 is determined as 1:1. Then, these samples were analysed using non-isothermally thermogravimetric analysis method by increase temperature from 45 to 800 °C and maintains at 800°C for 10 min. The O_2 gas with 10% concentration was used as the working gas.

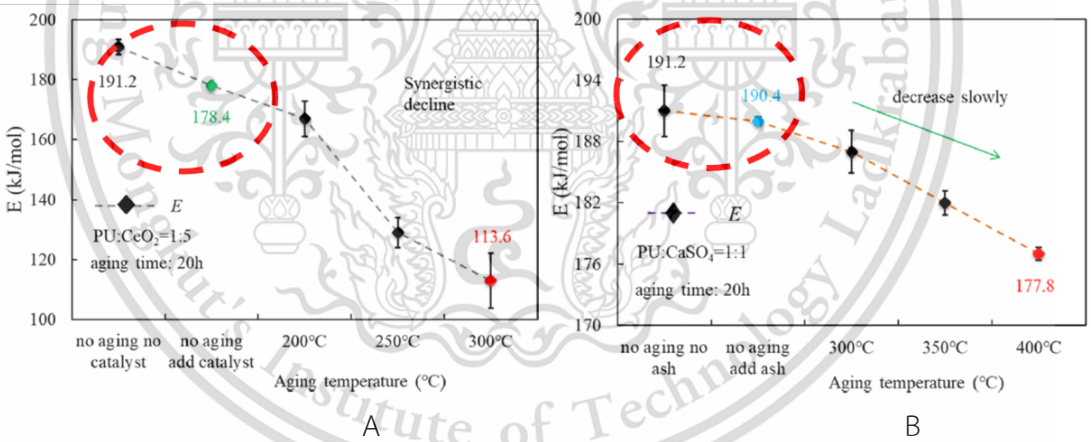

Figure 2.6 Activation Energy of PU mixed with CeO_2 (A) and $CaSO_4$ (B) after isothermally oxidized using TGA [28]

Focusing on results of activation energy depicted by red-dotted circles, it can be clarified that the activation energy in the sample contained CeO_2, 178.4 $\frac{kJ}{Mol}$(figure 2.6A), were significantly reduced compare with the sample contained $CaSO_4$, 190.4 $\frac{kJ}{Mol}$ (figure 2.6B). Therefore, CeO_2 exhibits higher catalysts effect on soot oxidation than $CaSO_4$, corresponding with previously reviewed.

2.5 Previous research on oxidation behaviours and characterization of PMs

(This section obtained from "Scanning electron microscopic time-lapse visualization of ash movement during soot cake oxidation in Diesel Particulate Filters" Tokyo Institute of Technology master thesis by author)

2.5.1 PMs generation method

Diesel Particulate Generator (DPG) was utilized to produce soot with ash components and introduced to the actual full-size DPF which is simulate the actual DPF system presents in the automobile, as shown in figure 2.7. The total flow rate and PM loading ratio was controlled by the main combustor based on the primary, secondary, and tertiary air supplies. Ash elements were introduced via spray combustion utilizing an oil injector with element concentrations shown in table 1 [29]. As a result, the PM included ash with a weight ratio of 11 wt.%. The main combustion gas consisting of PM and ash was then introduced into a DOC and full-size DPF [29, 30]. The PMs powder were collected from full sized DPF for an analysis of oxidation behaviours, elemental compositions, and desorption of oxygen from surface of ash particles.

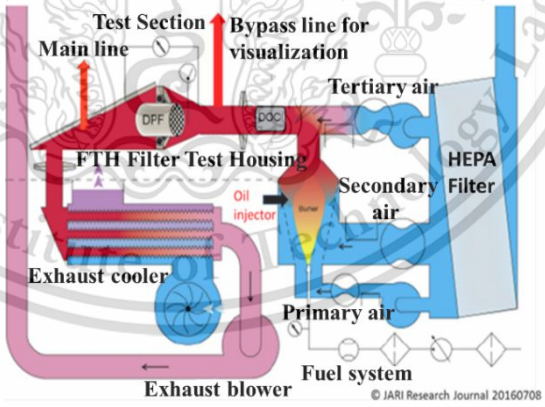

Figure 2.7 Schematic of the DPG [29, 30]

Table 2.1 Concentrations of ash elements introduced to DPG [29]

Ash Elements	Oil injector Concentrations (wt.%)
Calcium	0.5
Phosphorous	0.4
Zinc	0.4
Sulfur	0.8

2.5.2 Thermogravimetric analysis (TGA)

The PM sample powder, consists of pure soot and soot with 11 wt.% ash components (soot/ash=8), were analyzed their oxidation behaviors using a thermogravimetric analyzer (Shimadzu DTG-60). In a preheating process, the sample was heated up from room temperature with pure nitrogen gas at the increasing rate of 20°C/min until reaching the target temperature of 600°C. Then, the sample was oxidized isothermally with the 10% O_2 working gas conditions. Figure 2.8 (a) presents TGA results of soot and soot with 11% ash. The horizontal axis represent time in minutes, on the left and right vertical axis represent mass (%) and temperature (°C), respectively. The mass (%) was directly converted to mass reduction rate versus time (min.) as shown in figure 2.8 (b). During heating up process with pure nitrogen, mass losses were observed on both samples. A mass of soot has remained almost 100% during heating from 25°C to about 500°C, after that, it started to decrease until reached about 90% mass at 600°C. On the other hand, soot with 11% ash started to have a sharp decreased of mass at temperature of 400°C and it continuously decreased until reached 70% mass or had 30% mass loss at 600°C. In addition, the mass reduction rate of soot with 11% ash was about two times higher than pure soot just after an introduction of 10% O_2 for oxidation. As a result, an oxidation of soot with 11% ash was completed almost 50 minutes earlier than pure soot while 11% of residual mass was remained as indicated on a concentration of ash particle. The oxide of ash particles which are in the form such as oxides (-O), sulfates ($-SO_4$), and phosphates ($-PO_4$) may perform as the additional source of oxygen that promote soot oxidation. Since pure soot also had a mass loss during heating under inert gas (N_2), this mass loss can be a product of oxidation between carbon and decorated oxygen atoms, as well as volatile organic compounds (VOC) and soluble organic fraction (SOF). In order to verify this result, each PM powder was collected and analysed using organic elemental composition analysis as shown in the next section.

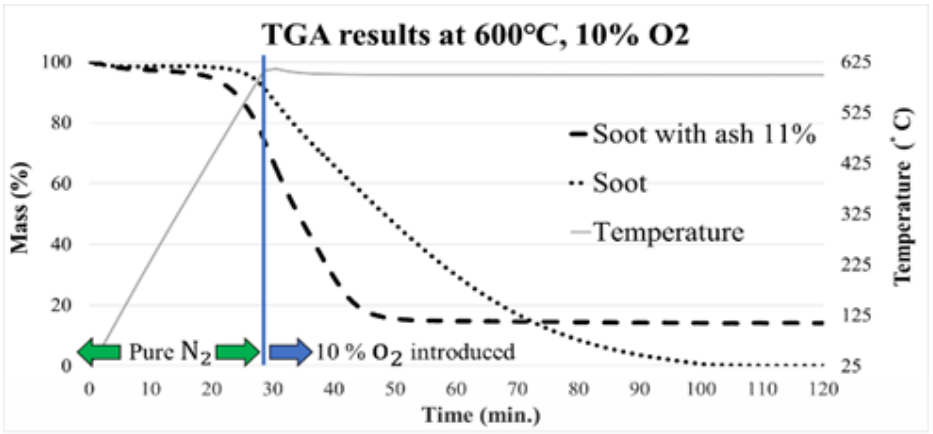

(a)

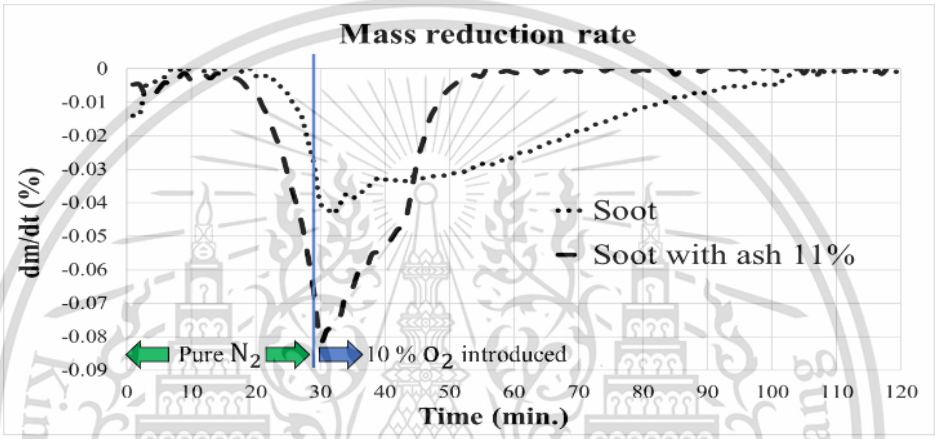

(b)

Figure 2.8 TGA results in mass % (a) and mass reduction rate (b).

2.5.3 Organic elemental composition

A Vario EL Cube organic element analyzer was used to analyze components of carbon(C), hydrogen(H), nitrogen(N), oxygen(O) and sulfur (S). The remaining unknown species was stated as ash. In addition, the Vario micro cube was used to analyze oxygen contents separately from C, H, N and S.

Table 2.2 presents the percent weight ratio of PM composition used in this study. Pure soot had the highest composition of C, while compositions of H and N from both samples were similar. The oxygen atom components of soot with 11% ash cannot be analyzed from the elemental analyzer due to its higher ash contents than 5%. Therefore, it was indicated as N/A. However, more than 10% of undetermined composition of soot with 11% ash might consists of O. As a result, soot with 11% ash had higher O atom than pure soot. This higher O atom may cause partially oxidized the C component during preheating, as well as accelerated oxidation reaction.

Table 2.2 organic elemental composition of pure soot and soot with 11% ash.

	Soot	11% ash
C [%]	88.85	74.49
H [%]	0.71	0.98
N [%]	0.15	0.17
O [%]	8.17	N/A
Total ash [%]	2.1	10.5
S	N/A	0.45
Total [%]	99.98	86.14

2.5.4 Desorption of oxygen from a surface of ash particles

A desorption of oxygen from surface of ash particle was measured by thermo mass/mass spectrometer system (Rigaku). The experiment was conducted with approximately 14 mg. of ash powder. The sample was heated under helium inert gas from room temperature to 1000 ℃ at heating rate of 20 ℃/min. The gases evolved in response to the sample heated were ionized and analyzed using quadruple type mass detector.

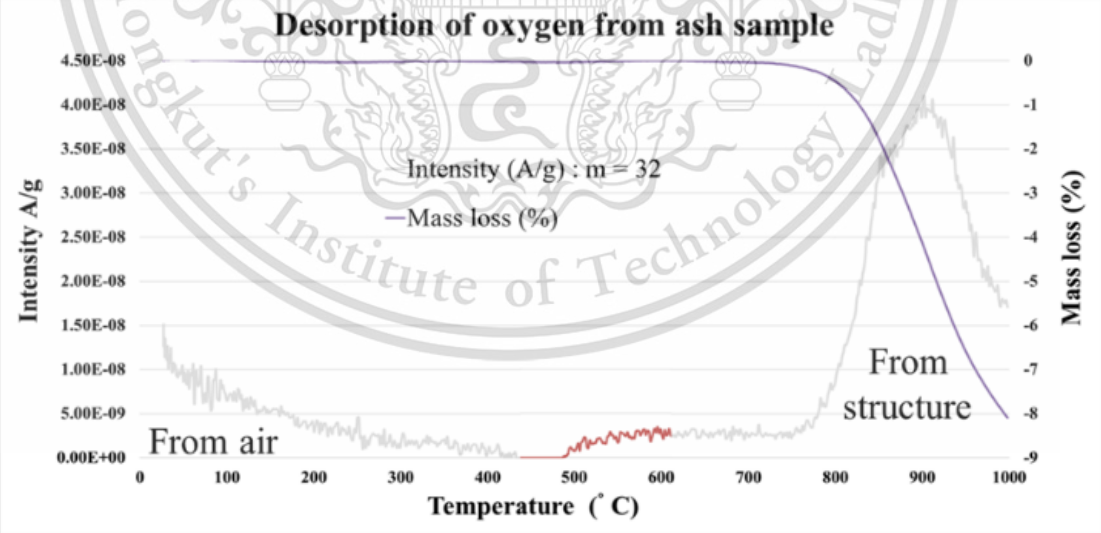

Figure 2.9 Intensity of oxygen desorbed from ash sample

Figure 2.9 presents intensity of oxygen in gas phase, desorbed from ash sample. The vertical axis presents an intensity of oxygen while horizontal axis presents temperature in degrees Celsius. At 27℃ room temperature, the signal of oxygen can

be detected as it continuously decreased and disappeared around 430℃. This low temperature signal came from the air that partially entered the ionization chamber. On the other hand, the sharp increase of oxygen signal simultaneously with a mass loss at a high temperature (>750℃) were the result of structure' s deformation. Both signals were not the result of oxygen desorbed from a surface of ash particle, therefore, they were depicted as grey line.

Focusing on the red line corresponding with a temperature from 500 to 600℃, the signal of desorbed oxygen can be detected around 500 ℃, and it continuously increased and remained constant at 600 ℃. Therefore, at 600 ℃ there were a desorption of oxygen from surface of ash particles. By making a comparison with a previous TGA result at the same temperature 600 ℃, there were a mass loss on both pure soot and soot with 11% ash during the preheating. A difference of a mass loss between these two samples is a result of the oxygen desorbed from a surface of ash particles causing a partial oxidized of soot and they also help accelerated and promoted soot oxidation. As a result, Soot with 11% ash exhibited higher mass loss than pure soot in any time intervals. In a practical DPF trapping process, oxygen has already absorbed on the surface of ash due to a high combustion temperature. Then, this oxygen will be desorbed resulting in an oxidation enhancement during DPF regeneration. The mechanisms of oxidation enhancement by ash particles can be explained using figure 2.10.

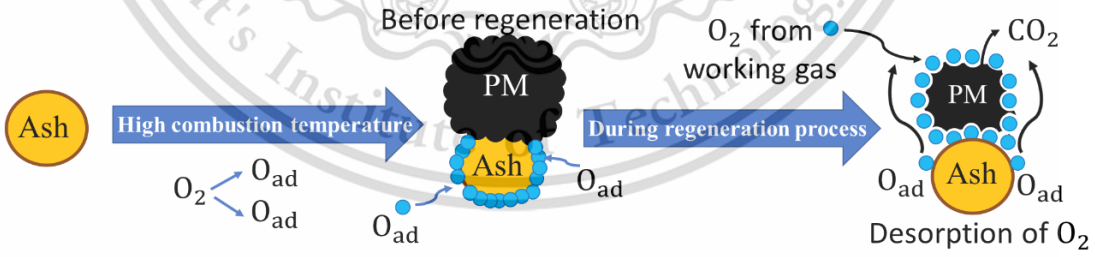

Figure 2.10 Mechanisms of catalysts as a physical impact on soot oxidation

2.5.5 Evaluation of reaction rate

From previous results, it can be clarified that ash has a catalyst effect that help promote soot oxidation. However, some quantitative analysis is needed to explain this catalyst effect whether it come from the chemical impact which is related to the reduction of activation energy or physical impact that mainly about the increasing of collision frequency contact with oxygen. In order to find out which parameters are dominant, a comparison of activation energies between pure soot and soot with 11% ash using Arrhenius plot was conducted.

The Arrhenius plot was obtained for both pure soot and soot with 11% ash as show in the following figures:

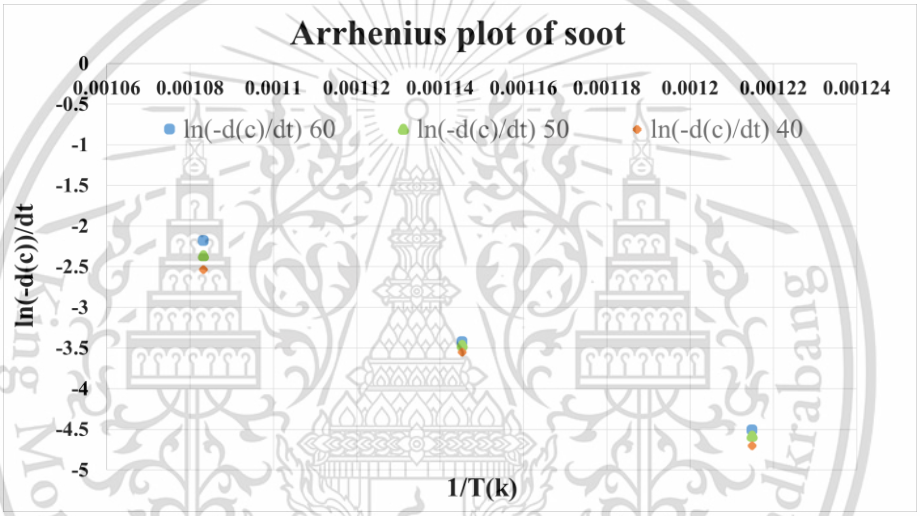

(A)

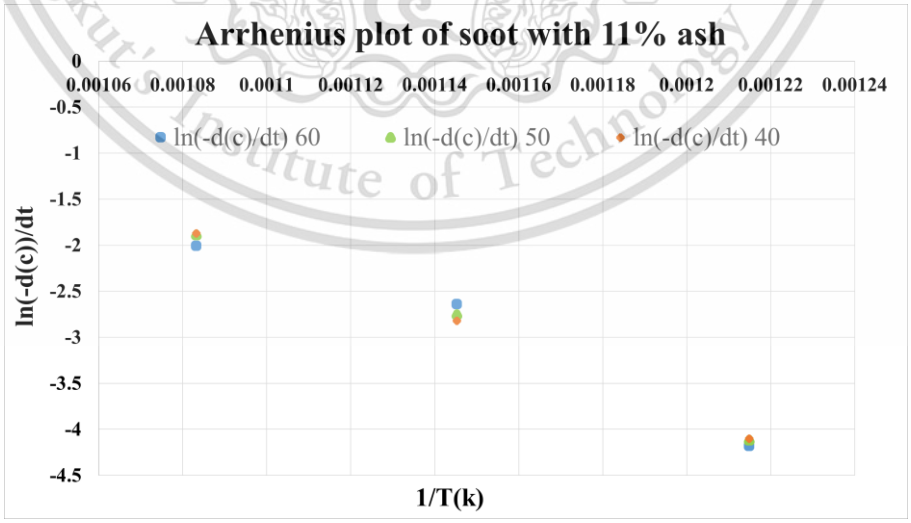

(B)

Figure 2.11 Arrhenius plot at mass percentage of 40, 50 and 60% for the pure soot (A) and soot with 11% ash (B).

Figure 2.11 (A) and (B) presents the Arrhenius plot used to obtain the characteristics of overall activation energy at mass percentage of 40, 50 and 60% for the pure soot and soot with 11% ash under the condition of 10% oxidation. The vertical axis represents reaction rate (ln(-d(c))/dt) and horizontal axis presents inverse of temperature (1/T(k)). It can be clearly observed from both graph that a distribution of data is not widely spread, each set of data (consists of three points) is concentrated in one point. As a result, it can be predicted that the overall activation energy of both sample at 40, 50 and 60% mass may not vary. The activation energy can be obtained as shown in table 2.3.

Table 2.3 presents activation energy of both PM samples at 40, 50 and 60% remaining mass.

Remaining C (%)	Ea of soot (KJ/mol)	Ea soot with 11% ash (KJ/mol)
40	136.92	140.99
50	139.99	140.91
60	147.05	137.14

From table 2.3, the activation energy at 40% C of pure soot was slightly less (about 4 KJ/mol) than soot with 11% ash. On the other hand, soot with 11% ash was about 10 KJ/mol less than a pure soot at 60%. At 50% remaining Carbon, both samples had almost the same activation energy. It can be concluded that ash particles do not have a chemical impact which is about a reduction of the activation energy on soot oxidation since the over all activation energy of both samples were nearly the same. To further investigate the effect of ash on soot oxidation, a comparison of arrhenius plot between pure soot and soot with 11% ash at the 50% mass, for example, was made as shown in figures 2.12. In addition, a comparison of activation energy and collision frequency term also present as shown in table 2.4.

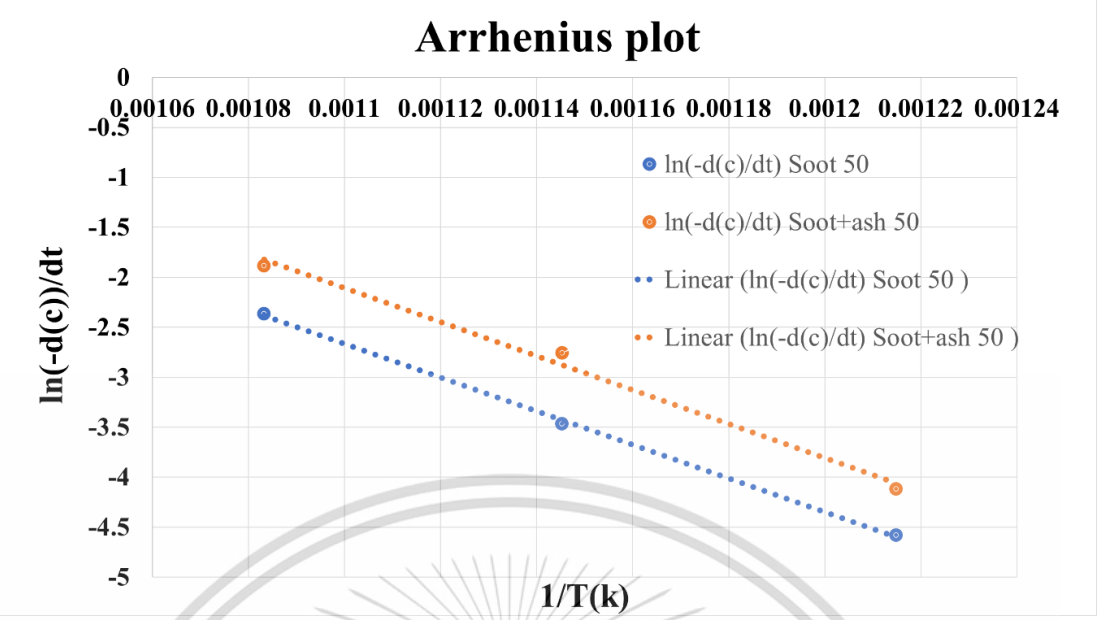

Figure 2.12 Arrhenius plot of PM samples at 50% mass.

Figure 2.12 presents a comparison of arrhenius plot between pure soot and soot with 11% ash at 50% mass. The trendlines, depicted by orange and blue dotted line, were added for an easier interpretation. It can be clearly observed that slope of a soot (depicted by a blue dotted line), and soot with ash (depicted by orange dotted line) were nearly the same. However, the y-interception, in the case of soot with ash (orange dotted line) was higher than pure soot (blue dotted line), corresponding with the collision frequency term (A) of sample contained ash that has about two times higher than pure soot, table 2.4. This can be concluded that ash has a physical impact which is an increasing of collision of frequency, in this case, an additional supply of desorbed oxygen on a surface of ash paricels resulting in an enhancement of soot oxidation.

Table 2.4 a comparison of activation energy and collision frequency of soot and soot with 11% ash at 50% mass

50 % Remaining mass	E_a (KJ/mol)	A ($\times 10^6$)
Soot	139.99	7.5
Soot + 11% ash	140.91	16.2

CHAPTER 3

RESEARCH METHODOLOGY

3.1 Experimental setup and procedures

3.1.1 Preparation of passenger car DPF

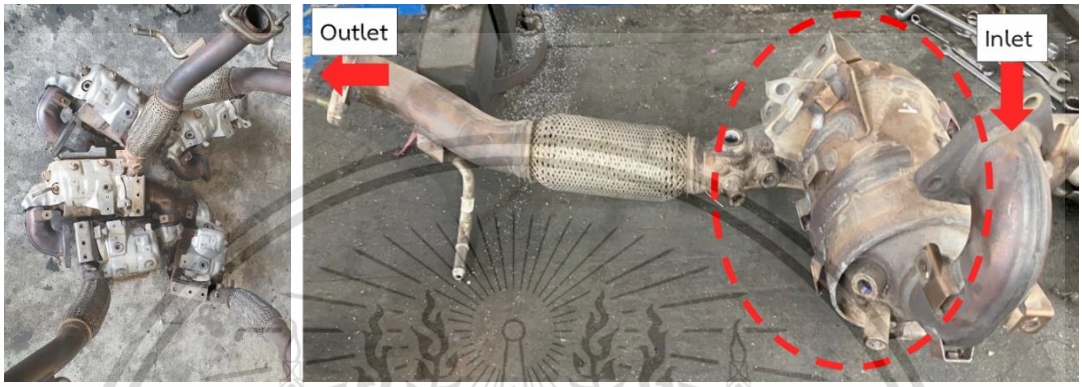

A B

Figure 3.1 several passenger cars DPF assembly (A), components and location of DPF case (B)

Figures 3.1(A) presents several DPF assemblies obtained from 1.5-liter diesel passenger cars used in this experiment. These DPF assemblies obtained from the muffler shop where car's owners decided to remove their DPF for engine tuning. The location of DPF case is depicted by the red-dotted circle, as shown in figure 3.1(B). The unessential components of this assembly, as well as the DPF case were removed utilizing electric saw. After the removal process was successful, the insulating materials can be clearly observed as it was wrapped around the DPF (figure 3.2A).

A B

C

D

Figure 3.2 insulating material around the DPF (A), DPF with honey-comb structure (B), 16 segments of DPF after the full-size DPF was disassembled (C), a removed top wall DPF (D).

The investigated DPF had ‘honey-comb’ structures (figure 3.2B) and consists of several ‘segments’, there were disassembled in their segment constituents, as shown in figure 3.2(C). There are a total of 16 segments in a DPF. Then, the horizon top wall of each segment was removed layer by layer utilizing abrasive papers and grinding machine (figure 3.2D). The macroscale analysis data of ash accumulation length, as well as distribution patterns in each layer were collected, as trapped within

the filter channels. In order to confirm the reproducibility of data, several DPFs from the same car manufactures were investigated in this experiment.

In addition, small pieces of DPF with deposited ash were collected from different locations of DPF (center, filter periphery) and mechanical removal of ash from the filter (figure 3.3) also performed for the microscale analysis utilizing instruments such as X-Ray Fluorescence (XRF), X-Ray Diffractometer (XRD), a field emission scanning electron microscope (FE-SEM), a transmission electron microscope (TEM), energy dispersive X-Ray spectroscopy (EDX), and thermogravimetric analysis (TGA) which will be discussed in next section.

Figure 3.3 small pieces of DPF and collected ash for microscale analysis

3.1.2 Physical characterization and Elemental analysis of particulate matters

For a microscopic visualization of metal oxide ash, a morphology, structure of nanoparticles, primary particles, as well as elemental compositions were investigated utilizing a field emission scanning electron microscope (FE-SEM), and a transmission electron microscope (TEM). The analytical facility was used at the National Nanotechnology Center (NANOTEC). The FE-SEM instrument was Hitachi SU5000 (figure 3.4 A), operation voltage from 0.1-30 kV, combined with an energy dispersive X-Ray spectroscopy (EDX) for qualitative chemical analysis. The majority of TEM study was made by using a transmission electron microscope (JEOL model JEM 2100) also equipped with an energy dispersive X-Ray spectroscopy (EDX), this instrument was operated at 200kV acceleration voltage (figure 3.4 B).

To ensure only ash particles were obtained for the analysis, the electrical furnace (figure 3.5) was used to oxidize soot at 900 ℃ for 30 minutes.

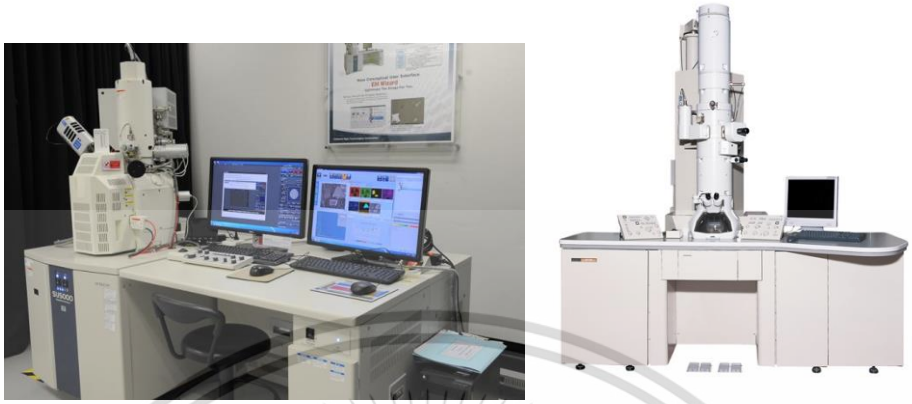

A B

Figure 3.4 FE-SEM SU5000 (A), JEOL model JEM 2100 (B)

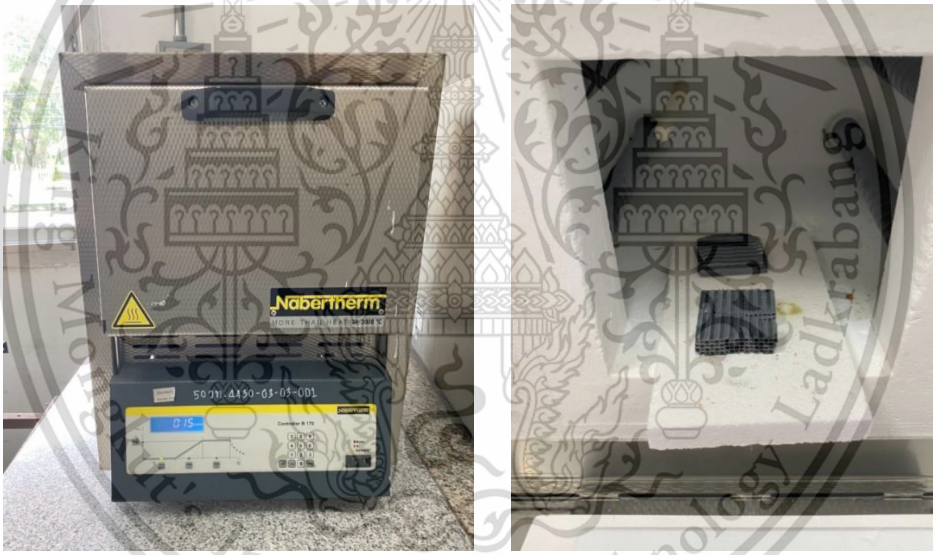

Figure 3.5 Electrical furnace used to remove deposited soot on DPF

In addition, ImageJ software was utilized to investigate agglomerated, primary particle, and the skeletonized nanostructure of metal oxide ash, carbon black (CBN 330) compares with other diesel engine soot. This analysis transformed the cropped TEM image (5 nm x 5 nm) as 25 nm^2 (figure 3.6A) into a binary image (black and white, figure 3.6B). Then, black and white binary image was transformed into skeletonized image (figure 3.6C) which reveals the different crystallites structure of particulate matters.

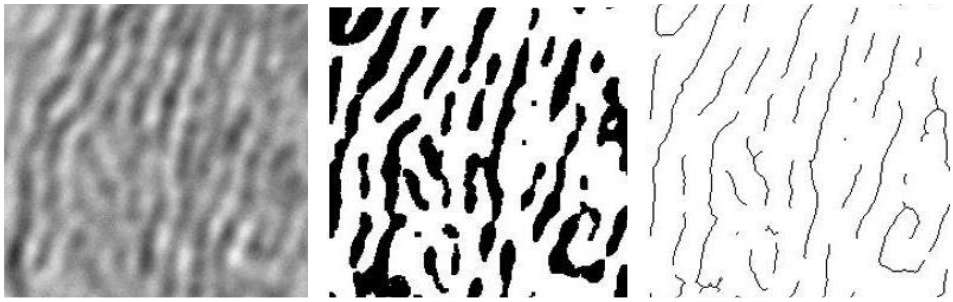

A B C

Figure 3.6 nanostructure analysis using ImageJ software

A natural aspirated, single cylinder, direct injection, compression ignition engine (Kubota RT 140 DI) was used to generate diesel engine soot. Engine displacement volume is 709 cm^3 and compression ratio is 18:1. Details of engine specifications are briefly described in Table 3.1.

Table 3.1 Kubota RT 140 DI engine specification

Items	**Details**
Engine type	1-cylinder, NA, direct injection CI engine
Bore x Stroke	(97 x 96) mm
Displacement	709 cm^3
Compression ratio	18:1
Power	9.2 kW @2400 RPM
Injection timing	19^{o} CA bTDC
Injection pressure	22 MPa

3.1.3 Archimedes method for porosity

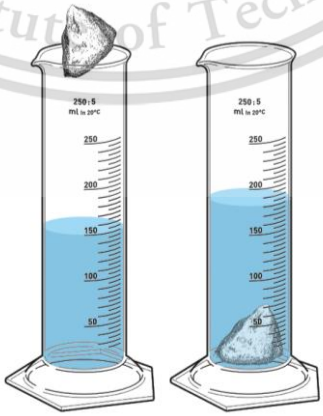

The porosity of SiC DPF can be measured using the Archimedes water displacement method

A DPF was cut into a small piece and its volume was estimate, indicated as V_{DPF} (Volume of DPF). This DPF was put into the scale test tube, then the volume of water was recorded before and after putting the DPF indicated as V_1 and V_2, respectively.

$$\text{Porosity } (\emptyset) = \frac{V_V}{V_T}$$

where; Total volume (V_T) = V_{DPF} = Volume of void (V_v) + Volume of solid (V_s), and

Volume of solid (V_s) = V_2 - V_1

$$\text{Therefore, } (\emptyset) = \frac{V_V}{V_{DPF}} = \frac{V_{DPF} - V_S}{V_{DPF}}$$

3.1.4 X-ray fluorescence and X-ray diffraction (XRD) analysis

The investigation of elemental compositions and chemical compounds of ash particles, as well as SiC DPF were carried out by X-Ray Fluorescence (XRF, Orbis PC), and X-Ray Diffractometer (XRD, D8 ADVANCE) at NSTDA Characterization and Testing Service Center (NCTC). The XRF and XRD instruments and sample loading locations are presented in figure 3.7 and 3.8, respectively.

Figure 3.7 XRF, Orbis PC

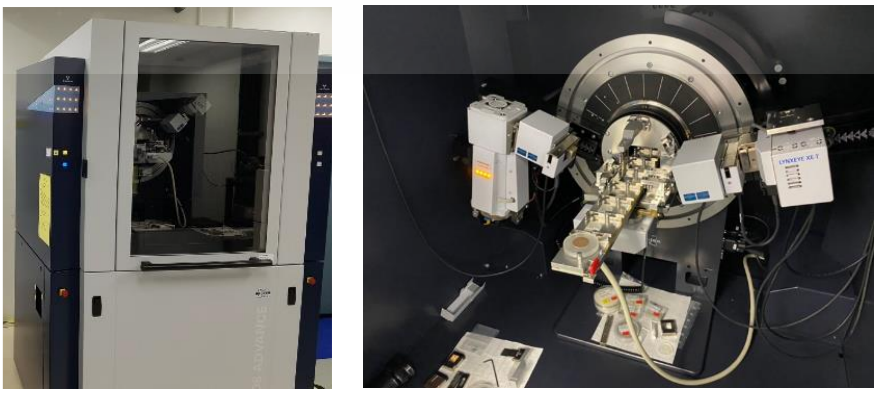

Figure 3.8 XRD, D8 ADVANCE

3.1.5 Elemental analysis of diesel fuels and lubricating oil

The wear, additive elements and contamination in used Lubricating Oils were further determined by the standard method ASTM D5185 utilizing Inductively coupled plasma atomic emission spectroscopy (ICP-AES) technique. This analytical technique detects chemical elements by emit the inductively coupled plasma to produce excited atoms and ions. These excited atoms and ions, then emit electromagnetic radiation at wavelengths which is a characteristic of particular element.

Approximately 1 litre of conventional diesel, diesel B10, diesel B20 and premium diesel fuels were collected from the PTT gas station. In addition, about 0.8 litre of the new Mazda fully synthetic engine oil (SUPRA DPF 0W-30, figures 3.9) and the used ones, were obtained from the MAZDA car dealership. The used lubricating oil samples were collected at the crankcase position from 4 different vehicles, each sample has about 10,000 kilometers oil service time.

Figure 3.9 The new MAZDA 0W-30 fully synthetic engine oil used for this analysis

All oil samples were collected into the specific opaque containers, as shown in figure 3.10 and figure 3.11, and it was submitted to the Focus lab for the analysis.

Figure 3.10 Used and new lubricating oil samples

Figure 3.11 Various type of fuels collected from PTT gas station

3.1.6 Thermogravimetric analysis (TGA)

The effect of ash particles on oxidation behaviors of PMs was analyzed using thermogravimetric analysis (TGA). PM samples were prepared by mixing powder of soot (CBN330), DPF (SiC) and ash with the conditions as follows:

Number of samples = 2

CBN330 50% + DPF(SiC) 50%

CBN330 50% + DPF(SiC) 40% + Ash 10%

These PM samples were analyzed their oxidation behaviors using a thermogravimetric analyzer (Shimadzu DTG-60AH). Approximately 10 mg. of each sample and the total gas flow rate of 30 ml/min were conducted in this experiment. It was previously confirmed this flow provides sufficient stoichiometry for oxidation. In a preheating process, the sample was heated up from room temperature with pure nitrogen gas at the increasing rate of 25℃/min, until reaching the target temperature of 575, 600, 625℃. Then, the sample was oxidized isothermally utilizing the atmospheric air as the working gas with the keeping time of 1.5 hour. A SiC DPF was blended into the samples to perform as the heat adsorption material, as well as to simulate a practical regeneration of DPF. A mass (%) curve versus time (sec.) were obtained at one second interval.

CHAPTER 4

RESULTS AND DISCUSSION

4.1 Physical characterization of particulate matters

4.1.1 Agglomerated and primary nanostructure of particulate matters

The transmission electron microscopy (TEM) was used to investigate a morphology, nanostructure of the agglomerated, primary particles of CBN330 and diesel engine, respectively. Figure 4.1 presents the agglomerated structure of PMs derived from CBN330 (A) and diesel engine (B).

A B

Figure 4.1 TEM images of agglomerated PMs from CBN330 (A), diesel engine soot (B)

The agglomerated structure of PMs from CBN330 are similar to the diesel engine, this structure composed of numerous spherical PMs primary particles agglomerated together. There is no significant difference in agglomerated structures between these two types of PMs, as shown in higher magnification images figure 4.2 (A, B).

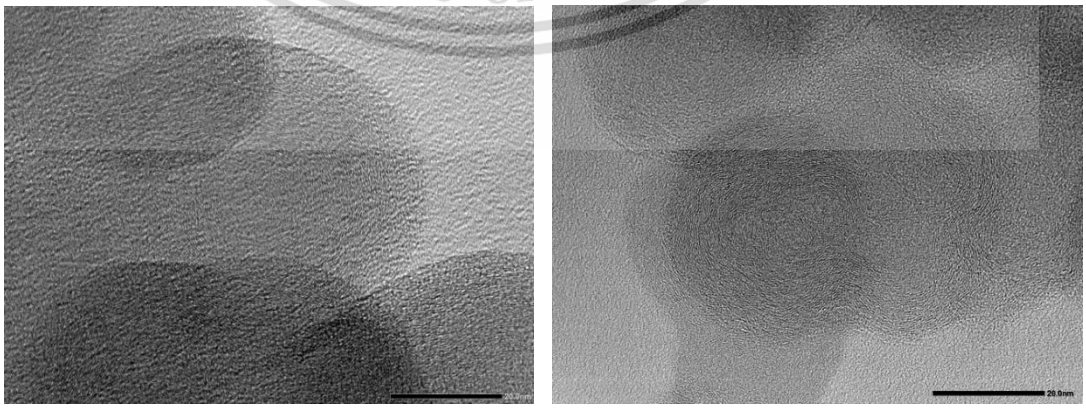

A B

Figure 4.2 Higher magnification TEM image of PMs from CBN330 (A), diesel engine soot (B)

Furthermore, figure 4.3 (A, B) presents the nanostructure of primary particles from carbon black (CBN330) compared with diesel PMs. It can be verified that the nanostructure of primary particles is spherical shape composed of curve line carbon crystallites.

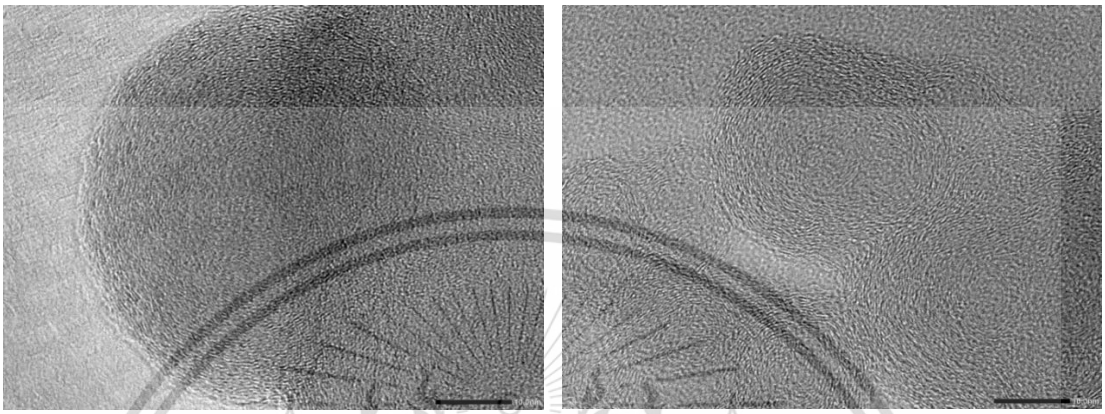

A B

Figure 4.3 TEM image of PMs from CBN330 (A), diesel engine soot (B)

Therefore, the carbon black CBN330 can be further analyzed as a representative of a diesel engine soot.

4.1.2 Skeletonized nanostructure of particulate matters

Image processing technique was utilized to investigate the skeletonized nanostructure of metal oxide ash, carbon black (CBN 330) and diesel engine soot. Figures 4.4, 4.5 and 4.6 present the skeletonized image analysis of PMs derived from carbon black (CBN 330) diesel engine soot and metal oxide ash, respectively. According to the CBN330 figure 4.4 and diesel engine soot figure 4.5 skeletonized images, they composed of similar curve lines carbon fringes as carbon crystallite structure.

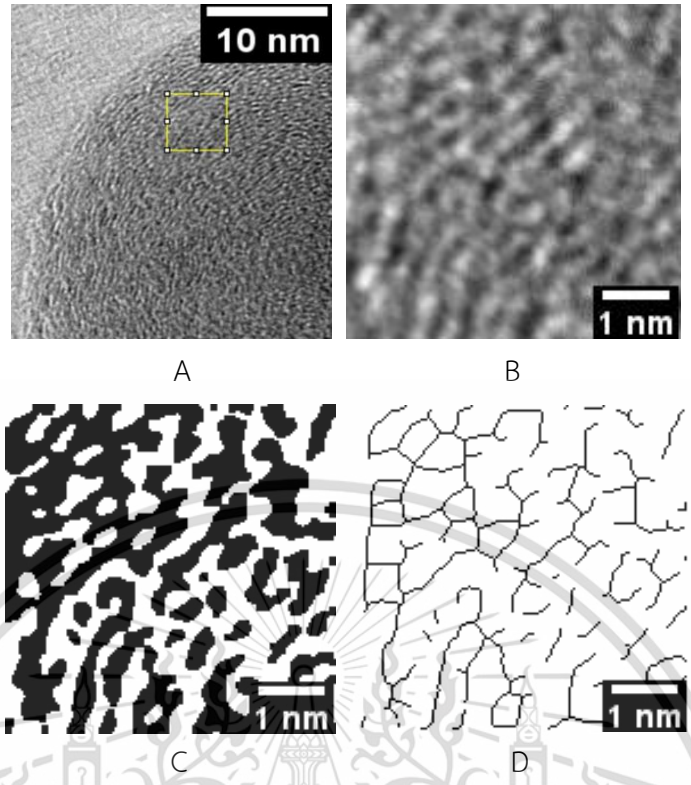

Figure 4.4 TEM nanostructure of CBN330 (A), 5 nm x 5 nm cropped images (B) black and white binary images, (C) skeletonized (D).

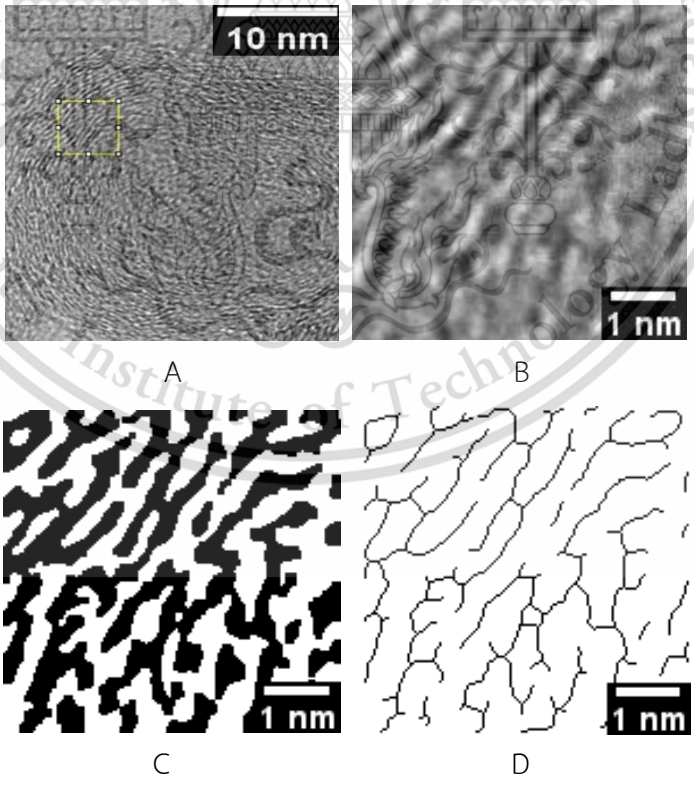

Figure 4.5 TEM nanostructure of diesel engine soot (A), 5 nm x 5 nm cropped images (B) black and white binary images, (C) skeletonized (D).

On the other hand, the skeletonized nanostructures of metal oxide ash consisted of straight-line lattice fringes. This metal oxide ash come from engine oil additives contained elements such as Calcium (Ca), Phosphorous (P), Sulfur (S), Iron (Fe) and Zinc (Zn).

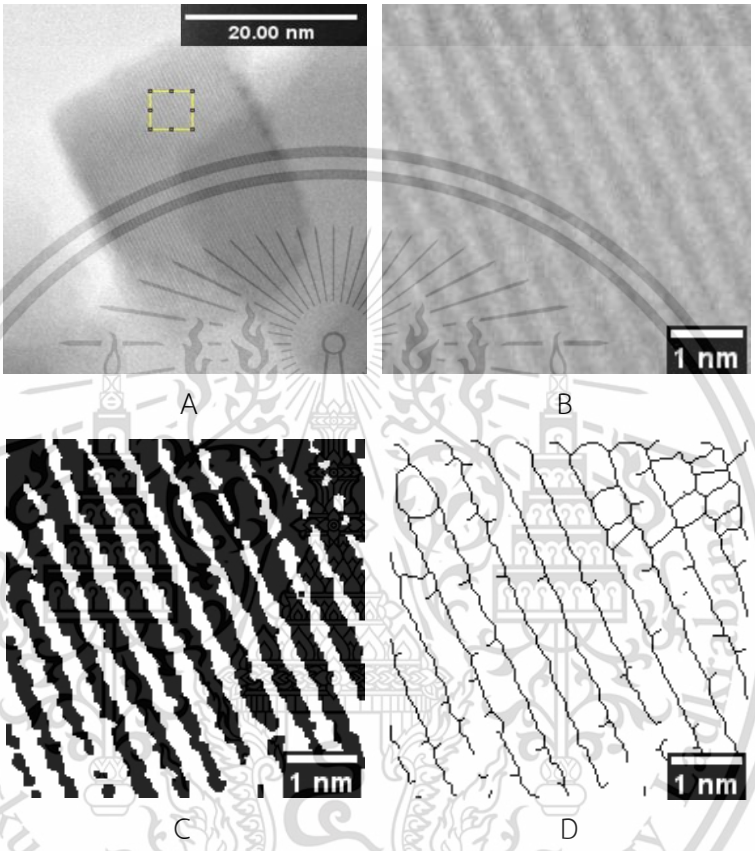

Figure 4.6 TEM nanostructure of metal oxide ash (A), 5 nm x 5 nm cropped images (B) black and white binary images, (C) skeletonized (D).

4.2 Porosity of SiC DPF

Figure 4.7 presents dimensions of a DPF sample used in this experiment. The volume of this

DPF (V_{DPF}) = Total Volume – Volume of channels

$$= (1 \times 1.2 \times 3.6) - (15 \times 0.1 \times 0.1 \times 3.6) - (15 \times 0.15 \times 0.15 \times 3.6)$$

$= 2.565\ cm^3$

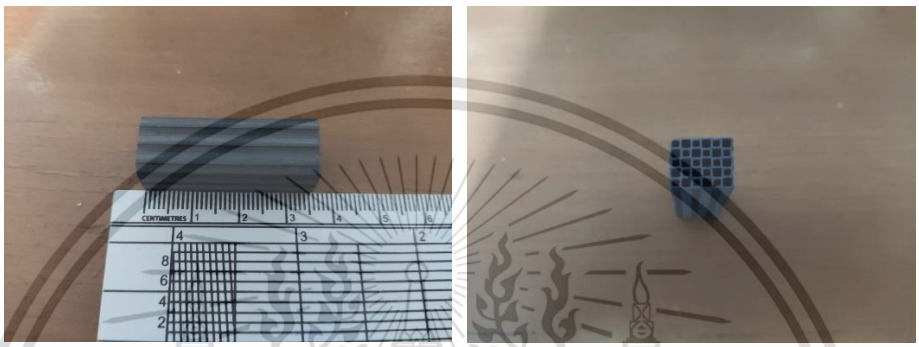

Figure 4.7 dimensions of DPF sample

Figure 4.8 presents volume of water before (V_1) and after (V_2) putting the DPF into the scale test tube. From this figure V_1 and V_2 equal to 15 ml. and 16.5 ml, respectively. A difference of water level (V_2-V_1) is equals to 16.5-15 = 1.5 ml.

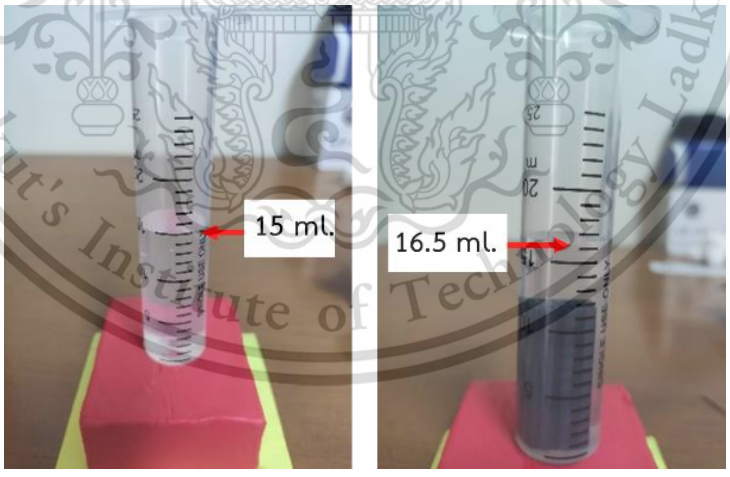

A B

Figure 4.8 Volume of water before (A) and after (B) putting the DPF.

$$\text{From} \quad (\emptyset) = \frac{V_V}{V_{DPF}} = \frac{V_{DPF} - V_S}{V_{DPF}}$$

$$\text{Thus,} \ (\emptyset) = \frac{V_V}{V_{DPF}} = \frac{2.565 - 1.5}{2.565} \times 100\% = 41.52\%$$

4.3 The macroscale analysis of plug ash in DPF

4.3.1 Ash accumulation in DPF

Figure 4.9 presents the twelfth DPF segment in which the horizontal top wall has already removed. This segment has the total of 9 inflow channels, as indicated on the right-hand side. Ash in DPFs tends to loosely accumulate, as a brown brittle powdery, and entirely filled up at the end of inflow channels (plug ash). The agglomeration of plug ash can be confirmed by SEM image (figure 4.9B). The asymmetrical can be observed in this sample as the plug ash lengths are varied depending on channels. Channel 1 has about 18 mm. which is the highest compare to others. The plug ash length drastically reduced to about 6.5 mm. in channel 7, however, the length gradually increased again to 7 and 7.3 mm. in channel 8 and 9, respectively. The amount of ash diminishing distinctively toward the inflow. The channels area without plug ash had a very thin ash layer (wall ash) attached on the channel wall, as well as deposited deep inside the surface pore along the filter length (figure 4.9 A). The mechanisms that altered ash particles from the channel walls to the end plug consists of flow-induced transport and regeneration-reduced transport [7]. Flow induced transport is a detachment and transport of ash particles by a shear force from the exhaust that can overcome the force of adhesion between the particle and filter wall (or neighboring particles).

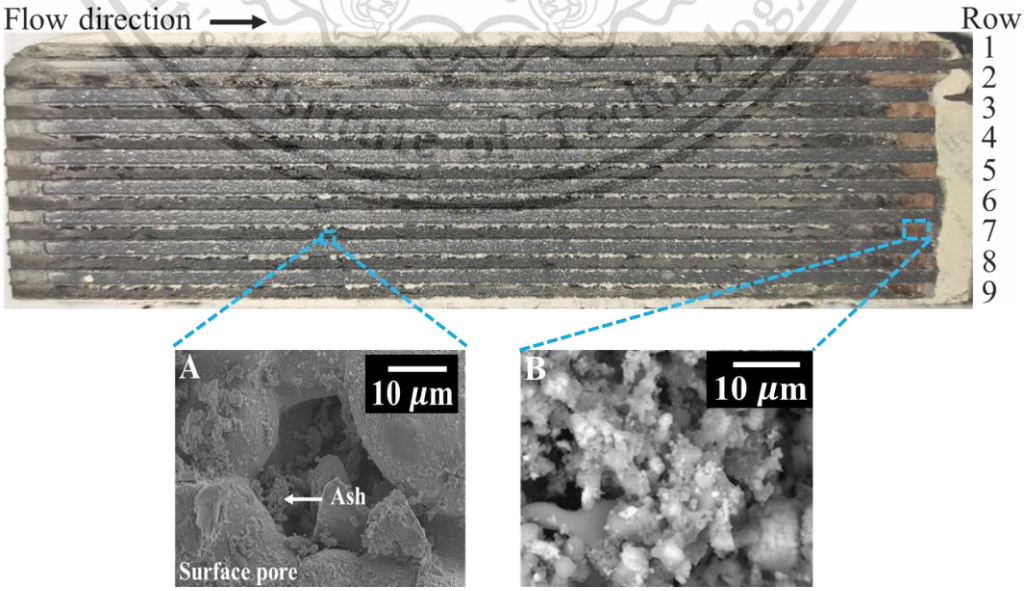

Figure 4.9 Deposited ash inside the surface pores of DPF (A), accumulation of plug ash (B).

During the regeneration process, soot cake continuously oxidized from the bottom [29]. The adhesive force between soot and ash, as well as DPF substrate are reduced. As a result, ash particles detach from DPF surface and subsequent transport to the end plug. The term “regeneration-reduced transport” can be used to describe this phenomenon.

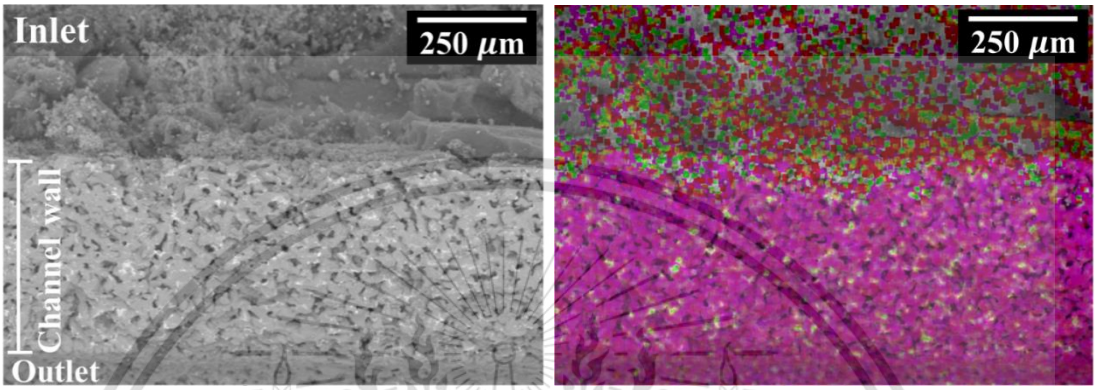

A B

Figure 4.10 SEM images show ash deposited on the channel wall (A), EDS layered image show ash penetration inside the channel wall toward the outlet channel (B).

In addition, ash is found also deep insides surface pores between inlet and outlet channels, as shown by bright white signals on the top wall in figure 4.10 A, corresponding with the EDS signals in figure 4.10 B. The ash particles directly distributed all over the channel wall, as well as in the outlet channel. Therefore, some ash particles may escape from the DPF and reach the atmosphere, however, in very small fraction. These results were similar to previous optical microscope observation of cross-sections of the DPF [32]. Since there was a variety of plug ash length accumulated in channels, therefore, ash distribution pattern was furthered investigated, as shown in the next section.

4.3.2 Ash distribution in DPF

Figure 4.11 presents plug ash length distribution in 16 segments of the DPFs. The horizontal axis represents “Segments number “in which each segment consists of 6-9 channels, depending on locations. The vertical axis represents plug ash length in millimeter (mm.). From this figure, deposited ash length fluctuates between 2-21 mm. with the average of 4.7 mm. from the 125 mm. long filter channel. Ash distribution in

most of segments were corresponding to the asymmetrical parabolic flow profile. At the filter center, ash length is varied between 2 to 8 mm., no significance difference of ash deposition in the same DPF segment. However, there were some significant increases of ash deposited length at the outer channel in the segments number 8, 12 and 16 which are close to filter periphery. The maximum length is up to 21 mm. which is almost 5 times more than the average. Previous study [32] on morphology and size of ash PM from the light truck DPF, found such a contradict result that the center part contained higher amounts of ash deposited than the periphery. One Possibility is the unique design of DPF inlet pipeline which is a characteristic of each vehicle. Thus, resulting in the difference inflow pattern inside the DPF.

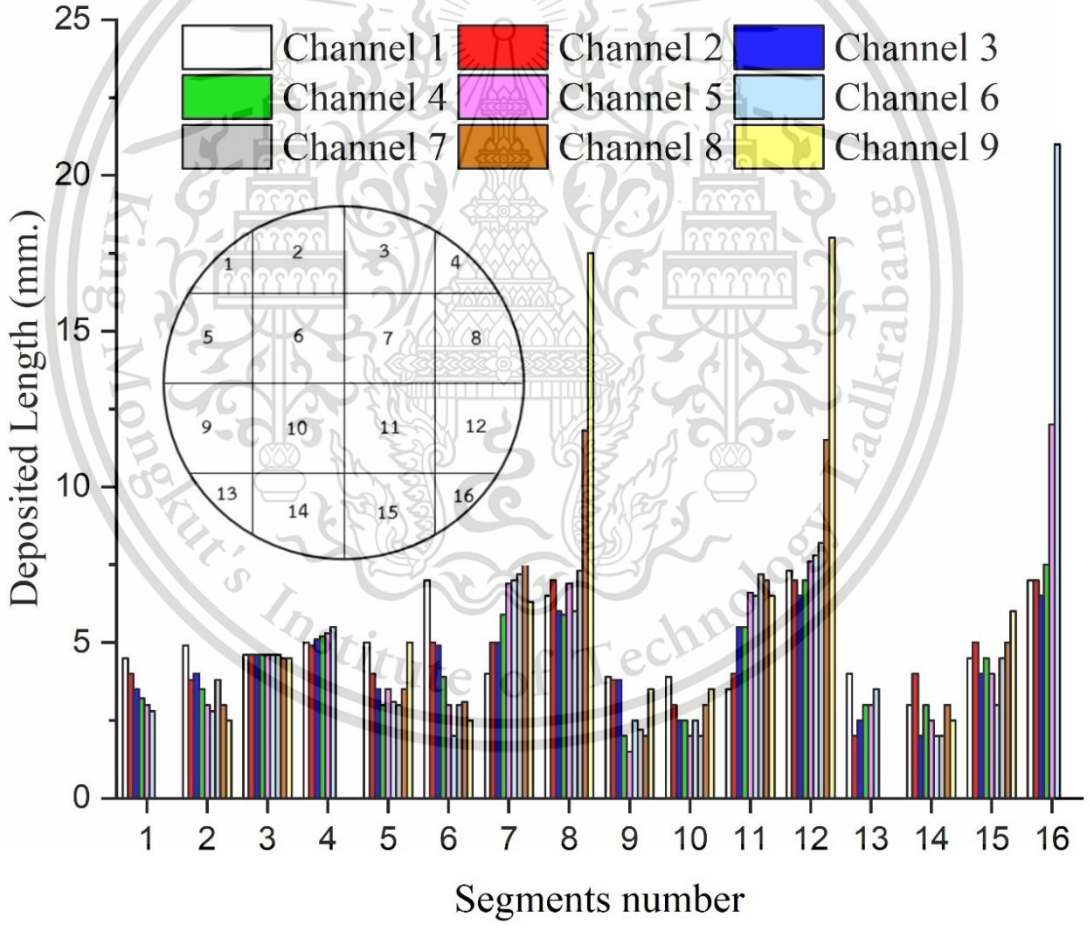

Figure 4.11 Ash distribution and deposited length inside the DPF.

4.4 The microscale analysis of ash powder

4.4.1 XRD analysis of DPF material

Before further investigation on ash elemental composition, the material analysis of DPF need to be conducted. Thus, a small piece of DPF was cut and made approximately 2 g. into a powder for XRD analysis. The main composition of this DPF is SiC as shown in XRD spectra figure 4.12 There is no signal of catalyst materials such as Pt, Pd, therefore, it can be concluded that the investigated DPF in this experiment is a non-coated type.

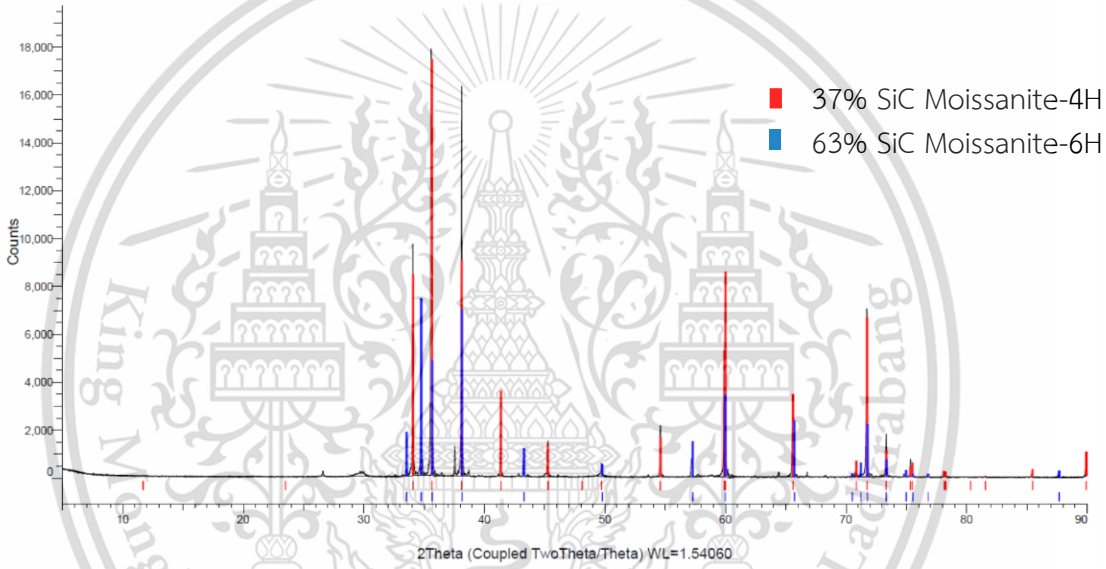

Figure 4.12 XRD spectra analysis of DPF material.

4.4.2 XRF and XRD analysis of ash components

Table 4.1 presents XRF analysis of elemental contained (wt.%) in ash sample. From the XRF result, the large proportion elements constitution of ash are Fe, Si, Ca, Cu, S, P, Zn, and Al which often presents in forms of $Cu_{0.5}Zn_{0.5}Cr_{1.1}Fe_{0.9}O_4$, $Ca(SO_4)$, Fe_2O_3 and $Ca_{19}Cu_2(PO_4)_{14}$, as shown in XRD spectra result (figure 4.13). There is no variation of ash components found in different locations. It is well-known that metal oxide ashes mainly derived from metal in the diesel fuel, engine wear, and lubricating oil. Sine Fe is the main constituent of ash, it is expected that a majority of Fe might produce from the fuel-borne additive (ferrocene) which is the Fe-based catalyst used to reduce the soot ignition and burning temperature. Another possibility is that Fe with

minor Ni and Cr may originate from the engine wear elements which are blended in lubricating oil [20].

Table 4.1 XRF elemental analysis of ash powder.

Elements	Wt%	Elements	Wt%
Fe	30.88	Zn	7.46
Si	16.18	Al	4.78
Ca	10.88	K	1.17
Cu	9.47	Ni	0.99
S	9.16	Cr	0.71
P	7.92	Mn	0.41

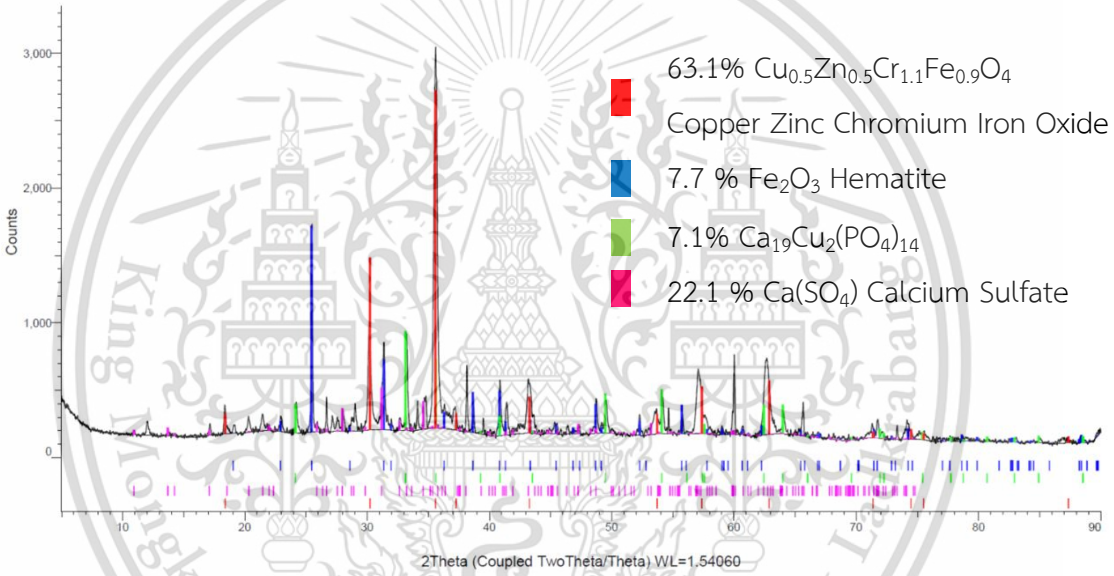

Figure 4.13 XRD spectra analysis of elements contained in deposited ash.

4.4.3 SEM-EDS analysis of ash particles

Figure 4.14 presents SEM image (A) and EDS elemental analysis (B) of Fe-oxide ash particle. This nearly spherical particle, with approximately 5 microns. in diameter, is a common type ash found in this sample. The elemental analysis revealed that Fe and O are the major elements included in this particle while Cu, Si, Zn, Al, P, Ca also found as minor components. This particle generated during the melting of iron at 1538℃ in cylinder. A surface tension draws the molten material into is spherical shape and rapidly solidified [32]. As a result, this particle has a cubic aggregation on its surface. Subsequently, transported by the exhaust gas and deposited in DPF as shown.

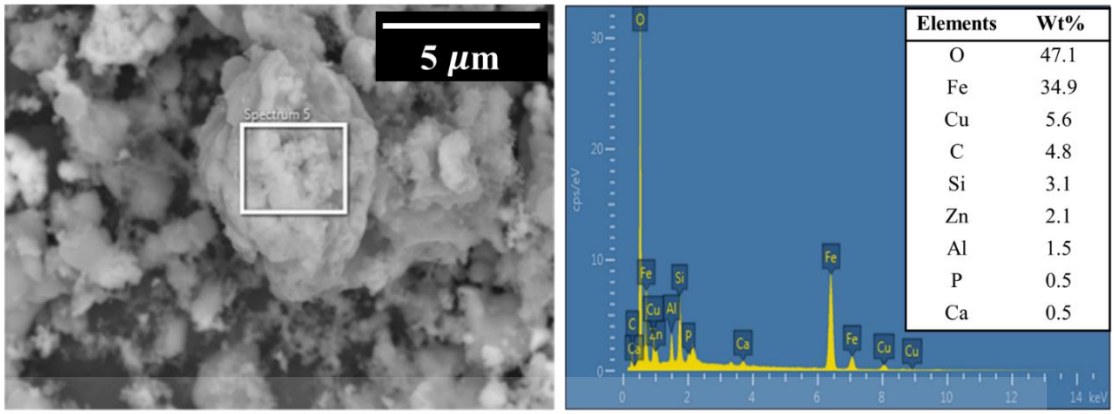

A B

Figure 4.14 SEM image of common type ash particles found in DPF (A) and EDS elemental analysis of ash particle (B).

Less commonly, another type of ash particle also found as shown in figure 4.15. This particle has nearly spherical shape with smooth surface, figure 4.15 A, consists mainly of O, Al and Si (figure 4.15 B). These Al, Si elements are components of the ceramic fiber blanket used as the insulating material around the DPF assembly. The melting point of Al_2O_3 and SiO_2 occurs above 1630°C which can only obtain in the combustion chamber. Therefore, these impurities may involve at some stage during combustion process.

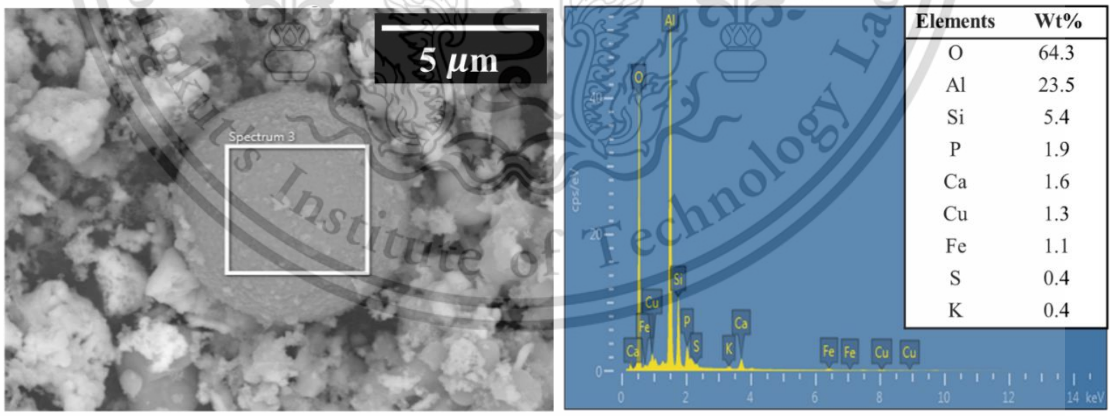

A B

Figure 4.15 SEM image of Al-Si ash particles (A) and EDS elemental analysis of ash particle (B).

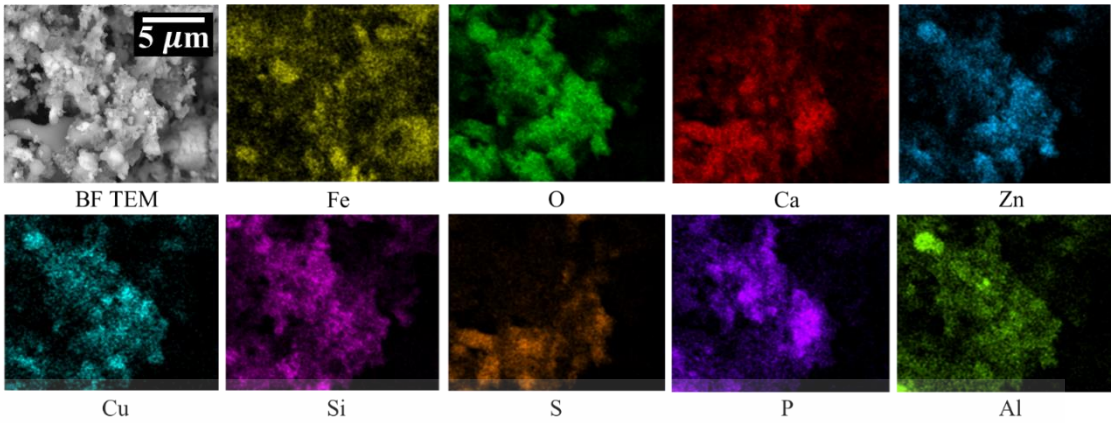

Figure 4.16 SEM image of agglomerated ash (Top left) and EDS elemental mappings analysis

Figure 4.16 presents SEM image with EDS mappings analysis of ash power. Ash agglomeration is shown on the top-left SEM image. The EDS analysis clarified the predominance of Fe, often present in form of Fe_2O_3, as the main component included in this sample. The distribution of O, Ca, Cu, Si, P, Al, for example, show similar pattern. Thus, they create compounds such as Al_2O_3, SiO_2 and $Ca_{19}Cu_2(PO_4)_{14}$ which are already confirmed in previous analysis.

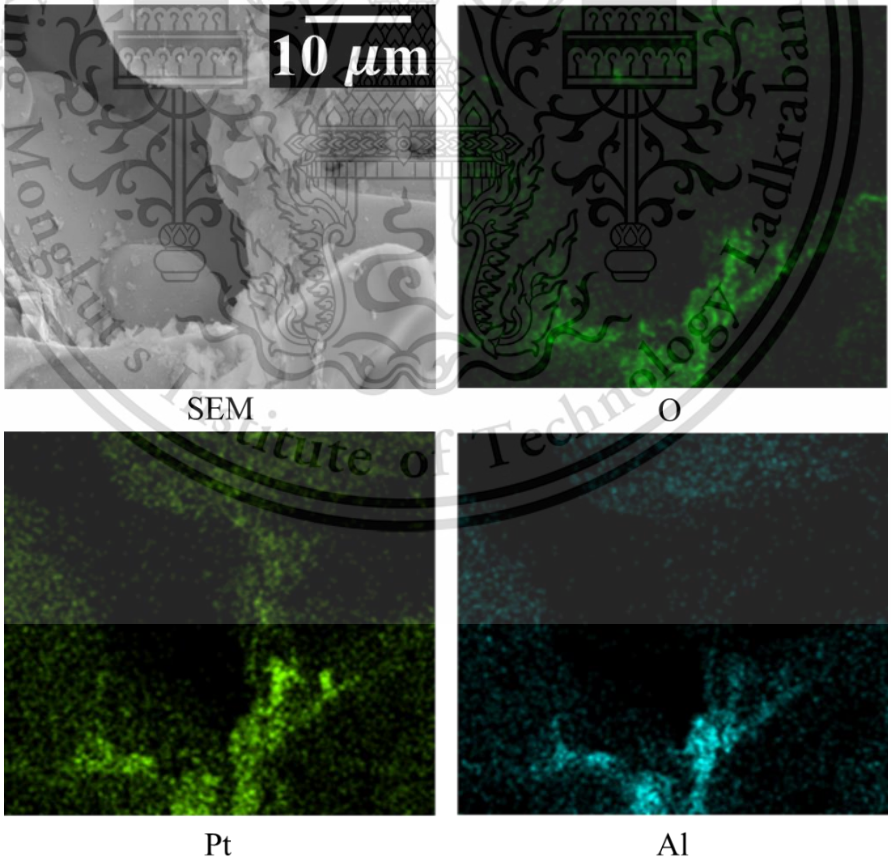

Figure 4.17 SEM image and EDS elemental mappings of deposited ash originating from DOC.

Furthermore, the agglomerated ash particles consist elements of Al and Pt originating from DOC, can also be found in this sample. Figure 4.17 presents SEM image (top left) and EDS mappings analysis of agglomerated ash particles. The conventional DOC, located upstream of DPF, usually comprised of a ceramic (cordierite) monolith with Al_2O_3 wash-coated Pt and Pd dispersion. Alumina is used for its porous structure which enables a high dispersion, as well as improvements in activity, selectivity and thermal resistance. The elemental analysis results reveal the presence of O, Al and Pt, corresponding to the composition of platinum catalyst coating on DOC. Therefore, it can be inferred that these Pt nanoparticles together with Al_2O_3 substrates were mechanically transported from the DOC to DPF by the exhaust stream.

4.4.4 TEM imaging

The bright field TEM image in figure 4.18 presents an agglomeration of ash particles with irregular round outlines shapes. Previous study suggested that this round ash particles derived from a condensation of hot combustion vapors from S which is a volatile species [33]. The right image (B) presents a higher magnification image of finer individual particle with approximately 25 nm. In diameter. A parallel straight-line hatch patterns can be clearly observed, indicated a crystalline structure which is similar to a nanostructure of metals (figure 4.19). This particle has a strong tendency to form an aggregation, and resulting in a densification of ash particle caused by repeated regenerations.

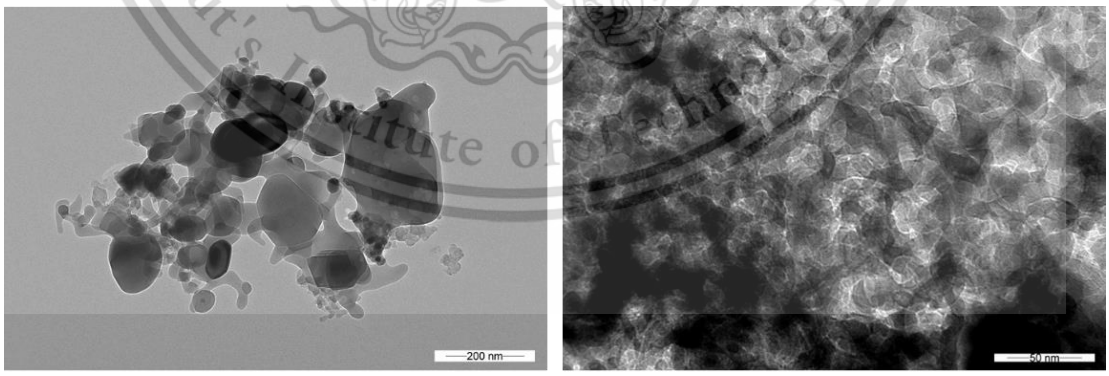

Figure 4.18 (A, B) bright field TEM image of various agglomerated ash particles

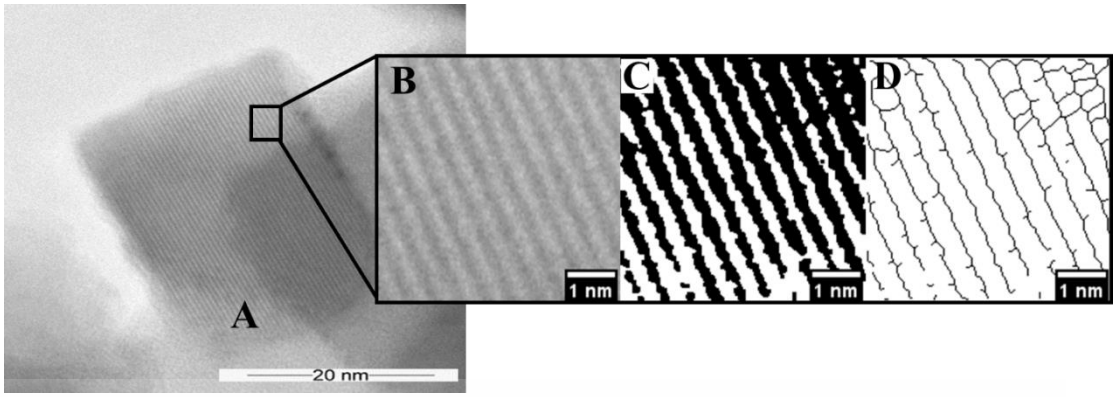

Figure 4.19 Bright field TEM presents nanostructure of metal oxide ash (A), a parallel straight-line hatch patterns indicate nanostructure of metal (B)

The top left figure 4.20 presents bright field TEM image of ash agglomeration, the EDS elemental mappings also shown. The agglomerates usually have round outlines with irregular shape, as shown in the bright field TEM image. EDS spectra mappings show an inhomogeneous of elemental distribution. Elements of Fe, O, Zn, Al, Ni, Cr and S are found in greater amounts, while Ca and P show some local concentrated. The presence of Ca, S, P, Fe, Zn and O are usually in form of $CaSO_4$, $Zn_3(PO_4)_2$, $FePO_4$ and $Ca_3(PO_4)_2$ which are a common diesel ash [34]. The EDS spectra mappings reveal some interesting information of element distribution P, S, Ca and O showed similar pattern, thus, formed compounds such as -O, -SO_4 and -PO_4 of Ca. Additionally, oxides of Fe, Al, Zn and minor Cr, Ni are considered to be the majority of ash compounds found within this sample. These compounds might be abrasion products of engine wear formed during movement of pistons. This inference is compliance with previous XRD, XRF analysis of ash powder which also show the presence of anhydrite ($CaSO_4$), hematite (Fe_2O_3), as well as minor fragment of Ni and Cr.

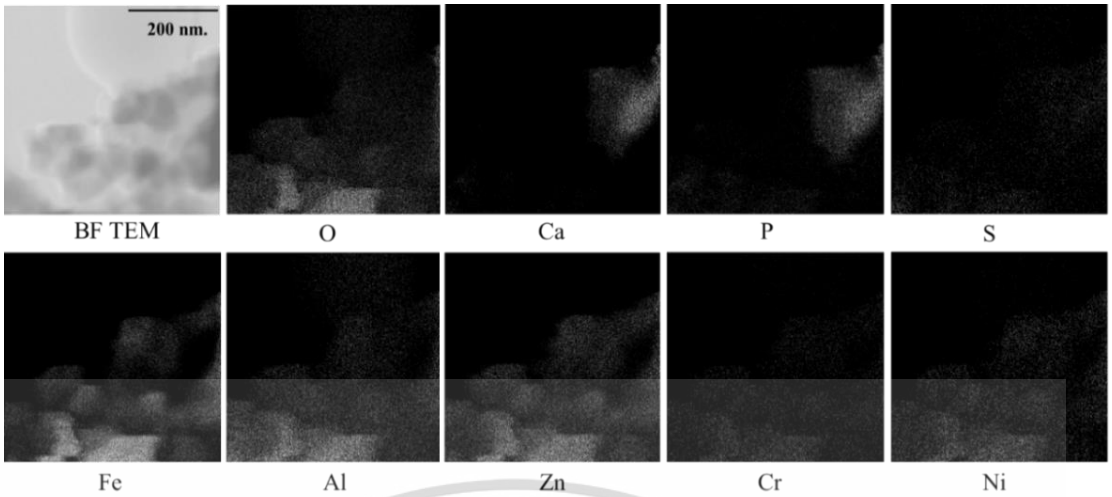

Figure 4.20 Bright field TEM image (Top-left) and EDS elemental distribution mappings.

To investigate more on how ash elements distributed on soot particles, 10-15 images were surveying and revealed some interesting result as shown in figure 4.21. In this observation area, elements of O, Ca, P, S were found in greater amounts and each component detected at nearly the same location. Cr and Ni were widely distributed but not highly concentrated while Fe, Al and Zn were local concentrated. This result appears to contradict the one previously carried out (figure 4.20). Therefore, ash distribution is considered as a non-homogenous because the signal intensity profiles, as well as concentration of each element are not the same and varied depend on the location.

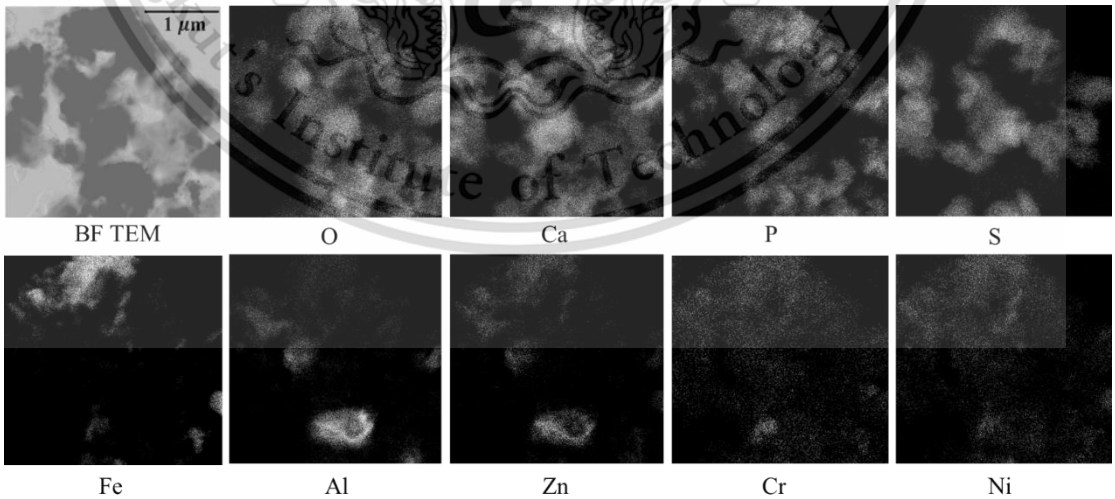

Figure 4.21 Bright field TEM image (Top-left) and EDS elemental distribution mappings in which O, Ca, P, S are dominant.

4.4.5 Analysis of diesel fuels and lubricating oil properties

The results of elemental contained in diesel fuels and lubricating oils are shown below.

4.4.5.1 Elemental compositions in diesel fuels

Table 4.2 Elemental compositions in diesel fuels

Elements (PPM)	Diesel	Diesel B10	Diesel B20	Premium Diesel
Lead	0	0.1	0	0
Tin	0.1	0.1	0	0
Aluminum	0.3	0.4	0.2	0.4
Silicon	0.2	0.2	0.2	0.3
Boron	1	0	0	0
Calcium	9	0	19	0
Phosphorus	2	1	2	4
Zinc	1	0	3	0

Table 4.2 presents properties and elemental compositions in four different types of diesel fuels in a unit of PPM. Aluminum and silicon are found in all kind of diesel fuels, while lead only presents in diesel B10. On the other hand, Tin can be found on both diesel and diesel B10. Since these elements contained in diesel fuels are in the unit of ppm and differences number of elements are less than 0.2 ppm, therefore, the constitution of these elements are negligibly small. There are no significant different of elements contained among these fuels.

Among additive elements such as Boron, Calcium, Phosphorus and Zinc, Calcium shows the highest element contained in Diesel B20. Diesel fuel contained about 9 ppm of elemental calcium. However, the amount of calcium is significantly increased to 19 ppm, in the case of diesel B20. This sharp increase of calcium might be a result of detergent additives that added from the oil refinery process. Although fuel samples were obtained from one gas station, stored fuel may derive from different oil refinery plant. In addition, the preparation of diesel B20 from diesel B100 might not be the cause of this jump of calcium since B100 is fatty acid which has alcohol as the main component.

4.4.5.2 Elemental compositions in diesel fuels

Table 4.3 elemental compositions of new and used MAZDA lubricating oils.

		New oil	Used oil			
			Sample 1	Sample 2	Sample 3	Sample 4
Wear element (PPM)	Iron	0	26.7	44.5	103.4	49.8
	Chromium	0.2	1.1	2.7	2.9	2.8
	Copper	0.4	3.6	3.7	6.3	34.5
	Tin	1.7	1.5	2.3	2.5	2.9
	Aluminum	0.9	4.6	19.8	7.2	8.1
	Nickel	0	3.1	0.6	0.4	0.6
	Silver	1	0.7	0.5	0.4	1.1
	Titanium	0	5.1	0	0	0
	Silicon	0.9	12.3	18.5	55	83.7
Additive Element (PPM)	Boron	191	138	31	26	188
	Magnesium	5	7	5	4	6
	Molybdenum	541.7	446.8	446.1	414.9	535.3
	Calcium	1035	1020	805	764	1447
	Barium	0	0	0	0	15
	Phosphorus	468	445	334	321	663
	Zinc	549	485	404	410	720

Table 4.3 presents wear element and additive element (ppm) contained in MAZDA lubricating oils. Since the collected data on table 4.3 were only based on 10,000 kilometres engine oil service life and there is no information related to the total mileage and engine conditions of tested vehicles, therefore, a comparison of the new and used oils will only be subjected to this discussion. Wear elements of used engine oil such as iron, chromium, copper, aluminium and nickel show some significant increase from the new one. Iron shows the highest elements contained in used oil, the increasing is up to 103.4 times (sample 3) compare with the new oil. Elements of copper and aluminium are the second and the third highest with the amount of 34.5

ppm (sample 4) and 19.8 ppm (sample 2), respectively. This result is compliance with previous XRF components analysis of ash powder (section 4.4.2) which also show that Fe is the main constituent of the deposited ash in DPF. It is well-known that engine block generally made of cast iron and aluminium, in addition, copper also found as the main components for head gasket in some engine. Therefore, these wear components are results from abrasion products of engine wear formed during movement of pistons and blended in lubricating oil, as discussed in previous TEM imaging section 4.4.4. Si also contaminated at higher amount in used oil than in the new oil. It is expected that Si may come from the atmospheric dust and the amount of this element is varied depend on vehicle conditions. For additive elements, it can be clarified that element such as Boron, Magnesium, Molybdenum, Calcium, Phosphorus, and Zinc are additives used in this lubricating oil. In addition, Calcium, Phosphorus, and Zinc are found in greater amount among additive Element, as well as other wear elements. The presents of these additive elements in used oil also correspond to a previous elemental analysis of ash powder. Therefore, it can be confirmed that most of ash found in a DPF originates from lubricant additives.

4.5 OXIDATION BEHAVIOR AND CHARACTERIZATION OF PMs

As discussed in previous section, a contamination of ash particle from lubricating oil can alter the physical properties of deposited PMs. In this section, the effect of ash particles on chemical properties of PM was further analyzed using thermogravimetric analysis (TGA).

4.5.1. Thermogravimetric analysis (TGA) results

Figure 4.22 A presents a normalized TGA results at 575, 600, 625℃ of two different samples: the first is soot mix with SiC (smooth line). The latter is soot mix with SiC and ash (dotted line). The vertical axis presents mass (%), while the horizontal axis presents time (sec.). The mass (%) was directly converted to mass reduction rate versus time (sec.) as shown in figure 4.22 B. In a preheating process with pure nitrogen, mass losses were observed as they were gradually decreased with the same slope and reached about 90% mass in all samples. This early mass loss is due to several reasons such as water evaporation, oxidation of soft components (VOC, SOF, HC) at low temperature (300-350℃), and some partial oxidation of carbon from decorated oxygen atoms at high temperature (550℃). During the oxidation process, the differences of mass loss can be clearly observed as PM included ash particles exhibited higher mass loss compare with PM sample without ash at the same temperature. The 625℃ oxidation temperature show the highest decreasing following with 600℃ and 575℃, respectively.

In addition, a mass reduction rate of sample contained ash increased up to about five times higher than sample without ash just after an introduction of atmospheric air for oxidation (at 1500 sec). As a result, an oxidation of soot, SiC mix with ash was completed earlier than sample contained only soot and SiC. The oxide of ash particles which are in the form such as oxides (-O), sulfates ($-SO_4$), and phosphates ($-PO_4$) may perform as the additional source of oxygen that promote soot oxidation.

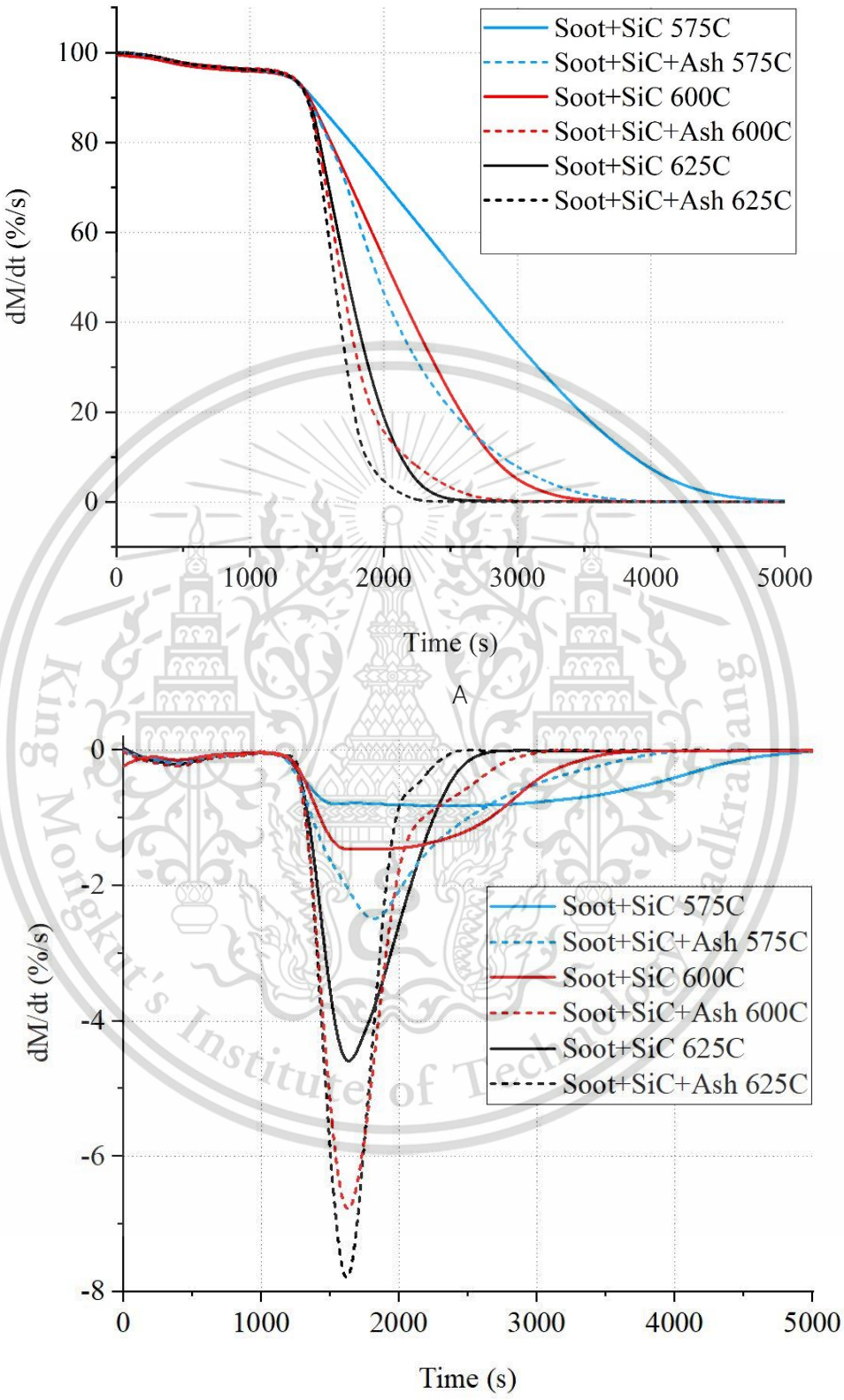

Figure 4.22 a normalized TGA results at 575, 600, 625℃ (A), mass loss rate versus time in sec. (B)

4.5.2. Evaluation of reaction rate.

From the previous TGA results, it can be clarified that ash shows some catalyst effect that help promote soot oxidation. However, some quantitative analysis is needed to explain this catalyst effect whether it come from the chemical impact which is related to the reduction of activation energy or physical impact that mainly about the increasing of collision frequency contact with oxygen. In order to find out which parameters are dominant, a comparison of activation energies between PM sample contained ash (Soot + SiC + Ash) and sample without ash (Soot + SiC) using Arrhenius expression was conducted. The particulate matters were assumed to be reacted with oxygen and produced products of CO and CO_2 as follows:

$$\text{Particulate matters} + O_2 \rightarrow CO_2 + CO$$

The production rate of CO and CO_2 can be described as follows:

$$-\frac{d[C]}{dt} = k[C]^m[O_2]^n$$

$$-\frac{d[C]}{dt} = A \cdot \exp^{-\frac{Ea}{RT}} \cdot [C]^m[O_2]^n$$

$$\ln\left[-\frac{d[C]}{dt}\right] = -\frac{Ea}{RT} + \ln A + m\ln[C] + n\ln[O_2]$$

$$\ln\left[-\frac{1}{[C]^m}\frac{d[c]}{dt}\right] = -\frac{Ea}{RT} + \ln A + n\ln[O_2] \ldots\ldots\ldots\ldots \quad 1$$

Where; C is mass of Carbon black (CBN330), A is the pre-exponential factor, E_a is the activation energy $\left(\frac{kJ}{mol}\right)$, R is the value of ideal gas constant in 8.314$\left(\frac{J}{mol\ K}\right)$, m and n are the reaction order. Generally, soot particles are assumed to be spherical shape with the reaction order (m) equal to 2/3 follow a shrinking core model. However, the reaction order (m) also depends on physical structure of soot, ash, as well as oxidation conditions of a PMs. Therefore, the rection order (m) of sample contained ash (Soot + SiC + Ash) and sample without ash (Soot + SiC) were calculated specifically as equal to 0.41 and 0.40, respectively.

The first terms of equation 1 represents reaction rate. The second term, third together with fourth terms represent chemical impact and physical impact, respectively.

By making a comparison of equation 1 with the linear equation

$$y = ax + b$$

The activation energy (E_a) can be obtained from

$$Slope = a = -\frac{Ea}{R}$$

Three differences points on the mass loss curves at 40, 50 and 60 mass (%), obtain from figure 4.22 A were collected and substituted into equation 1. The Arrhenius plots were obtained for both samples as show in the following figures:

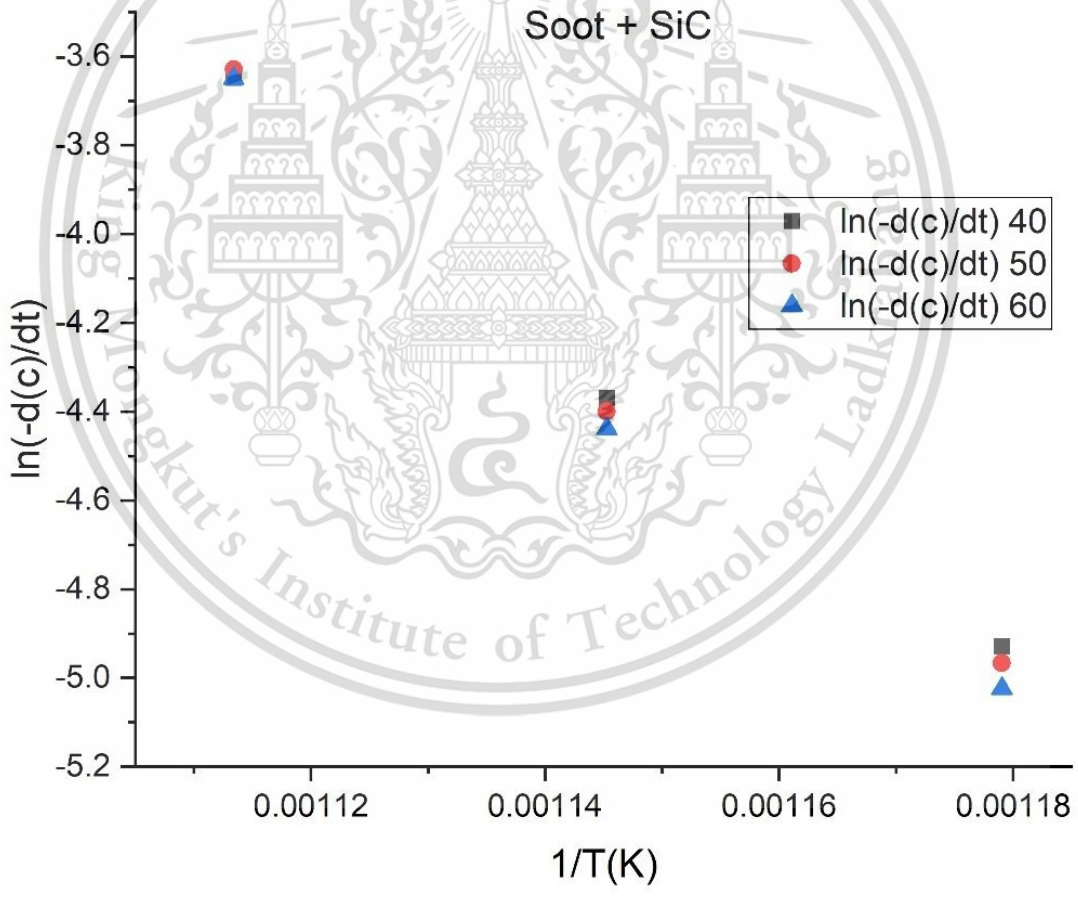

A

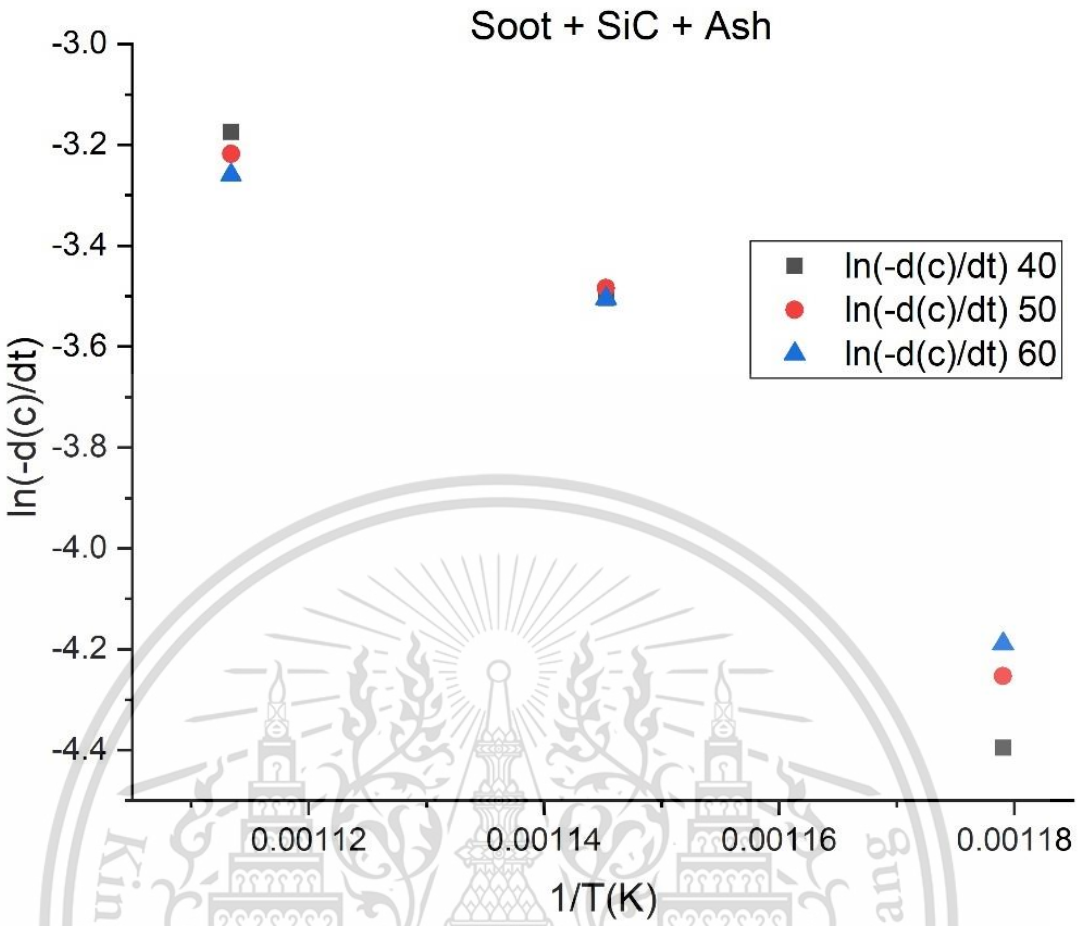

B

Figure 4.23 the Arrhenius plot at mass percentage of 40, 50 and 60% for the Soot + SiC (A) and Soot + SiC + Ash (B).

Figure 4.23 (A) and (B) presents the Arrhenius plot used to obtain the characteristics of overall activation energy at mass percentage of 40, 50 and 60% for Soot + SiC and Soot + SiC + Ash, respectively. The vertical axis represents reaction rate (ln(-d(c))/dt) and horizontal axis presents inverse of temperature (1/T(k)). There are differences of data distribution patterns between these two samples. Each set of data (consists of three points) in soot with SiC (figure 4.23A) tends to concentrated in one point, while data distribution is more widely spread in Soot + SiC + Ash (figure 4.23B). As a result, it can be predicted that the overall activation energy of sample contained ash particles at 40, 50 and 60% mass may be slightly different.

Since the overall activation energy (E_a) can be obtained from a slope of equation 1, the activation energy and logarithm of frequency factor can be obtained as shown in table 4.4.

Table 4.4 presents activation energy and frequency factor of both PM samples at 40, 50 and 60% mass.

Mass (%)	Soot + SiC		Soot + SiC + Ash	
	E_a (kJ/mol)	InA	E_a (kJ/mol)	InA
40	162.16	18.00	154.62	17.71
50	169.33	18.97	131.11	14.50
60	173.99	19.57	117.74	12.65
Average	168.49	20.49	134.49	16.64

From table 4.4, the activation energy at 40% mass of sample contained soot, SiC and ash was slightly less (about 8 kJ/mol) than sample contained only soot and SiC. In addition , a difference of activation energy between two samples at 50% and 60% mass were continuing to increase as the oxidation process proceeded. A study on Experimental and Modelling Study of Catalytic Diesel Soot Oxidation [31] suggested that a global activation energies for soot oxidation with O_2 are in the range of 140 to 170 kJ/mol. As a result, the results of activation energies in this study are comparable with others. The logarithm frequency factor (In A) terms also show the same trend as there were reduced when ash included. It can be concluded that ash particles have a chemical impact which is a reduction of the activation energy on soot oxidation since the average of over all activation energy of samples contained ash were less than sample without ash particles. On the other hand, ash particles had a negative effect on physical impact. This is due to the non-catalytic ash particles that may impede the reactive surfaces of soot that usually exposed to the oxygen. The reduction of activation energy, in a case of Soot + SiC + Ash, shows such a contradict to the previous result investigated by authors, as discussed in literature review section. One reason may come from the differences in ash generation method. Ash generated by the oil burner may experience lower internal combustion pressure, as well as some temperature differences inside the burner pipelines compare to the actual engine combustion chamber. These differences might effect the formation, and properties of deposited ash. Another important reason is the difference of injected oil elements. Ash generated from the oil burner contains only Ca, P, S, Zn elements, while lubricating oil-derived ash included also wear and additive elements such as Fe, Cr, Cu, Ni, Mo, etc.

To further investigate the effect of ash on soot oxidation, a comparison of arrhenius plot between Soot + SiC and Soot + SiC + Ash at the same mass precentage was made as shown in figures 4.24 (A, B, C).

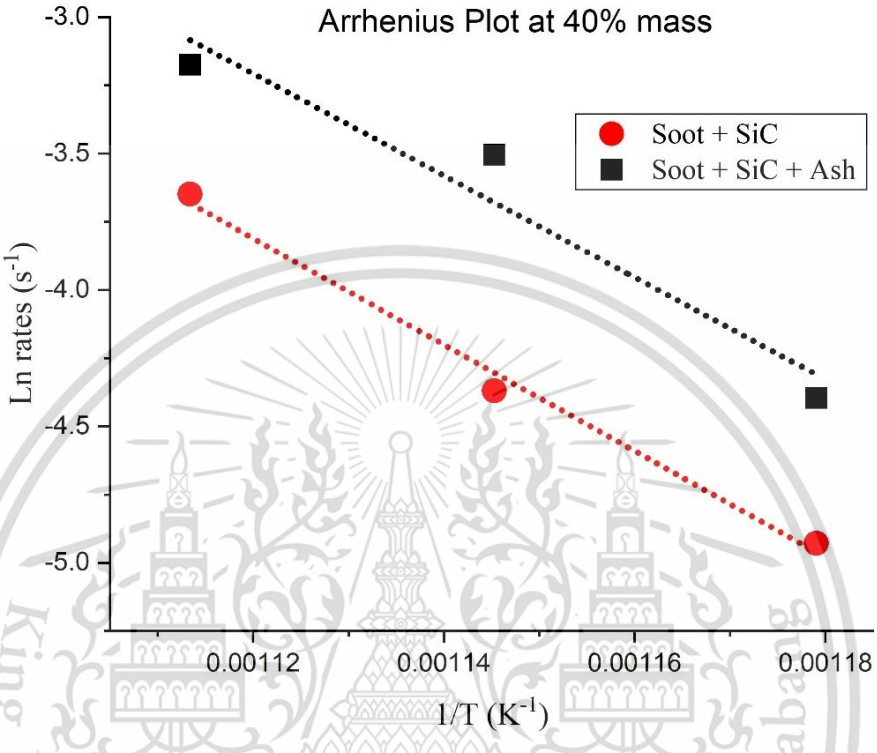

A

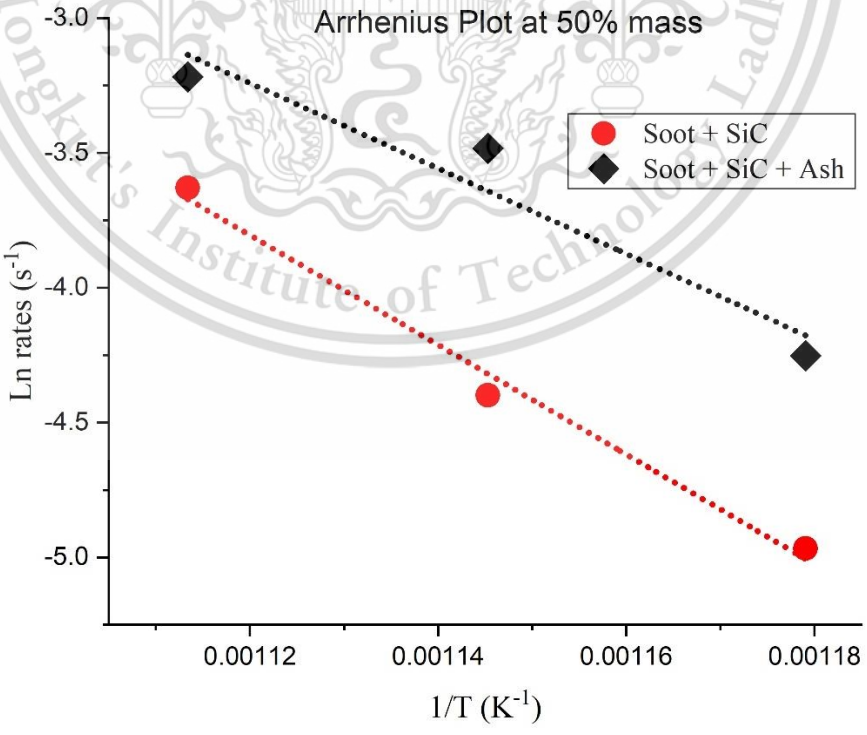

B

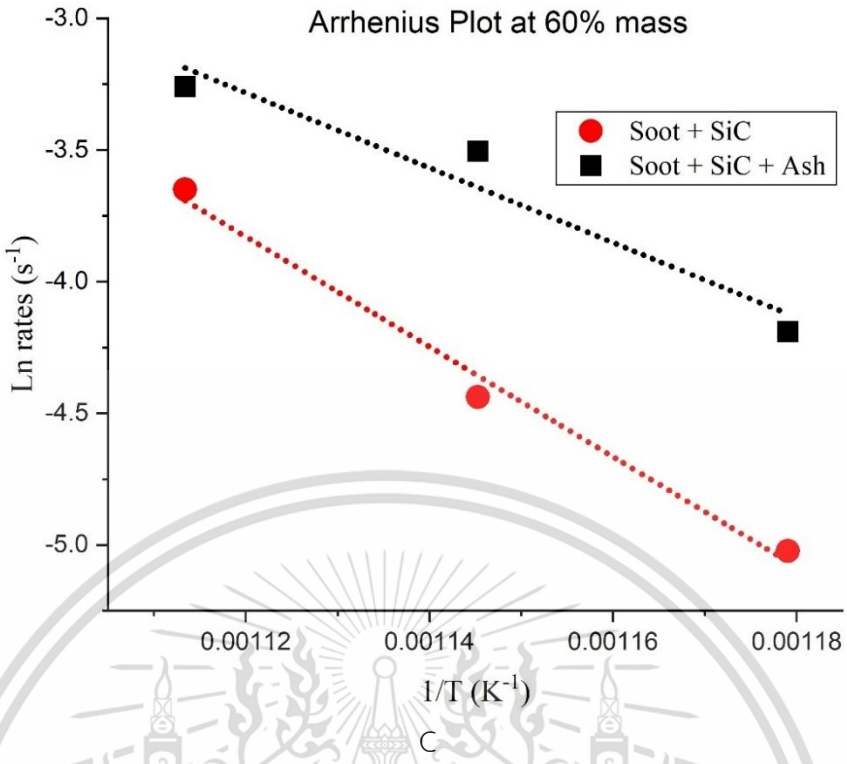

C

Figure 4.24 the arrhenius plot of PM samples at 40% (A), 50% (B) and 60% (C) mass.

Figure 4.24 presents a comparison of arrhenius plot between soot and soot with ash at 40% (A), 50% (B) and 60% (C) mass. The trendlines, depicted by red and black dotted line, were added for an easier interpretation. It can be clearly observed that slope of soot with SiC (depicted by red dotted lines), and soot, SiC with ash (depicted by black dotted lines) were different corresponding to a variation of activation energy, as shown in table 4.4. However, the interested plot area in this experiment are only focusing on three points temperature (575 ℃, 600 ℃, 625 ℃) which this range is quite narrow and far from the origin point. As a result, plot of Soot + SiC+ Ash is higher than Soot + SiC. If these two plots were observed at x=0, the y-interception of Soot + SiC (red dotted line) will be higher than Soot + SiC+ Ash (black dotted line) in all three mass conditions. This indicated that ash has a negative effect on physical impact as already discussed in previous section.

4.5.3. Mechanisms of oxidation enhancement by ash particles

From previous XRF and XRD analysis results of ash particles, it was clarified that Fe is the main constituent of ash element and it was mainly presented in the form of Fe_2O_3, also $Cu_{0.5}Zn_{0.5}Cr_{1.1}Fe_{0.9}O_4$. The mechanisms of the catalytic soot oxidation by Fe_2O_3 can be explained using schematic diagram figure 4.25. During the PM oxidation process, oxygen is transferred from the catalyst surface to the soot by both bulk lattice and surface mechanisms. The resulting of oxygen vacancies on the catalyst surface are refilled either by surface migration or re-oxidation from gas-phase oxygen, and diffusing of bulk lattice oxygen. The oxygen deficiency of the lattice is balanced by migration of oxygen from the surface or sub-surface to the bulk of the catalyst. Since there is a replacement and rearrangement of oxygen ions, this mechanism is considered as the chemical impact of Fe_2O_3 catalysts on soot oxidation. This chemical impact is in compliance with the reduction of activation energy in Soot + SiC +Ash sample, as discussed in section 4.5.2.

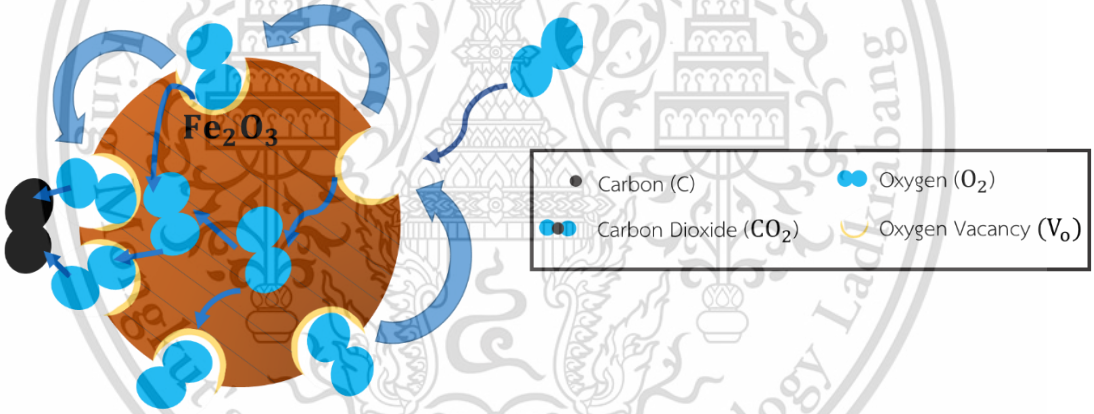

Figure 4.25 Mechanisms of Fe_2O_3 catalysts as a chemical impact on soot oxidation

For $CaSO_4$ and other ash components, previous experiment conducted in Tokyo tech already confirmed that components of Ca, P, S, and Zn don't have chemical impact which is a reduction of activation energy on soot oxidation. However, only physical impact related to an additional O_2 desorbed from the surface of ash particles play an important role in oxidation enhancement. In a combustion process, an unstable oxygen (O_{ad}) is adsorbed on the surface of ash particles, then they were deposited inside the DPF. During regeneration process, this oxygen desorbed form the surface of ash and supply to enhance the reaction rate, in addition to the oxygen from working gas.

CHAPTER 5

CONCLUSIONS AND DISCUSSION

5.1 Macro/micro scale analysis of deposited ash in DPF

The actual DPFs acquired from a diesel passenger car was disassembled for an investigation of macro/microscale analysis of metal oxide ashes. The macroscale analysis results found that ash entirely filled up the end plug of channels, and much amounts of ash were deposited at the filter periphery with the maximum length of 21 mm. due to the unique design of DPF inlet pipeline. The XRF microscale analysis revealed that Fe is the main component of deposited ash on the SiC non-coated DPF, while XRD analysis confirmed the presence of $Cu_{0.5}Zn_{0.5}Cr_{1.1}Fe_{0.9}O_4$, $Ca(SO_4)$, Fe_2O_3 and $Ca_{19}Cu_2(PO_4)_{14}$. The TEM results confirmed that the agglomerated ashes are mostly round and consist chemically of Fe, O, Zn, Al, Ni, Cr, S and minor Ca and P in form of sulfates, phosphates and oxides. It was clarified that majority of ash components found within DPFs samples are oxides of Fe, Al, Zn and minor Cr, Ni. These components originated from engine wear metal, exhaust corrosion products, as well as lubricant additives.

In the Analysis of diesel fuels and lubricating oil properties, diesel fuels show less influence on deposited ash in DPF since elements were found only in small amount. On the other hand, wear elements from used engine oil such as iron, chromium, copper, aluminum and nickel show some significant increase from the new oil. Fe shows the highest elements contained in used oil corresponding with previous XRF ash components analysis, and the increasing is up to 103.4 times compare with the new engine oil.

5.2 Influence of metal oxide ash on soot oxidation

Two different type of PMs samples: carbon black (CBN330) mixed with SiC and carbon black (CBN330) mixed with SiC and ash, were investigated their oxidation behaviors utilizing TGA. The PMs sample which contained ash exhibited higher oxidation rate up to four times high compare with sample without ash. This is due to the catalytic effect of ash particles, especially Fe_2O_3, in which a diffusing of bulk lattice and surface mechanisms of oxygen (chemical impact) plays an important role on soot oxidation enhancement. This catalyst effect can be described by a reduction of activation energy (E_a) in Arrhenius expression.

REFERENCES

[1] Plotkin, S. and Ribeiro, S. K. Energy Efficiency Technologies for Road Vehicles 2009; 2:125-137

[2] Heywood, J. B. Internal Combustion Engine Fundamentals. McGraw-Hill. Singapore; 1988.

[3] Bagi, S., R. Bowker, and R. Andrew. 2016. Understanding chemical composition and phase transitions of ash from field returned DPF units and their correlation with filter operating conditions. SAE International Journal of Fuels and Lubricants 9:239–59. doi:10.4271/2016-01-0898.

[4] Gao, J., C. Ma, S. Xing, L. Sun, and L. Huang. 2018. A review of fundamental factors affecting diesel pm oxidation behaviors. Science China-Technological Sciences 61:330–45. doi:10.1007/s11431-016-9117-x.

[5] P. Karin,: "Microscopic Visualization and Characterization of Particulate Matter Trapping and Oxidation in Diesel Particulate Filters and Membrane Filters", Doctoral thesis, Tokyo Institute of Technology, 2010

[6] Viswanathan, S., Rakovec, N., and Foster, D. ： Microscale Study of Ash Accumulation Process in DPF Walls Using the Diesel Exhaust Filtration Analysis (DEFA) System, ASME, ICEF 2012-92104, (2012)

[7] Sappok, A., Wang, Y. et al. ： Theoretical and Experimental Analysis of Ash Accumulation and Mobility in Ceramic Exhaust Particulate Filters and Potential for Improved Ash Management, SAE Technical paper, 2014-01-1517, (2014)

[8] Sappok, A. ： The Nature of Lubricant-Derived Ash-Related Emissions and Their Impact on Diesel Aftertreatment System Performance, PhD Thesis, Massachusetts Institute of Technology, 2009.

[9] W.A. Majewski and M.K. Khair, Diesel Emissions and Their Control, SAE Order No.R-303, SAE International, 2006.

[10] Leslie, R. Rudnick : Lubricant Additives: Chemistry and Applications, Third edition, Taylor & Francis, (2017)

[11] P, Tornehed. And U, Olofsson : Lubricant ash particles in diesel engine exhaust, Journal of automobile engineering, Vol.225 Part D, (2011)

[12] M.M. Maricq, Review Chemical Characterization of particulate emissions from diesel engine: A review, Journal of Aerosol Science, Vol.38, pp.1079-1118,2007.

[13] Eastwood, P. (2008). Particle Emission from vehicles. John Wiley & Sons, Ltd, England.

[14] Dec, J. (1997). A Conceptual Model of DI Diesel Combustion Based on Laser-Sheet Imaging. SAE Technical Paper 970873.

[15] Sappok, A.: "Ash Accumulation in Diesel Particulate Filters, "Revision 2013.01, DieselNet. https://dieselnet.com/tech/dpf_ash.php.

[16] Aravelli K., Heibel, A., "Improved Lifetime Pressure Drop Management for Robust Cordierite (RC) Filters with Asymmetric Cell Technology (ACT)," SAE 2007-01-0920, 2007.

[17] Mc Geehan, J., "API CJ-4: Diesel Oil Category for Both Legacy Engines and Low Emission Engines Using Diesel Particulate Filters", SAE 2006-01-3439, 2006.

[18] Murray, T. : The Effect of Lubricant Derived Ash on the Catalytic Activity of Diesel Particulate Filters, Master Thesis, Massachusetts Institute of Technology, 2014.

[19] Kamp, C. J., et al., "Direct Measurements of Soot/Ash Affinity in the Diesel Particulate Filter by Atomic Force Microscopy and Implications for Ash Accumulation and DPF Degradation," SAE International 2014-01-1486, 2014.

[20] Sappok, A., and Wong, V., "Detailed Chemical and Physical Characterization of Ash Species in Diesel Exhaust Entering Aftertreatment Systems," SAE 2007-01-0318, 2007.

[21] Dittler, A. : Ash Transport in Diesel Particulate Filters, SAE Technical paper, 2012-01-1732, (2012)

[22] Ishizawa, T., H. Yamane, H. Satoh, K. Sekiguchi, M. Arai, N. Yoshimoto, and T. Inoue. 2009. Investigation into ash loading and its relationship to DPF regeneration method. SAE International Journal of Commercial Vehicles 2:164–75. doi:10.4271/2009-01-2882.

[23] Sappok, A., I. Govani, C. Kamp, Y. Wang, and V. Wong. 2013. In-situ optical analysis of ash formation and transport in diesel particulate filters during active and passive DPF regeneration processes. SAE International Journal of Fuels and Lubricants 6:336–49. doi:10.4271/2013-01-0519.

[24] MacKee, D. (1983). Mechanism of the Alkali Metal Catalyzed Gasification of Carbon, *Fuel*, 62, pp. 170–175.

[25] Junko, U., Akira, O., Tetsuya, N. Soot Oxidation in Particulate Filter Regeneration, Handbook of Advanced Methods and Processes in Oxidation Catalysis, pp. 25-50 (2014)

[26] Steffen Wagloehner, Sven Kureti,Study on the mechanism of the oxidation of soot on Fe2O3 catalyst, Applied Catalysis B: Environmental, Volume 125, 2012, Pages 158-165, ISSN 0926-3373,

[27] McKee, D. (1981). The Catalyzed Gasification Reactions of Carbon, *Abstracts of Papers of the American Chemical Society*, **181**, pp. 1–118.

[28] Huang, Junfeng., et al., Effect of Different Aging Conditions on the Soot Oxidation by Thermogravimetric Analysis, ACS Omega, Vol 5, number 47, pages 30568-30576,2020,

[29] Rodvanna, S., Srilomsak, M., Mitsuhiro, S., and Katsunori, H.: Scanning electron microscopic time-lapse visualization of ash movement during regeneration of Diesel Particulate Filters, International Journal of Automotive Engineering, Vol. 11, No.2(2020).

[30] Rodvanna, S., Srilomsak, M., Mitsuhiro S., and Katsunori H.: Time-lapse Visualization of agglomeration and growth of ash during regeneration of Diesel Particulate Filter, JSAE proceedings Number: 20195139 May, 2019 Issued No.29-19

[31] Kirsten Leistner. Experimental and Modelling Study of Catalytic Diesel Soot Oxidation. Chemical engineering. Université Pierre et Marie Curie - Paris VI, 2012. English. fftel-00858763

[32] Liati, A., P. Dimopoulos Eggenschwiler, E. Müller Gubler, D. Schreiber, and M. Aguirre. 2012a. Investigation of diesel ash particulate matter: A scanning electron

microscope and transmission electron microscope study. Atmospheric Environment 49:391–402. doi:10.1016/j.atmosenv.2011.10.035.

[33] Buhre, B.J.P., Hinkley, J.T., Gupta, R.P., Wall, T.F., Nelson, P.F., 2005. Submicron ash formation from coal combustion. Fuel 84, 1206e1214.

[34] Nemoto, S., Kishi, Y., Matsuura, K., Miura, M., Togawa, S., Ishikawa, T., Hashimoto, T., Yamazaki, T., 2004. Impact of Oil-derived Ash on Continuous Regeneration-type Diesel Particulate Filter- JCAPII Oil WG Report JCAPII Oil WG Report SAE Technical Paper 2004-01-1887.

APPENDIX A

EXPERIMENTAL ANALYSIS REPORTS

NCTC
NSTDA Characterization and Testing Service Center

Micro-EDXRF Analysis Report 8/17/2020

Prepared by: NSTDA Characterization and Testing Service Center

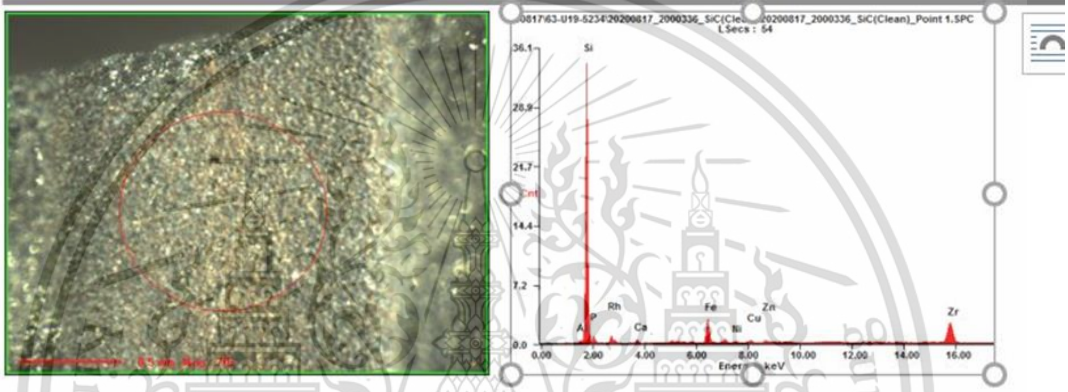

Element	*Wt%*	*At%*
Al	1.55	1.66
Si	87.66	90.40
P	5.94	5.56
Ca	1.14	0.82
Fe	1.68	0.87
Ni	0.08	0.04
Cu	0.10	0.05
Zn	0.09	0.04
Zr	1.75	0.56

A-1: XRF analysis of DPF material

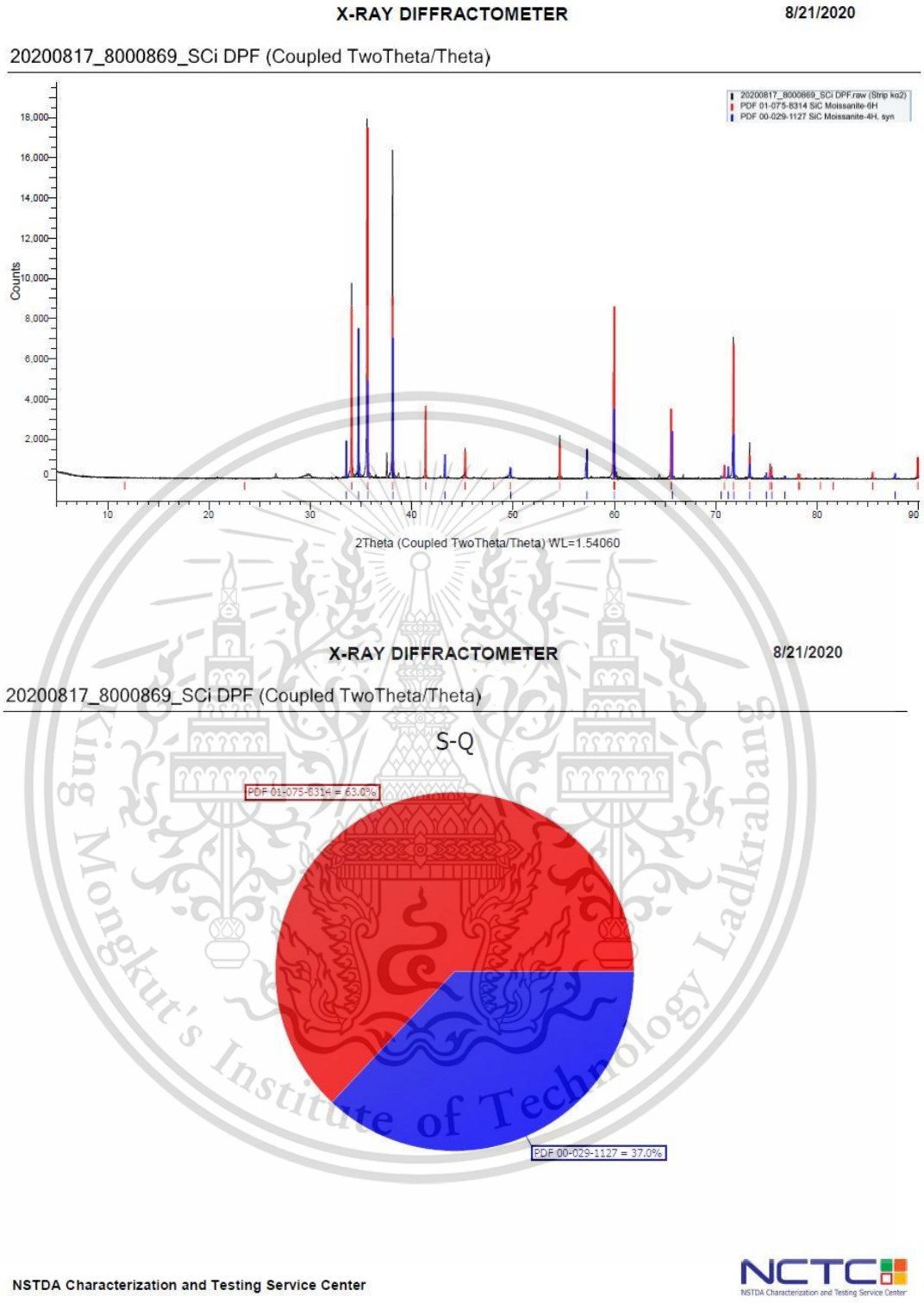

A-2: XRD analysis of DPF material

NCTC
NSTDA Characterization and Testing Service Center

Micro-EDXRF Analysis Report

8/7/2020

Prepared by: NSTDA Characterization and Testing Service Center

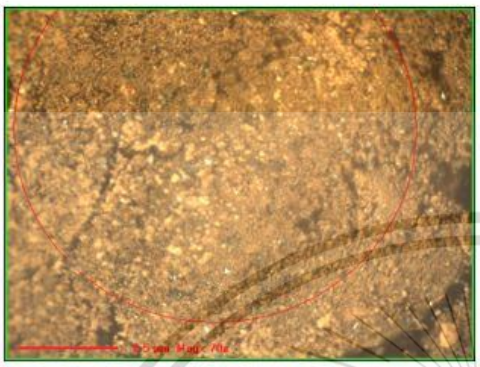

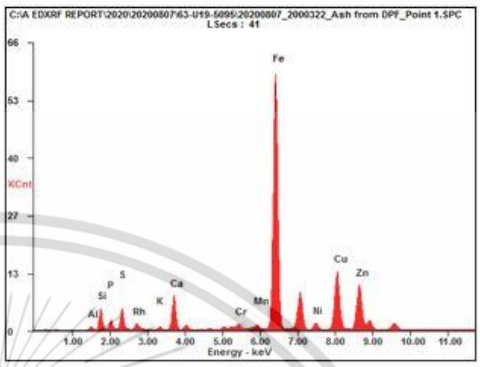

Element	Wt%	At%
Al	4.78	7.23
Si	16.18	23.51
P	7.92	10.44
S	9.16	11.66
K	1.17	1.22
Ca	10.88	11.08
Cr	0.71	0.56
Mn	0.41	0.31
Fe	30.88	22.57
Ni	0.99	0.69
Cu	9.47	6.09
Zn	7.46	4.66

A-3: XRF analysis of Ash

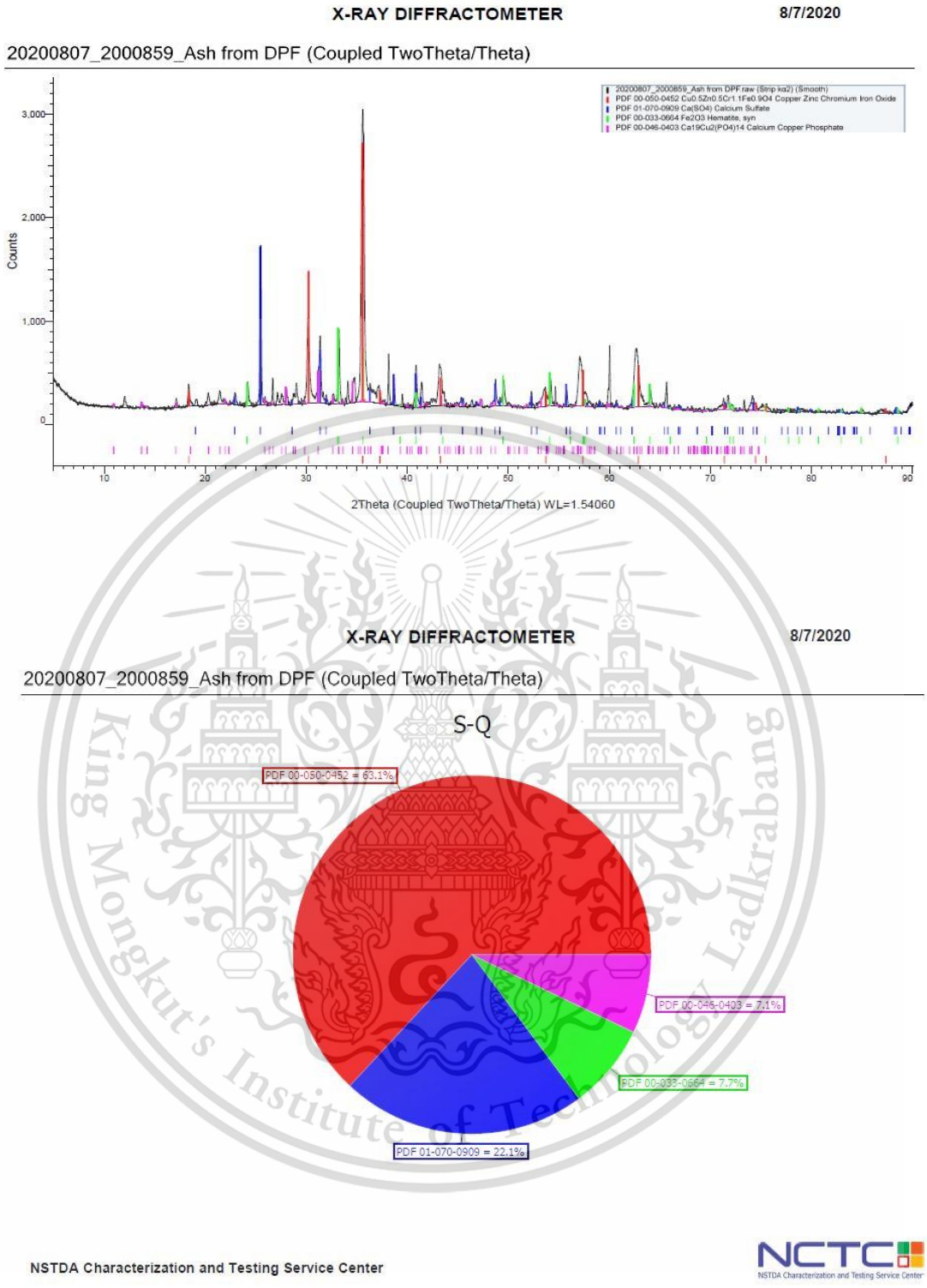

A-4: XRD analysis of Ash

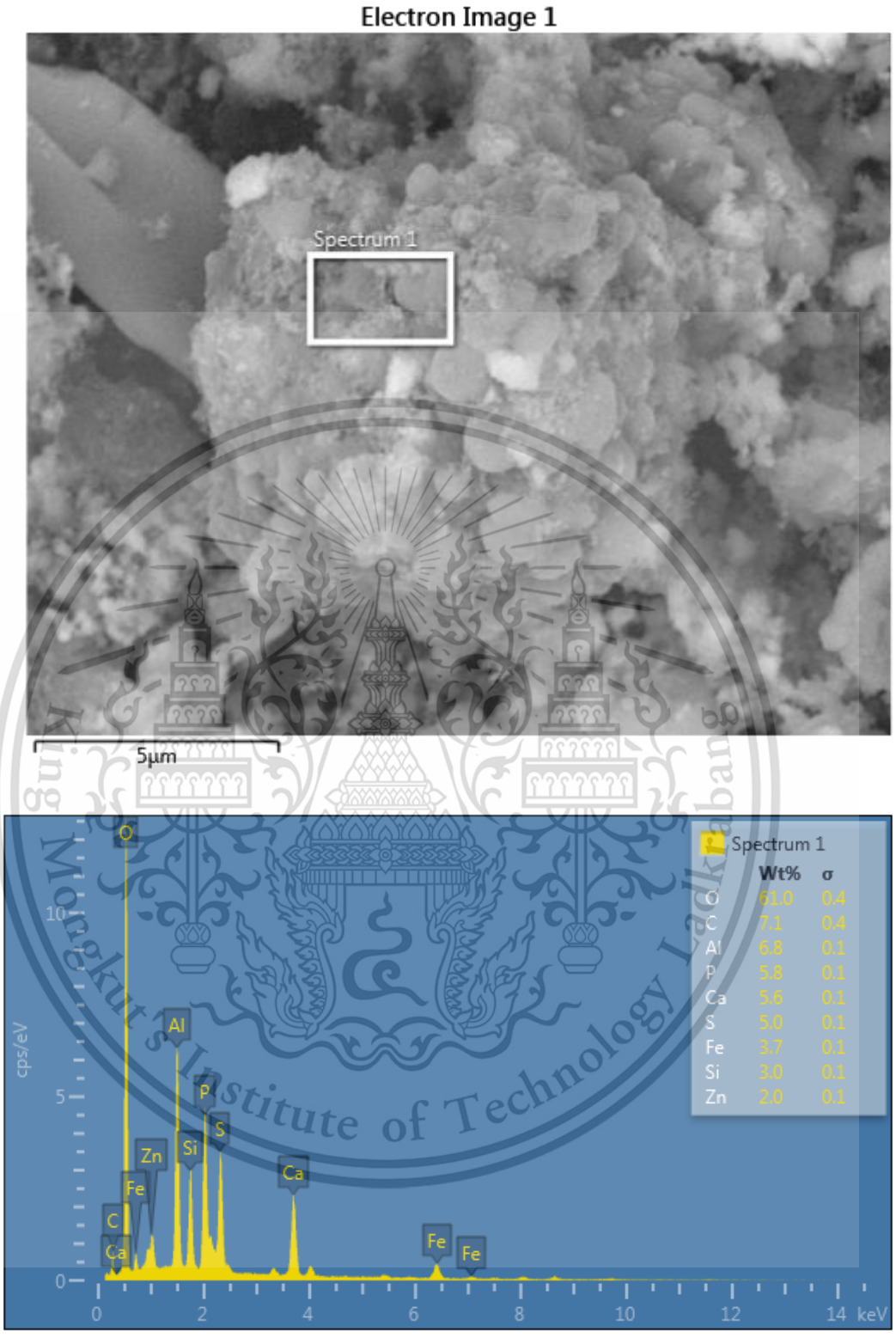

A-5: SEM and elemental analysis images of ash particle

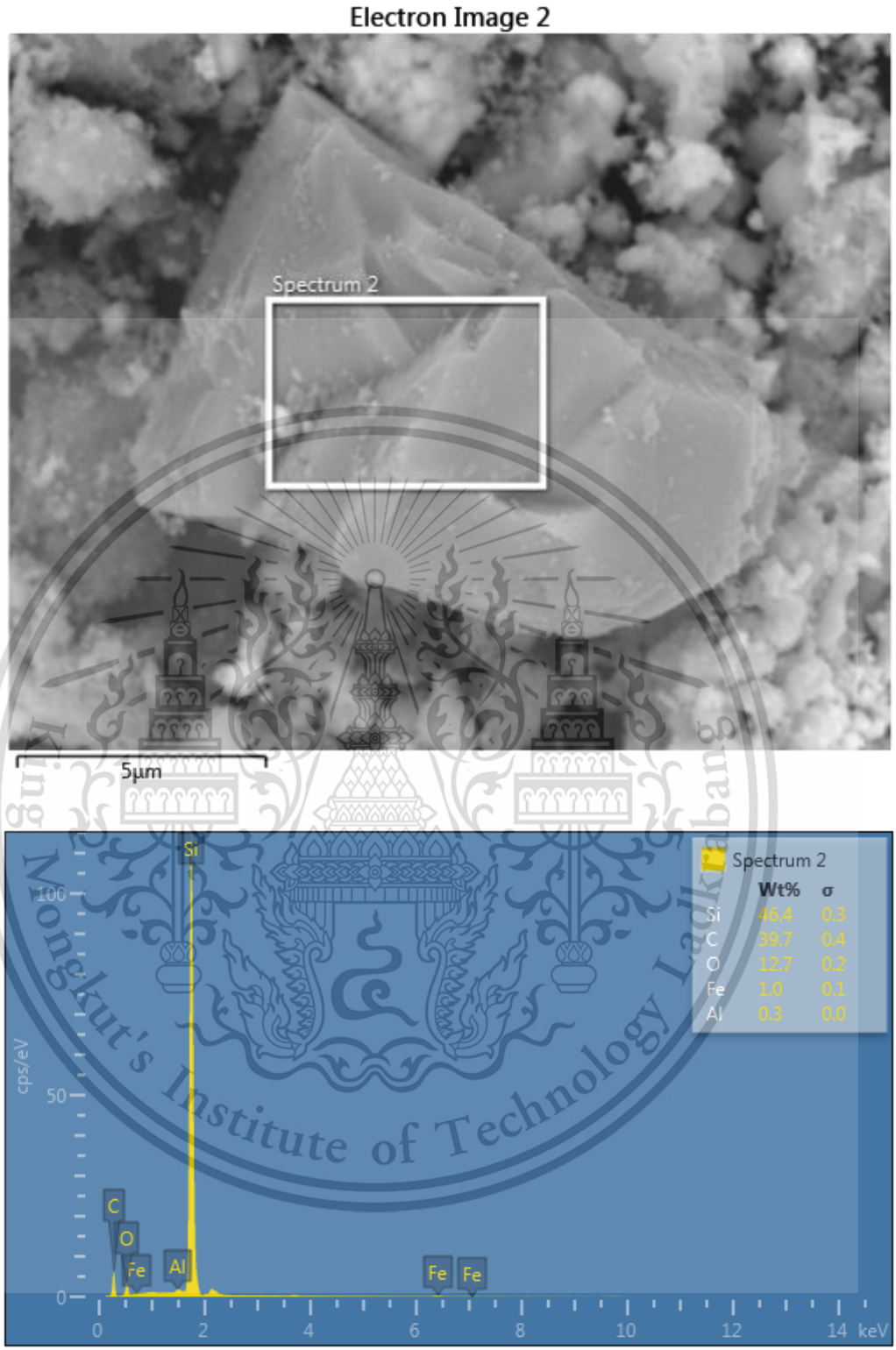

A-6: SEM and elemental analysis images SiC DPF materials

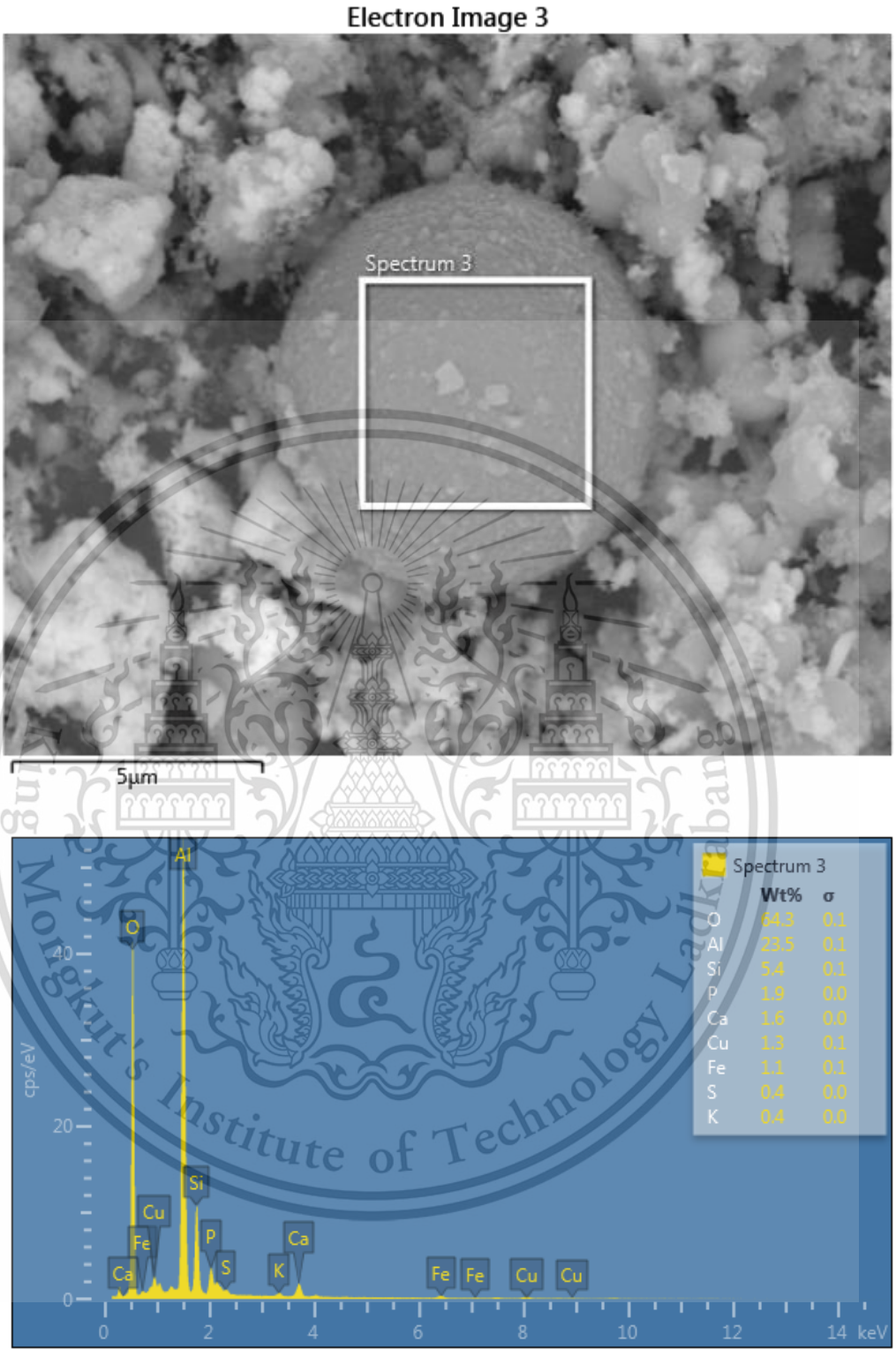

A-7: SEM and elemental analysis images Al-Si ash particle

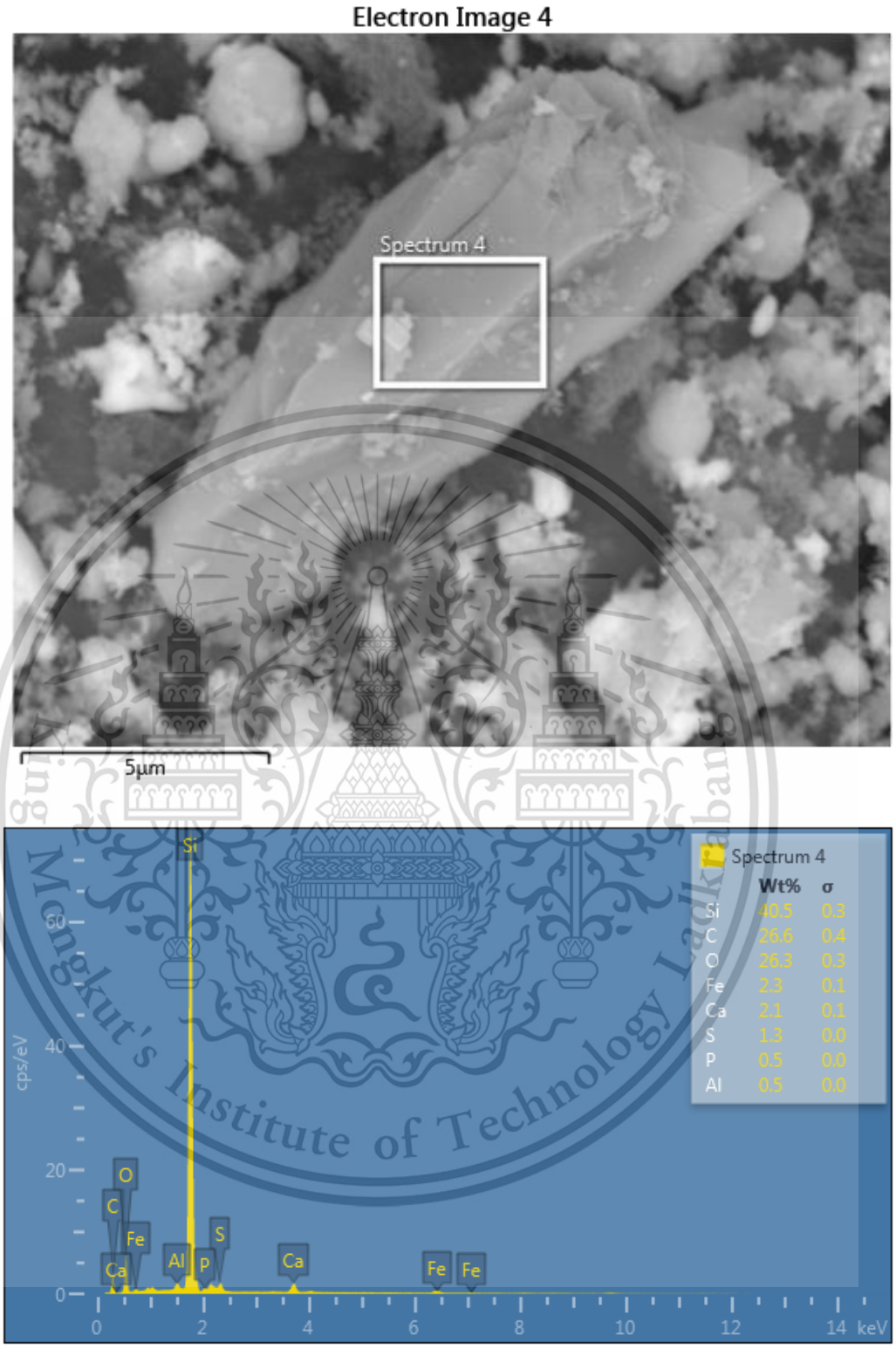

A-8: SEM and elemental analysis images SiC DPF materials

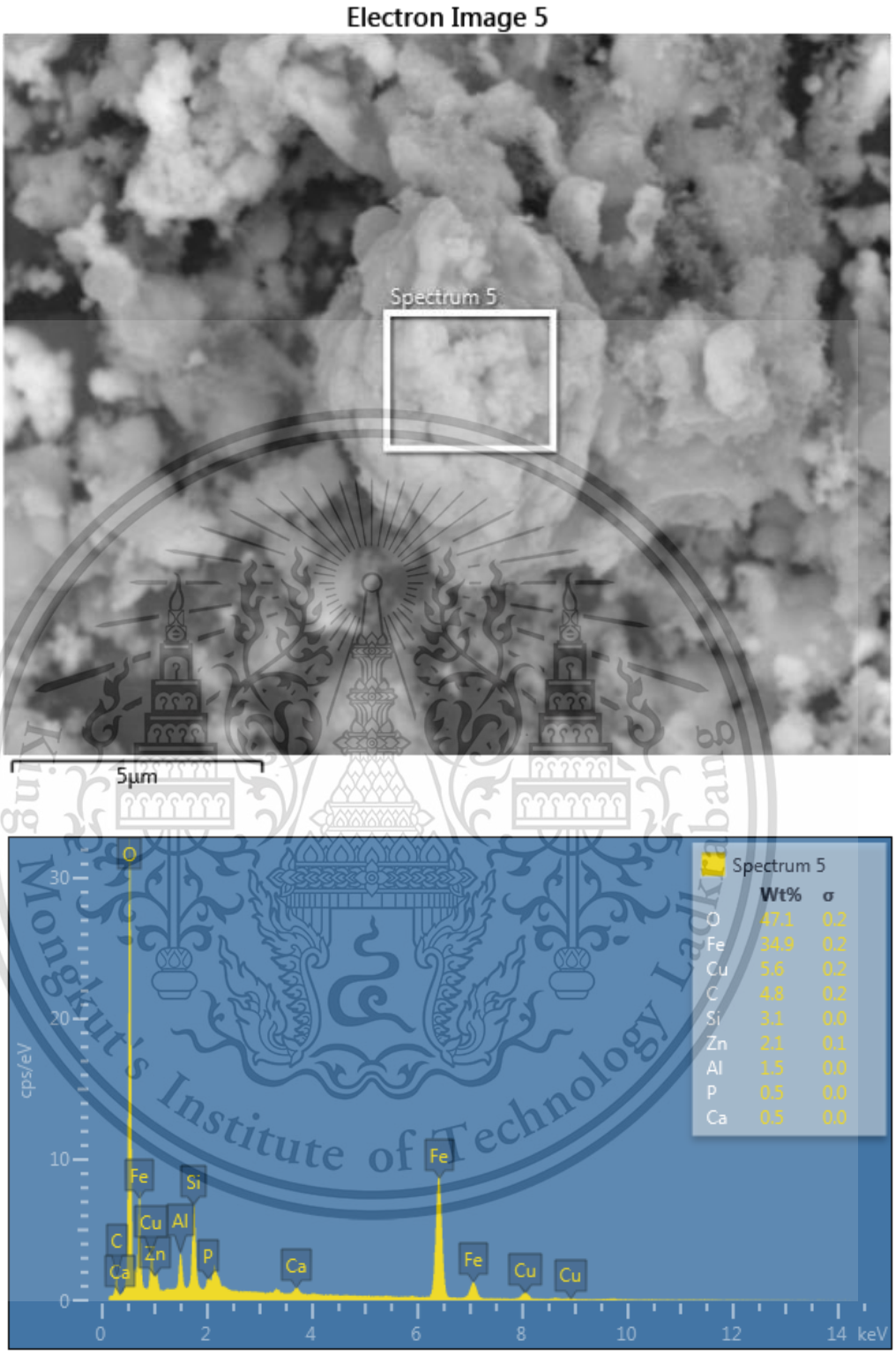

A-9: SEM and elemental analysis images oxide of Fe ash particle

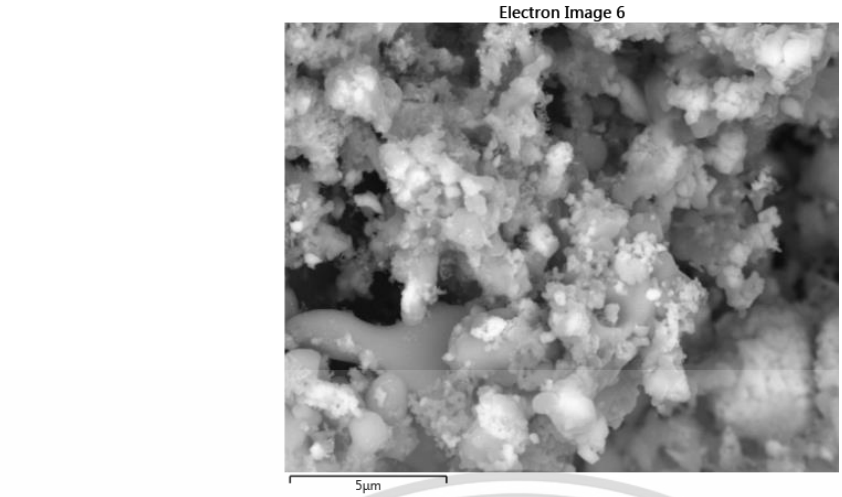

A

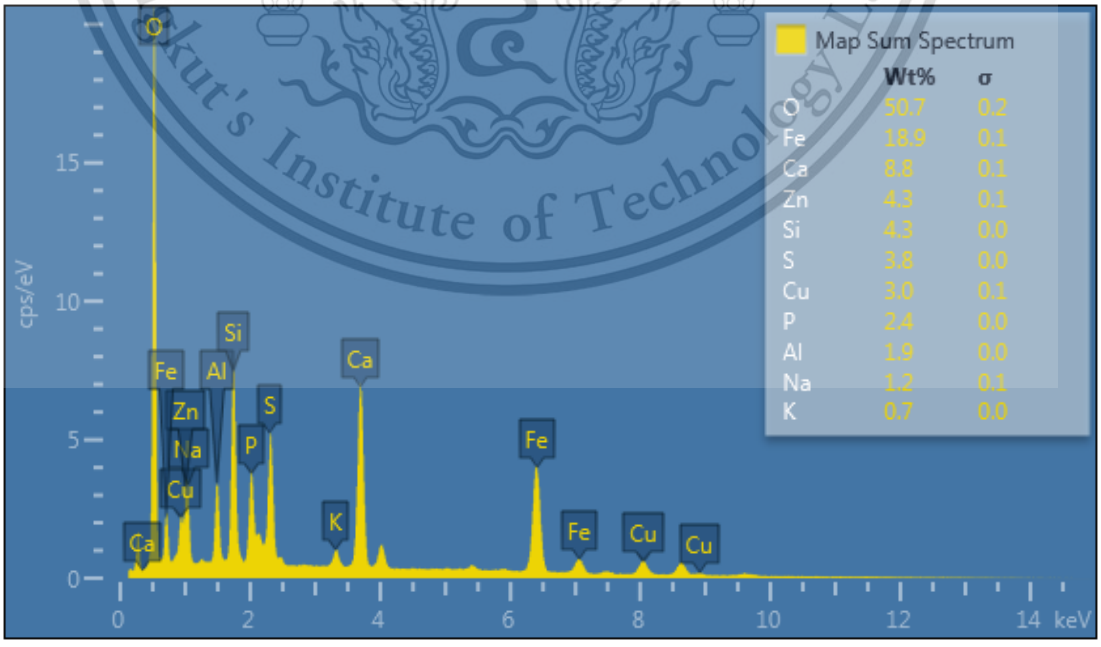

B

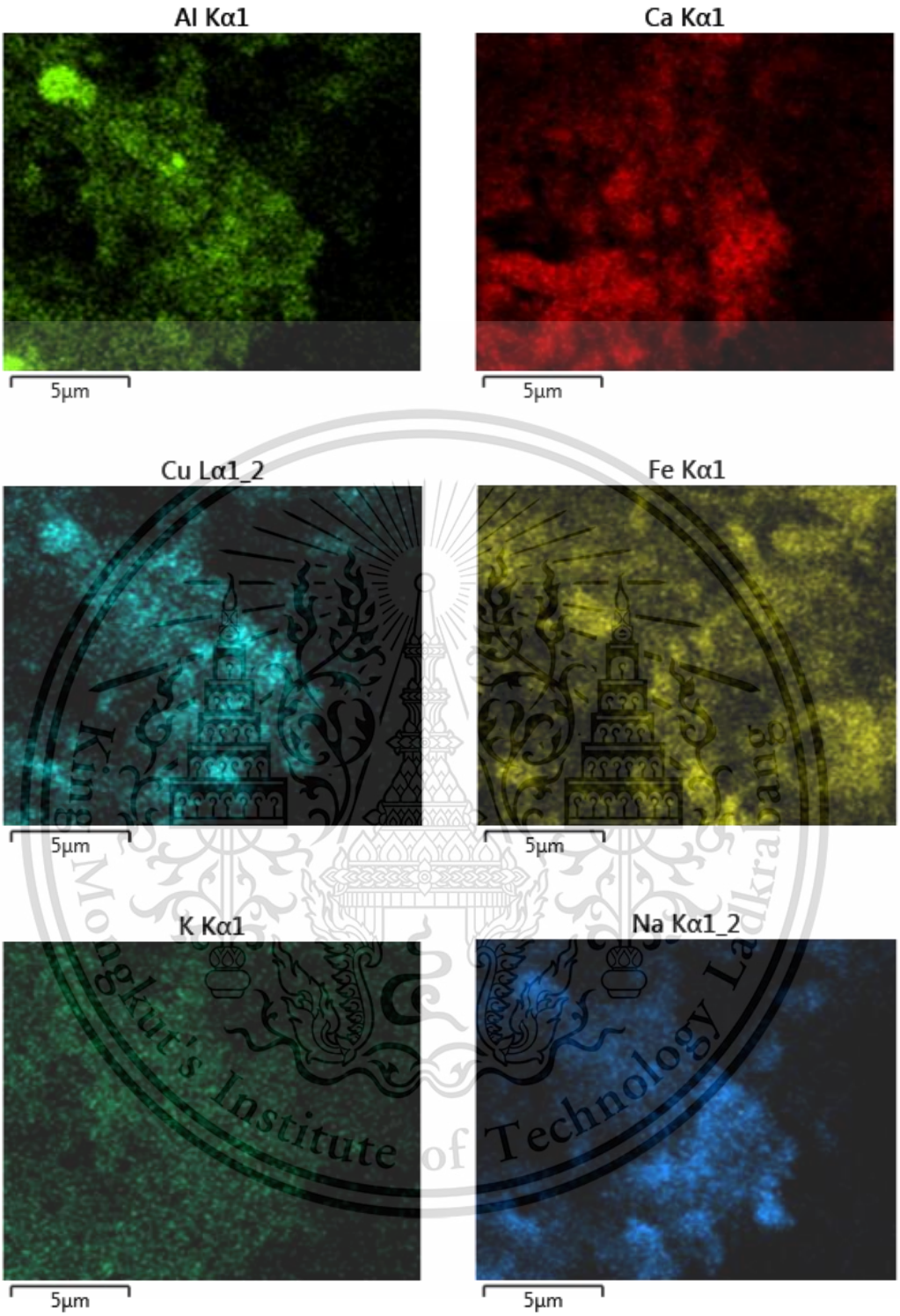

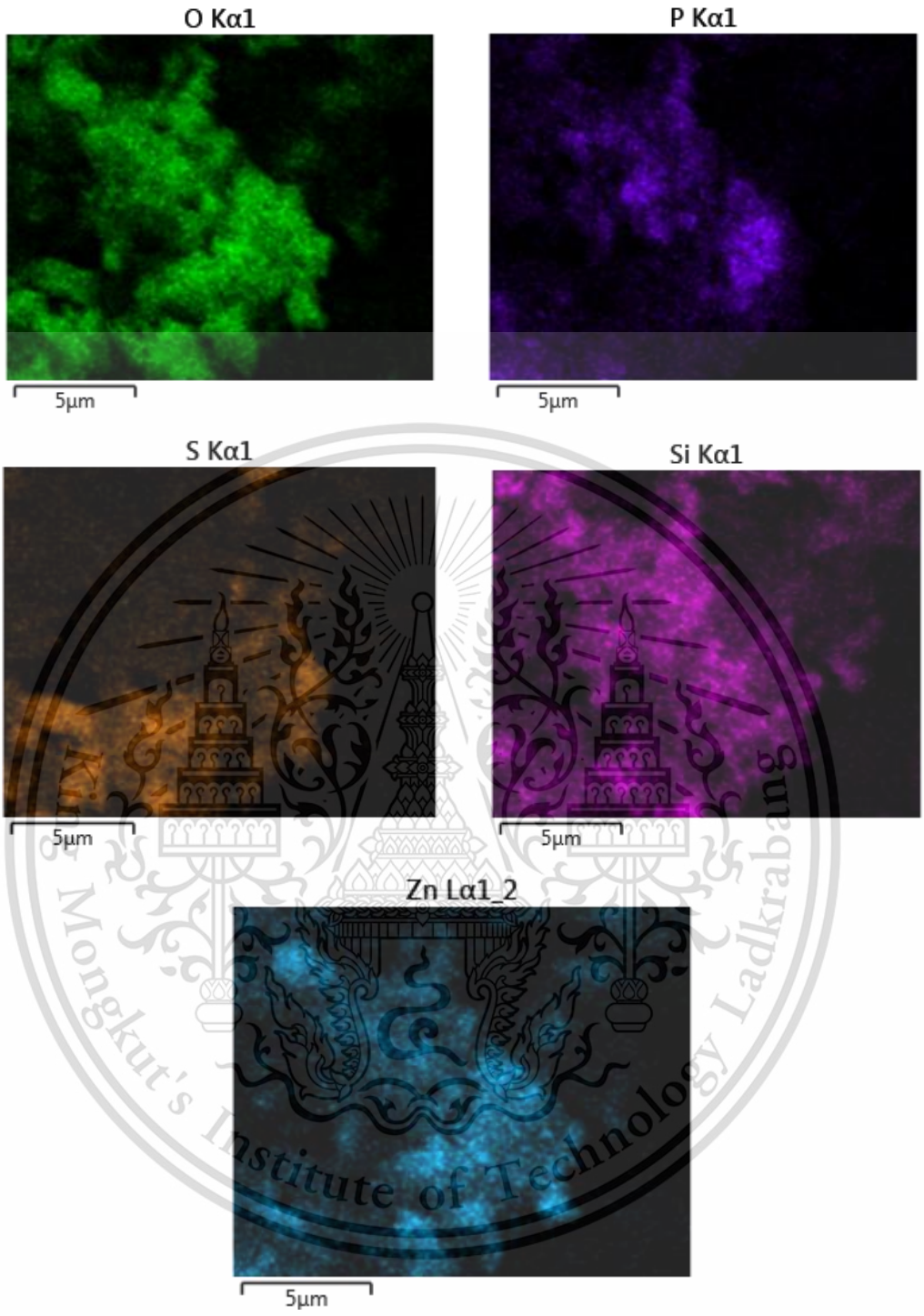

C

A-10: SEM image (A), elemental analysis data (B) and elemental distribution mappings (C) of ash particles

A-11: SEM image and elemental analysis of SiC wall of DPF

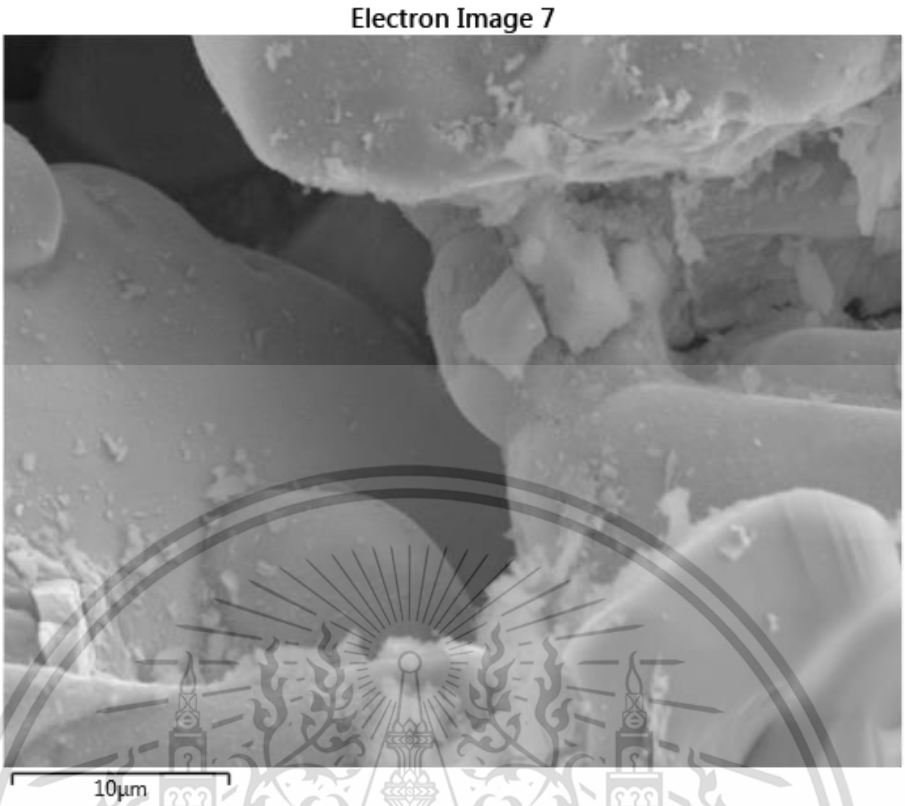

A

B

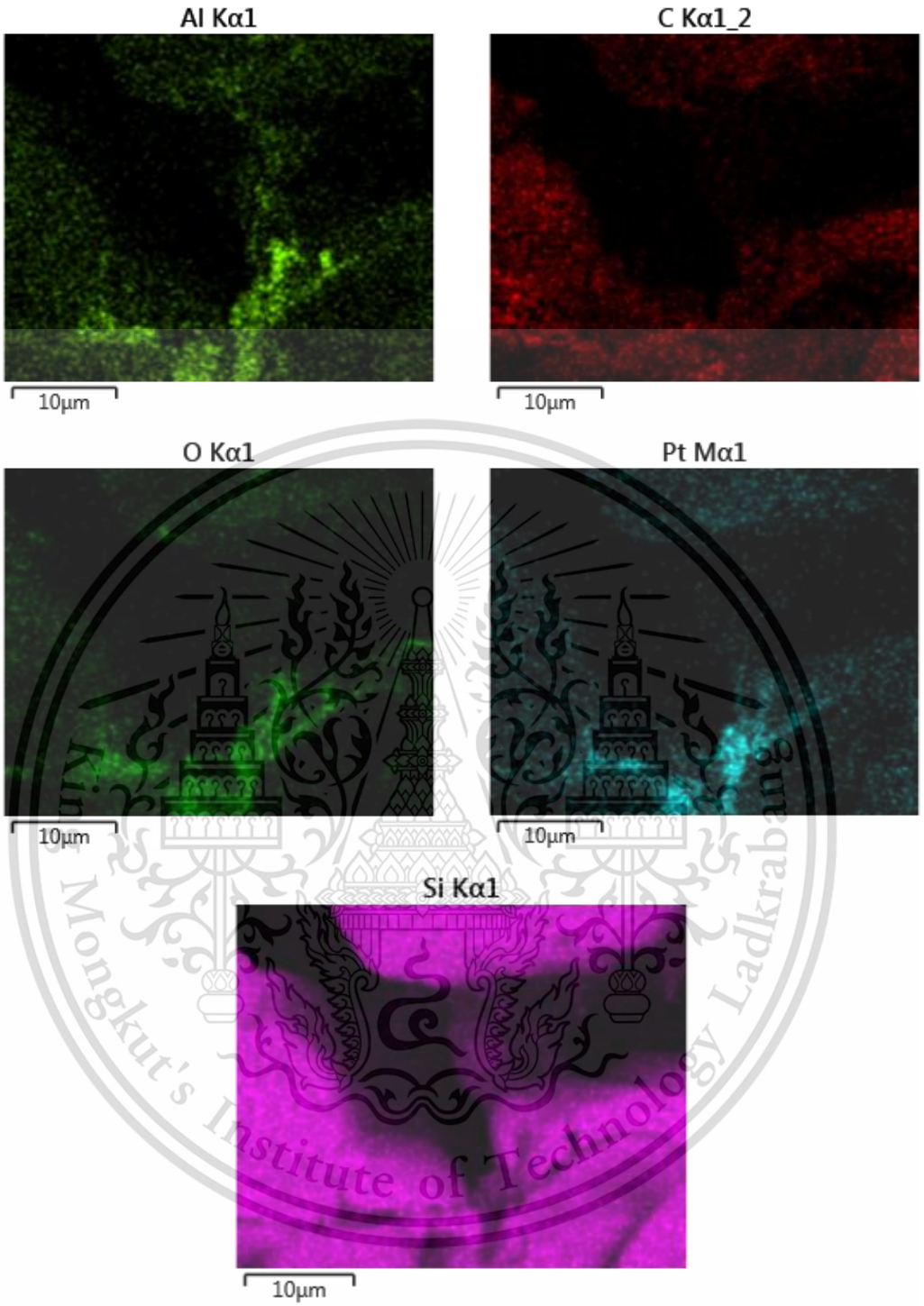

C

A-12: SEM image (A) and elemental analysis area shows ash elements originated from DOC (B, C)

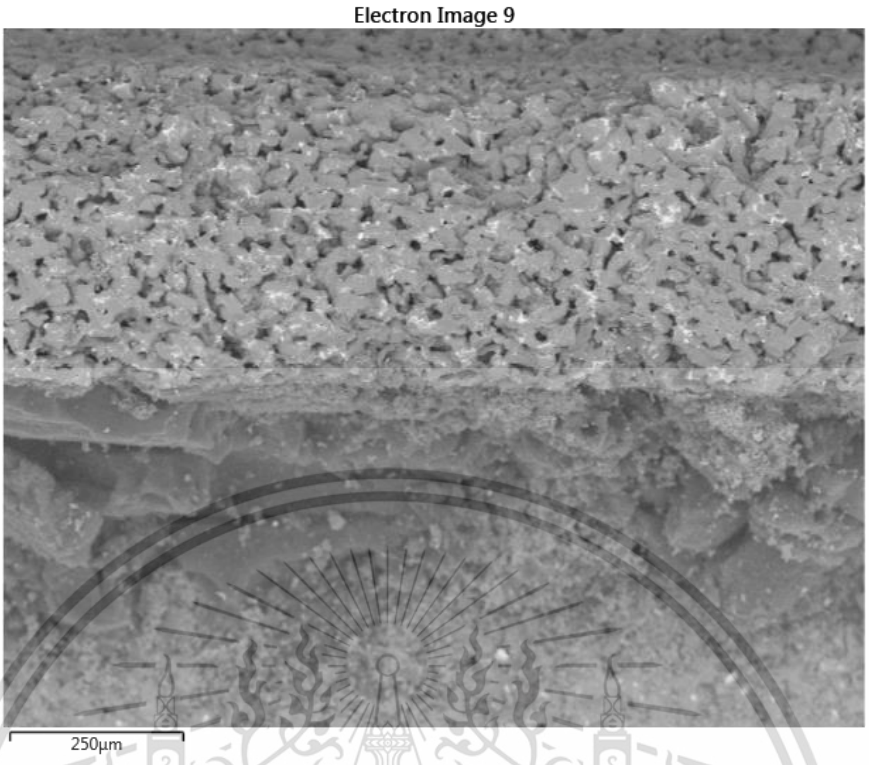

A

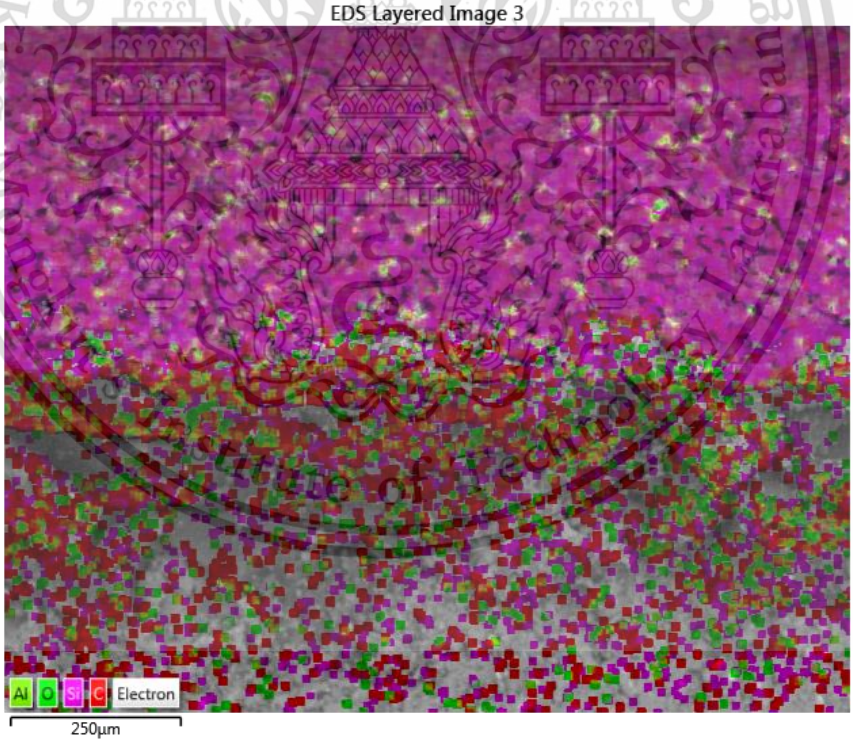

B

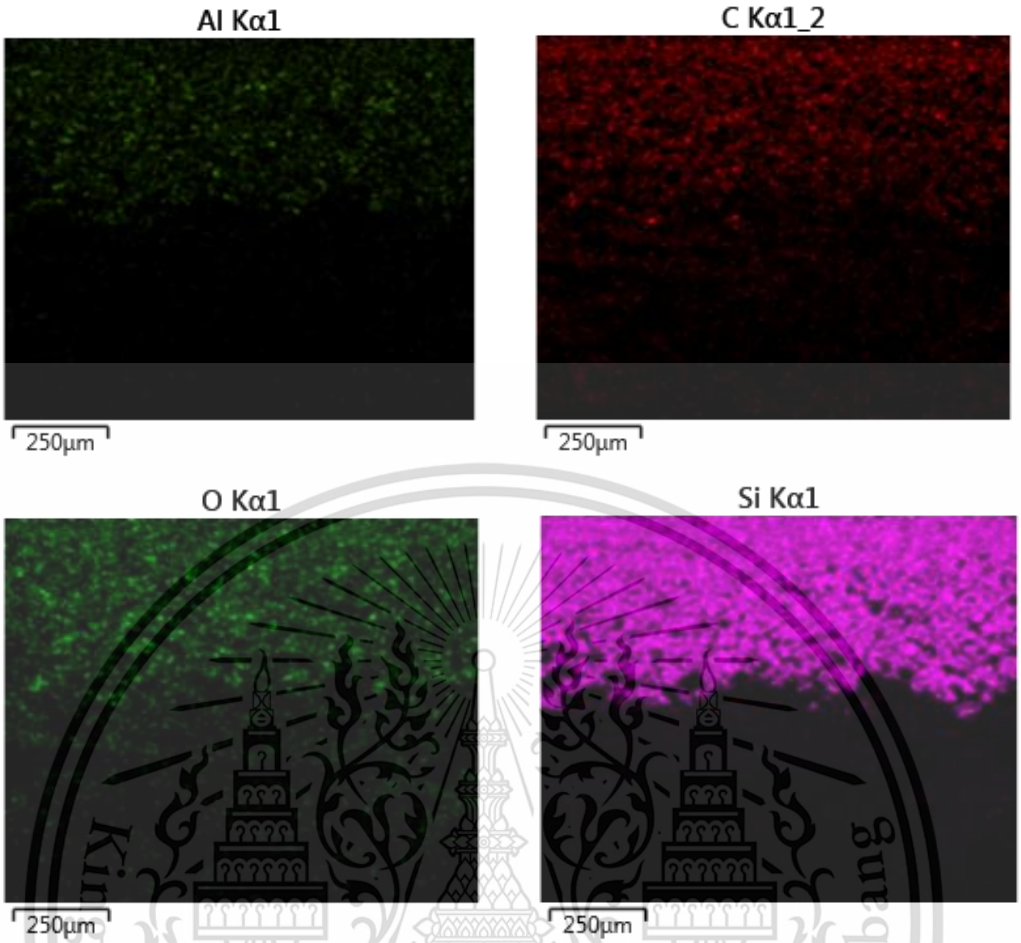

C

A-13: SEM images show ash deposited on the channel wall (A), EDS layered image and mappings show penetration and distribution of ash inside the channel wall toward the outlet channel (B, C).

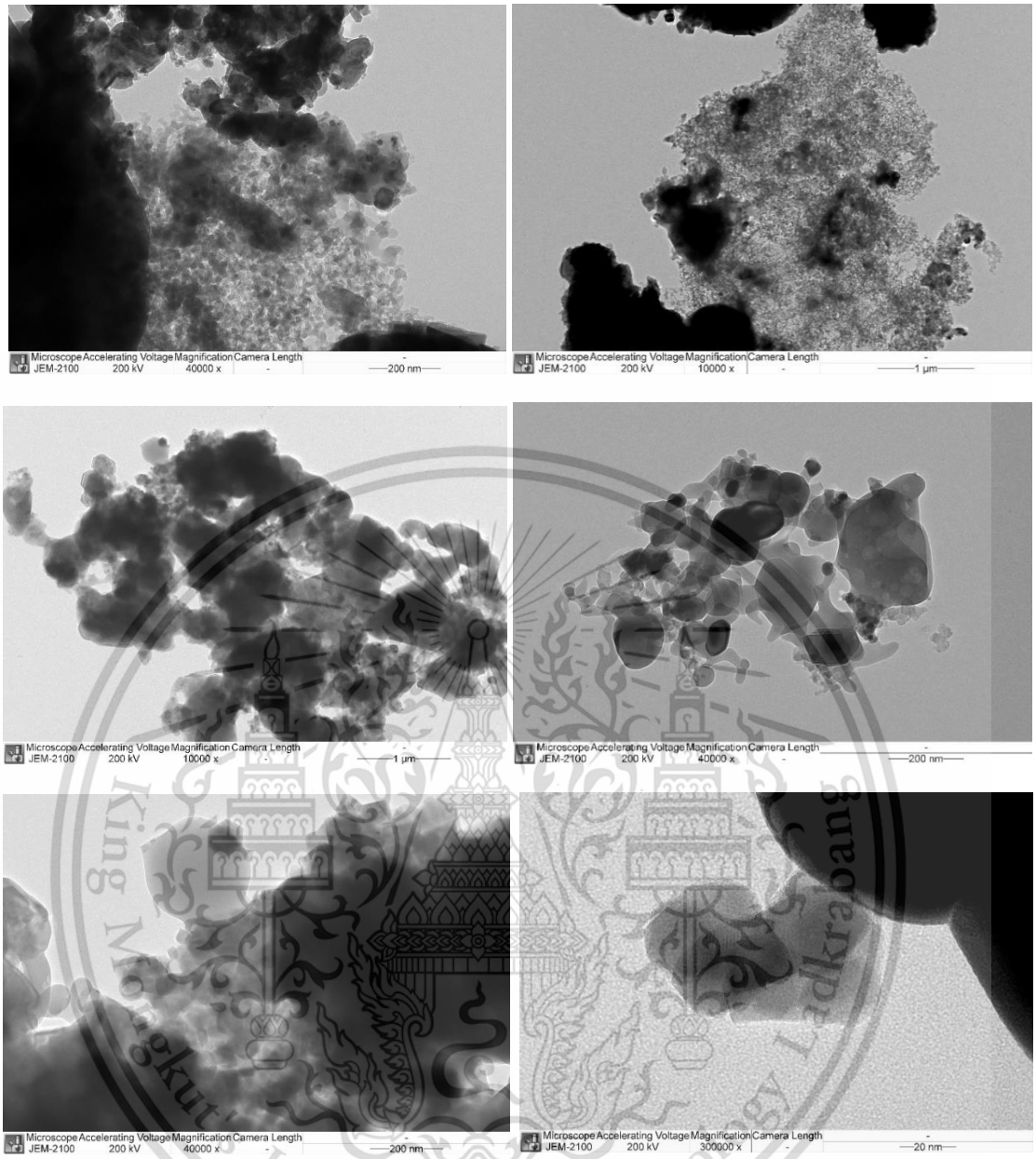

A-14: Bright field TEM images show agglomerated ash particles

A-15: Bright field TEM image (Top) and EDS elemental distribution mappings.

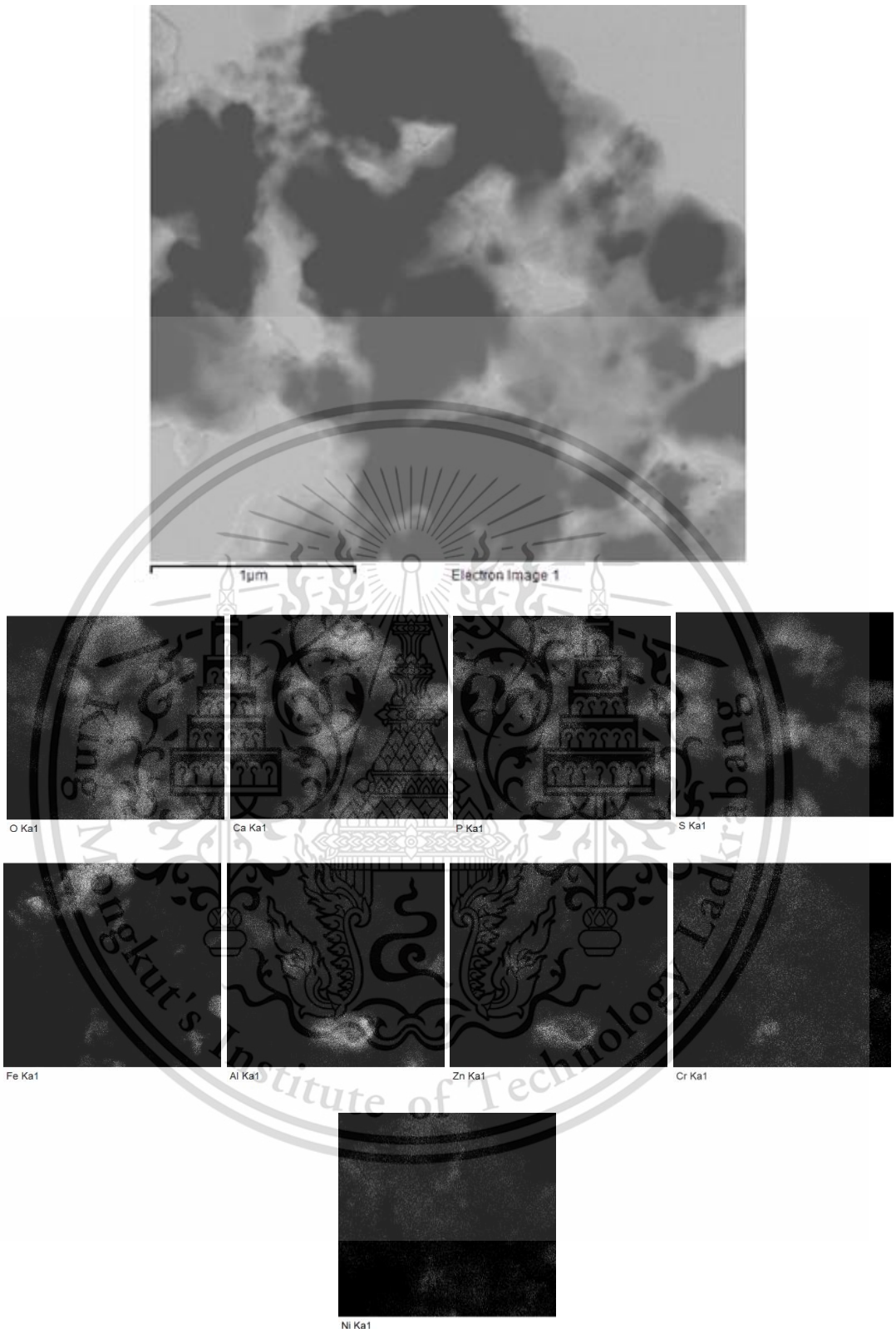

A-16: Bright field TEM image (Top) and EDS elemental distribution mappings.

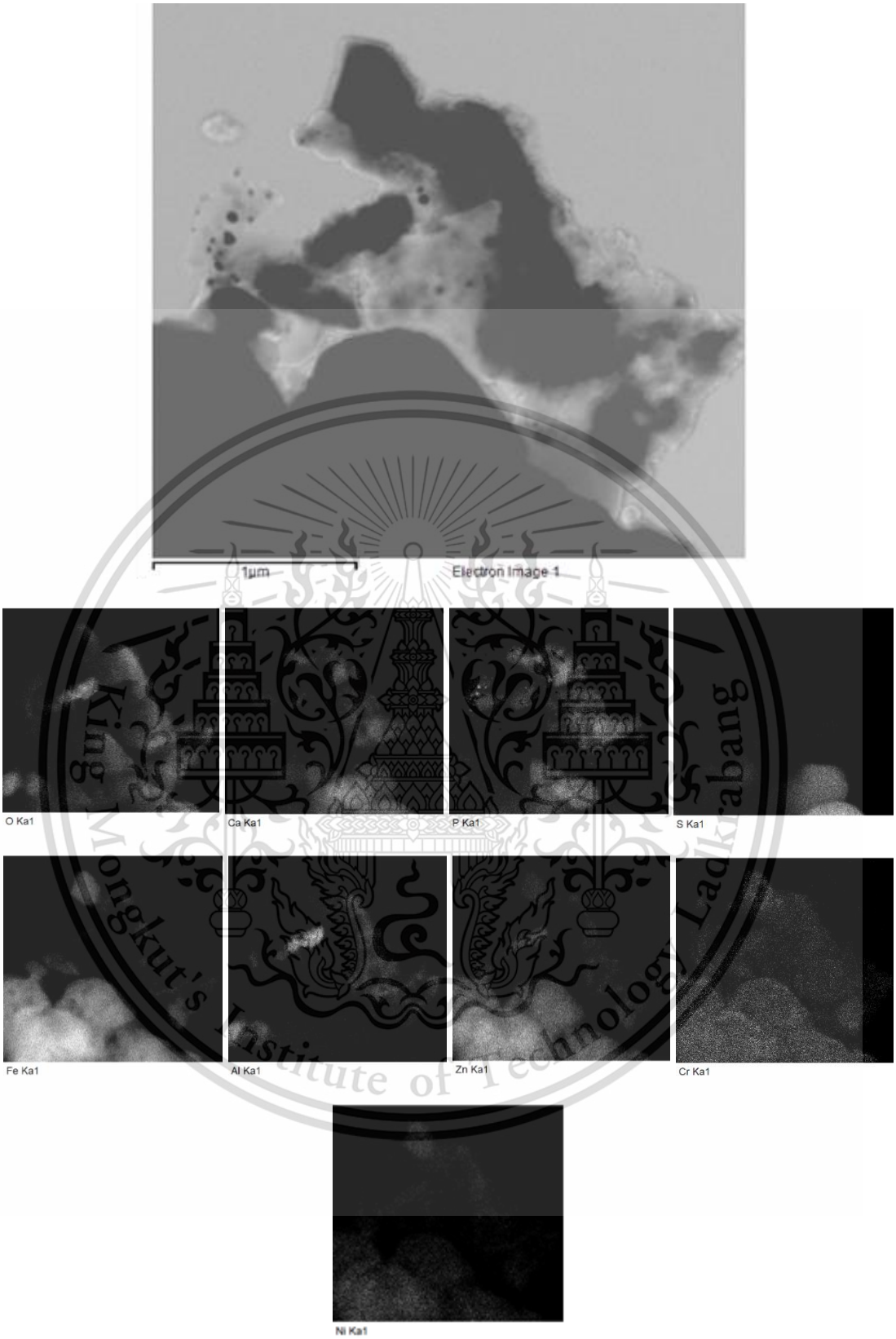

A-17: Bright field TEM image (Top) and EDS elemental distribution mappings.

APPENDIX B

DIESEL, LUBRICATING OILS ANALYSIS REPORTS

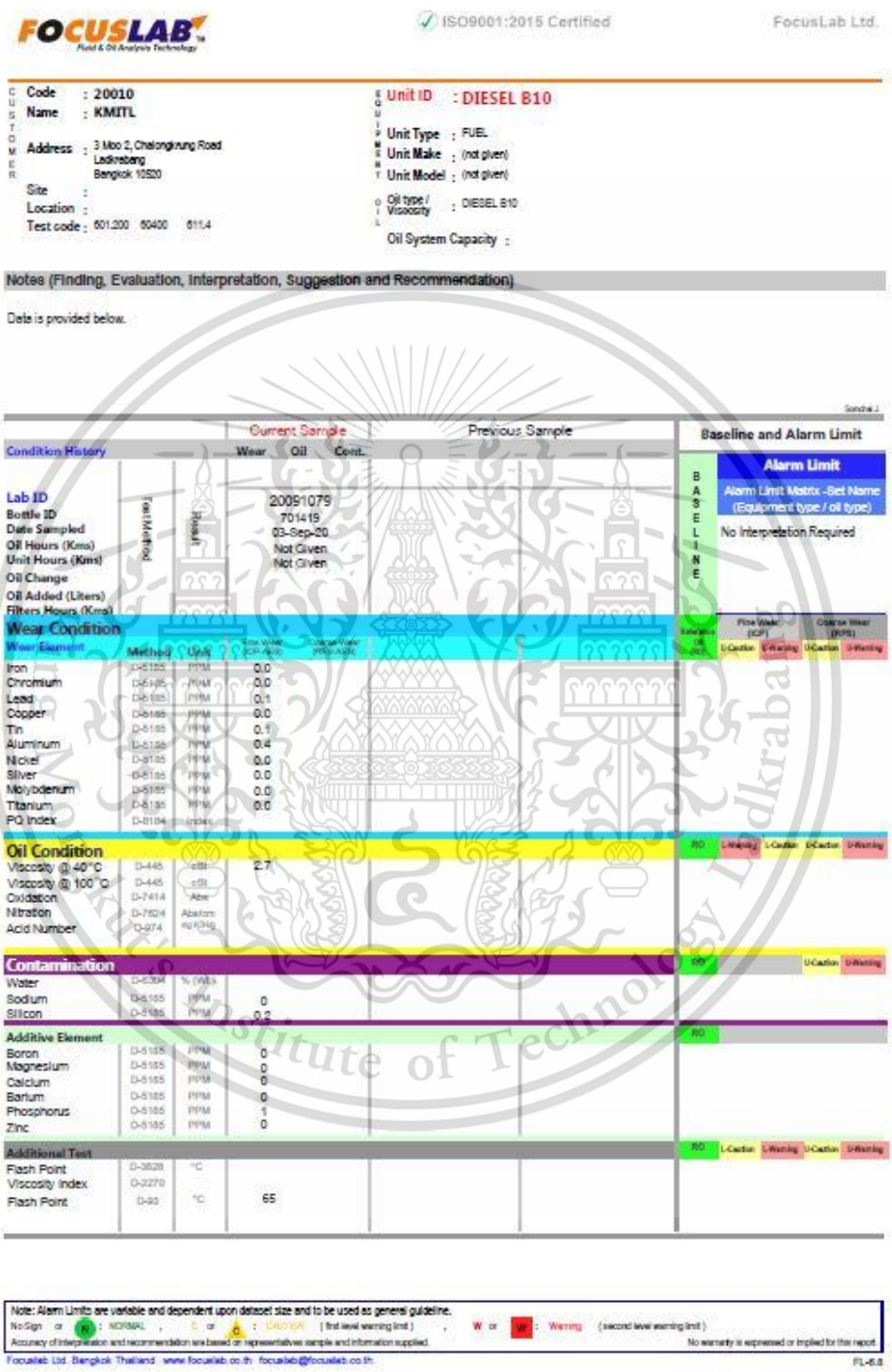

FOCUSLAB
Fluid & Oil Analysis Technology

ISO9001:2015 Certified

FocusLab Ltd.

CUSTOMER
Code : 20010
Name : KMITL
Address : 3 Moo 2, Chalongkrung Road
Ladkrabang
Bangkok 10520
Site :
Location :
Test code : 601.200 60400 611.4

EQUIPMENT
Unit ID : DIESEL B10
Unit Type : FUEL
Unit Make : (not given)
Unit Model : (not given)

OIL
Oil type / Viscosity : DIESEL B10
Oil System Capacity :

Notes (Finding, Evaluation, Interpretation, Suggestion and Recommendation)

Data is provided below.

Condition History	Test Method	Unit	Current Sample Wear Oil Cont.	Previous Sample	Baseline and Alarm Limit
Lab ID			20091079		Alarm Limit
Bottle ID			701419		Alarm Limit Matrix -Set Name (Equipment type / oil type)
Date Sampled			03-Sep-20		
Oil Hours (Kms)			Not Given		No Interpretation Required
Unit Hours (Kms)			Not Given		
Oil Change					
Oil Added (Liters)					
Filters Hours (Kms)					
Wear Condition					
Wear Element	Method	Unit			
Iron	D-5185	PPM	0.0		
Chromium	D-5185	PPM	0.0		
Lead	D-5185	PPM	0.1		
Copper	D-5185	PPM	0.0		
Tin	D-5185	PPM	0.1		
Aluminum	D-5185	PPM	0.4		
Nickel	D-5185	PPM	0.0		
Silver	D-5185	PPM	0.0		
Molybdenum	D-5185	PPM	0.0		
Titanium	D-5185	PPM	0.0		
PQ Index	D-8184	Index			
Oil Condition					
Viscosity @ 40°C	D-445	cSt	2.7		
Viscosity @ 100°C	D-445	cSt			
Oxidation	D-7414	Abs/cm			
Nitration	D-7624	Abs/cm			
Acid Number	D-974	mg KOH/g			
Contamination					
Water	D-6304	% (Wt.)			
Sodium	D-5185	PPM	0		
Silicon	D-5185	PPM	0.2		
Additive Element					
Boron	D-5185	PPM	0		
Magnesium	D-5185	PPM	0		
Calcium	D-5185	PPM	0		
Barium	D-5185	PPM	0		
Phosphorus	D-5185	PPM	1		
Zinc	D-5185	PPM	0		
Additional Test					
Flash Point	D-3828	°C			
Viscosity Index	D-2270				
Flash Point	D-93	°C	65		

Note: Alarm Limits are variable and dependent upon dataset size and to be used as general guideline.
No Sign or N : NORMAL , C or C : CAUTION (first level warning limit) , W or W : Warning (second level warning limit)
Accuracy of interpretation and recommendation are based on representative sample and information supplied. No warranty is expressed or implied for this report.
Focuslab Ltd. Bangkok Thailand www.focuslab.co.th focuslab@focuslab.co.th FL-6.8

B-1: elemental compositions of Diesel B10.

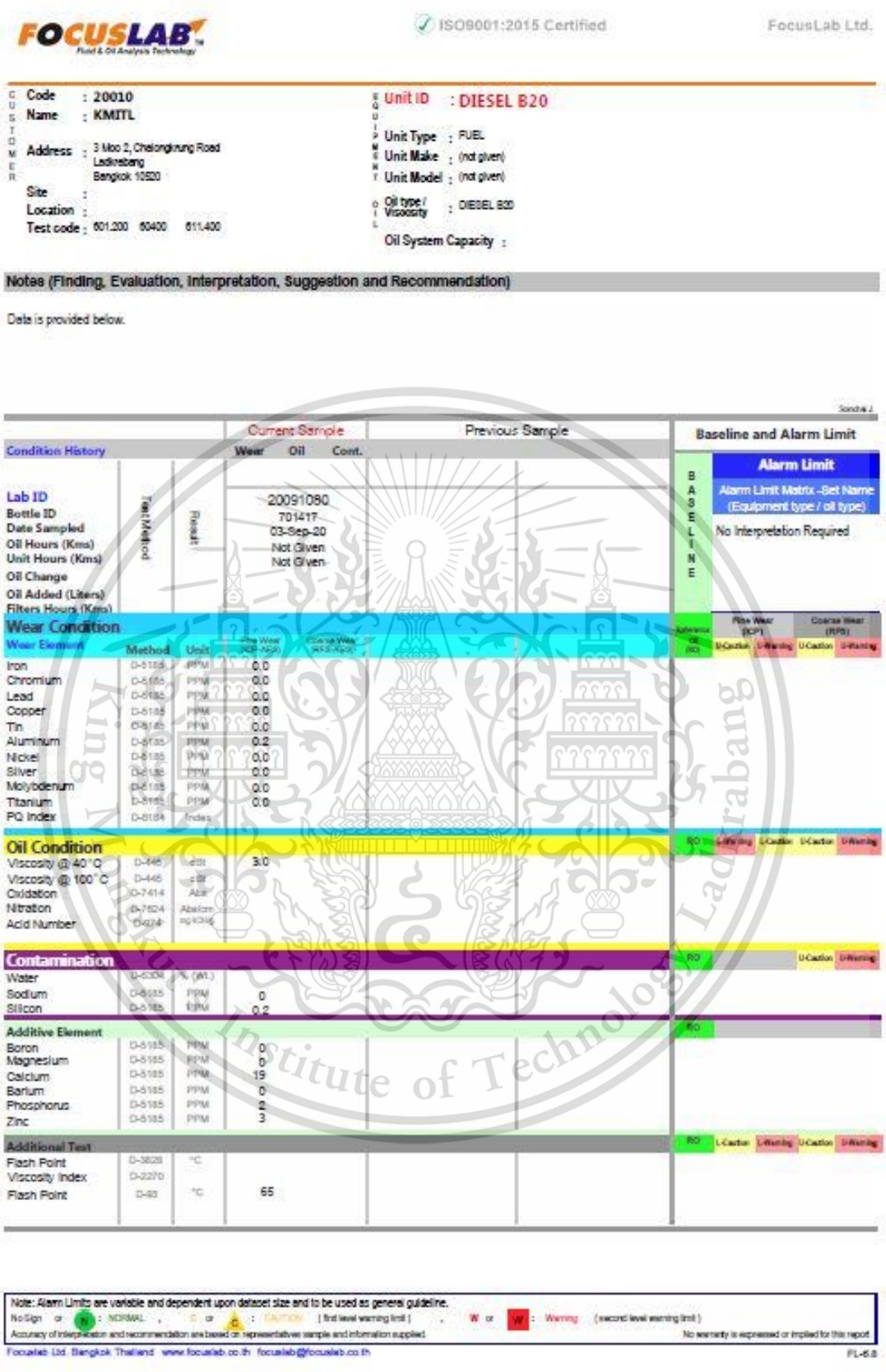

FOCUSLAB Fluid & Oil Analysis Technology — ISO9001:2015 Certified — FocusLab Ltd.

CUSTOMER
Code : 20010
Name : KMITL
Address : 3 Moo 2, Chalongkrung Road, Ladkrabang, Bangkok 10520
Site :
Location :
Test code : 601.200 60400 611.400

EQUIPMENT / OIL
Unit ID : DIESEL B20
Unit Type : FUEL
Unit Make : (not given)
Unit Model : (not given)
Oil type / Viscosity : DIESEL B20
Oil System Capacity :

Notes (Finding, Evaluation, Interpretation, Suggestion and Recommendation)

Data is provided below.

Condition History	Test Method	Result	Current Sample: Wear / Oil / Cont.	Previous Sample	Baseline and Alarm Limit
Lab ID			20091080		Alarm Limit
Bottle ID			701417		Alarm Limit Matrix -Set Name (Equipment type / oil type)
Date Sampled			03-Sep-20		No Interpretation Required
Oil Hours (Kms)			Not Given		
Unit Hours (Kms)			Not Given		
Oil Change					
Oil Added (Liters)					
Filters Hours (Kms)					
Wear Condition					Reference / Oil (RO) / Fine Wear (ICP) L-Caution / L-Warning / Coarse Wear (RPS) U-Caution / U-Warning
Wear Element	Method	Unit	Fine Wear (ICP-AES) / Coarse Wear (RPS-AES)		
Iron	D-5185	PPM	0.0		
Chromium	D-5185	PPM	0.0		
Lead	D-5185	PPM	0.0		
Copper	D-5185	PPM	0.0		
Tin	D-5185	PPM	0.0		
Aluminium	D-5185	PPM	0.2		
Nickel	D-5185	PPM	0.0		
Silver	D-5185	PPM	0.0		
Molybdenum	D-5185	PPM	0.0		
Titanium	D-5185	PPM	0.0		
PQ Index	D-8184	Index			
Oil Condition					RO / L-Warning / L-Caution / U-Caution / U-Warning
Viscosity @ 40°C	D-445	cSt	3.0		
Viscosity @ 100°C	D-445	cSt			
Oxidation	D-7414	Abs/cm			
Nitration	D-7624	Abs/cm			
Acid Number	D-974	mg KOH/g			
Contamination					RO / U-Caution / U-Warning
Water	D-6304	% (Wt.)			
Sodium	D-5185	PPM	0		
Silicon	D-5185	PPM	0.2		
Additive Element					RO
Boron	D-5185	PPM	0		
Magnesium	D-5185	PPM	0		
Calcium	D-5185	PPM	19		
Barium	D-5185	PPM	0		
Phosphorus	D-5185	PPM	2		
Zinc	D-5185	PPM	3		
Additional Test					RO / L-Caution / L-Warning / U-Caution / U-Warning
Flash Point	D-3828	°C			
Viscosity Index	D-2270				
Flash Point	D-93	°C	65		

Note: Alarm Limits are variable and dependent upon dataset size and to be used as general guideline.
No Sign or N : NORMAL , C or ⚠ : CAUTION [first level warning limit] , W or W : Warning (second level warning limit)
Accuracy of interpretation and recommendation are based on representative sample and information supplied. No warranty is expressed or implied for this report.
Focuslab Ltd. Bangkok Thailand www.focuslab.co.th focuslab@focuslab.co.th FL-6.8

B-2: elemental compositions of Diesel B20.

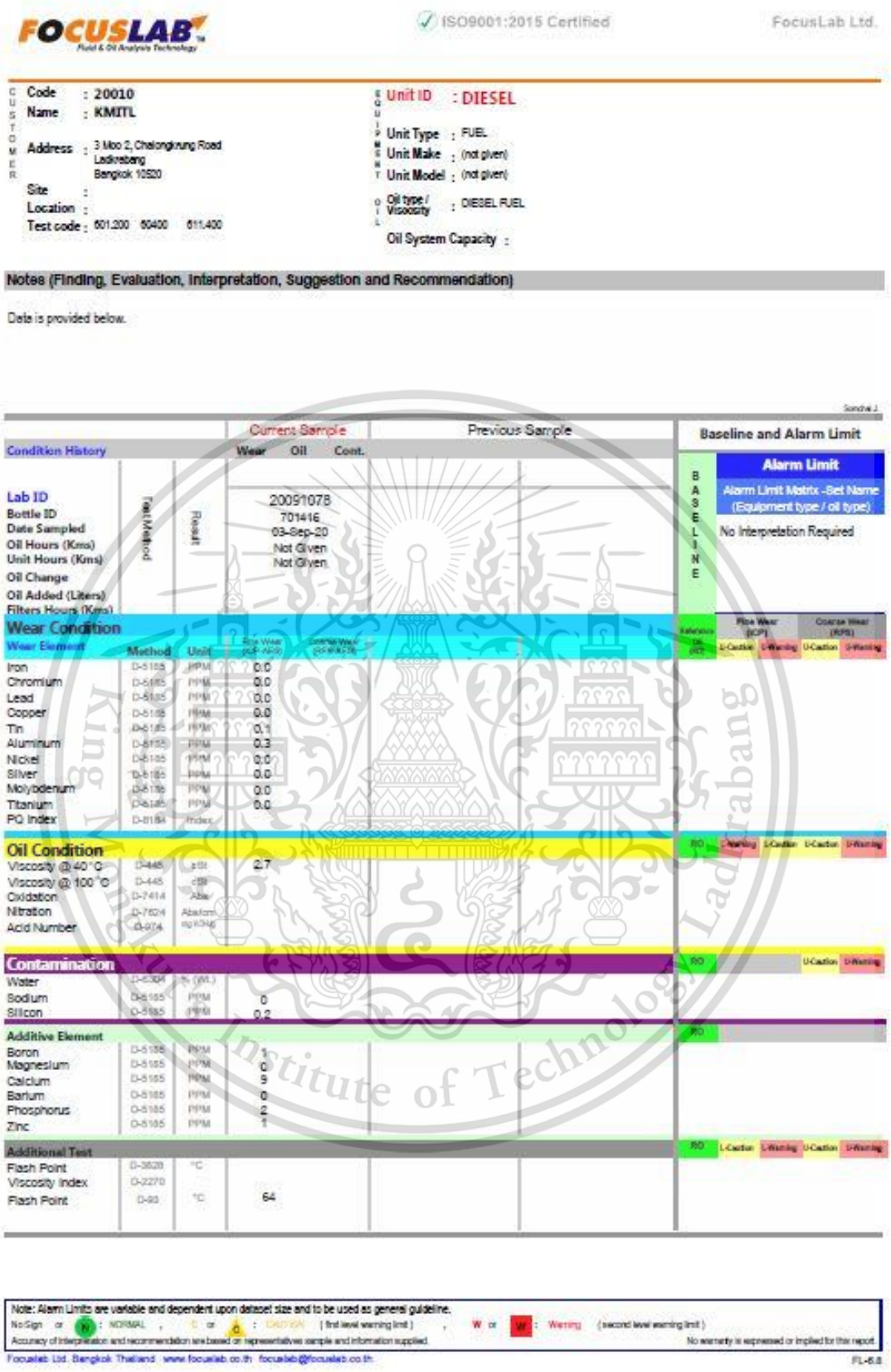

FOCUSLAB Fluid & Oil Analysis Technology

ISO9001:2015 Certified

FocusLab Ltd.

CUSTOMER
Code : 20010
Name : KMITL
Address : 3 Moo 2, Chalongkrung Road Ladkrabang Bangkok 10520
Site :
Location :
Test code : 601.200 60400 611.400

EQUIPMENT
Unit ID : DIESEL
Unit Type : FUEL
Unit Make : (not given)
Unit Model : (not given)

OIL
Oil type / Viscosity : DIESEL FUEL
Oil System Capacity :

Notes (Finding, Evaluation, Interpretation, Suggestion and Recommendation)

Data is provided below.

Condition History	Test Method	Result	Current Sample Wear Oil Cont.	Previous Sample	Baseline and Alarm Limit
Lab ID			20091078		Alarm Limit
Bottle ID			701416		Alarm Limit Matrix -Set Name (Equipment type / oil type)
Date Sampled			03-Sep-20		
Oil Hours (Kms)			Not Given		No Interpretation Required
Unit Hours (Kms)			Not Given		
Oil Change					
Oil Added (Liters)					
Filters Hours (Kms)					
Wear Condition					
Wear Element	Method	Unit			
Iron	D-5185	PPM	0.0		
Chromium	D-5185	PPM	0.0		
Lead	D-5185	PPM	0.0		
Copper	D-5185	PPM	0.0		
Tin	D-5185	PPM	0.1		
Aluminum	D-5185	PPM	0.3		
Nickel	D-5185	PPM	0.0		
Silver	D-5185	PPM	0.0		
Molybdenum	D-5185	PPM	0.0		
Titanium	D-5185	PPM	0.0		
PQ Index	D-8184	Index			
Oil Condition					
Viscosity @ 40 °C	D-445	cSt	2.7		
Viscosity @ 100 °C	D-445	cSt			
Oxidation	D-7414	Abs			
Nitration	D-7624	Abs/cm			
Acid Number	D-974	mg KOH/g			
Contamination					
Water	D-6304	% (Wt.)			
Sodium	D-5185	PPM	0		
Silicon	D-5185	PPM	0.2		
Additive Element					
Boron	D-5185	PPM	1		
Magnesium	D-5185	PPM	0		
Calcium	D-5185	PPM	9		
Barium	D-5185	PPM	0		
Phosphorus	D-5185	PPM	2		
Zinc	D-5185	PPM	1		
Additional Test					
Flash Point	D-3828	°C			
Viscosity Index	D-2270				
Flash Point	D-93	°C	64		

Note: Alarm Limits are variable and dependent upon dataset size and to be used as general guideline.
No Sign or N : NORMAL , C or C : CAUTION [first level warning limit] , W or W : Warning [second level warning limit]
Accuracy of interpretation and recommendation are based on representatives sample and information supplied. No warranty is expressed or implied for this report.
Focuslab Ltd. Bangkok Thailand www.focuslab.co.th focuslab@focuslab.co.th FL-6.8

B-3: elemental compositions of Diesel.

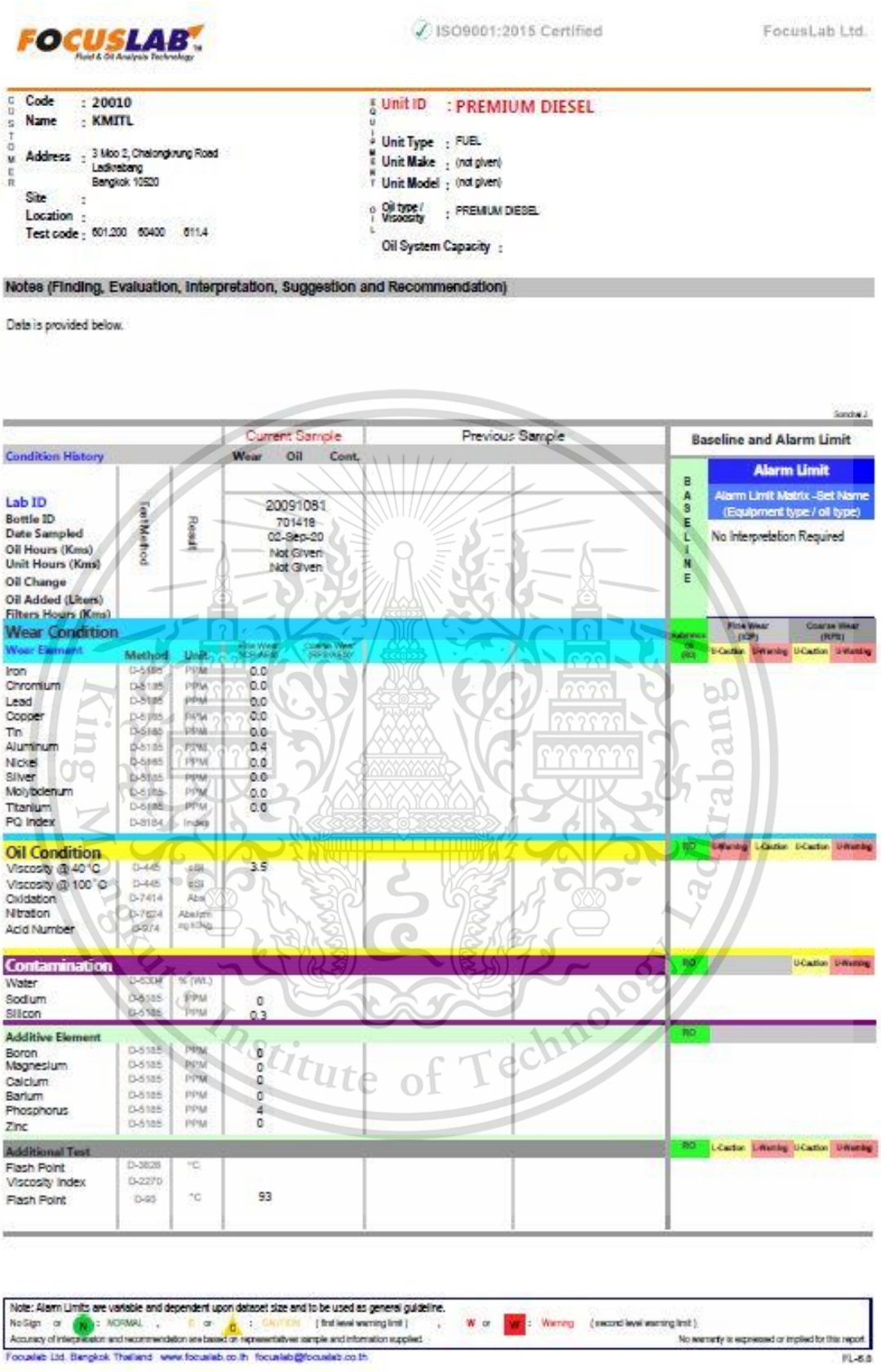

FOCUSLAB Fluid & Oil Analysis Technology

ISO9001:2015 Certified

FocusLab Ltd.

CUSTOMER
Code : 20010
Name : KMITL
Address : 3 Moo 2, Chalongkrung Road Ladkrabang Bangkok 10520
Site :
Location :
Test code : 601.200 60400 611.4

EQUIPMENT
Unit ID : PREMIUM DIESEL
Unit Type : FUEL
Unit Make : (not given)
Unit Model : (not given)

OIL
Oil type / Viscosity : PREMIUM DIESEL
Oil System Capacity :

Notes (Finding, Evaluation, Interpretation, Suggestion and Recommendation)

Data is provided below.

Condition History	Test Method	Result	Current Sample Wear Oil Cont.	Previous Sample	Baseline and Alarm Limit
Lab ID			20091081		BASELINE: Alarm Limit
Bottle ID			701418		Alarm Limit Matrix -Set Name (Equipment type / oil type)
Date Sampled			02-Sep-20		No Interpretation Required
Oil Hours (Kms)			Not Given		
Unit Hours (Kms)			Not Given		
Oil Change					
Oil Added (Liters)					
Filters Hours (Kms)					
Wear Condition					Fine Wear (ISO) / Coarse Wear (RPS)
Wear Element	Method	Unit	Fine Wear / Coarse Wear		Reference (%) (RO) / L-Caution / L-Warning / U-Caution / U-Warning
Iron	D-5185	PPM	0.0		
Chromium	D-5185	PPM	0.0		
Lead	D-5185	PPM	0.0		
Copper	D-5185	PPM	0.0		
Tin	D-5185	PPM	0.0		
Aluminum	D-5185	PPM	0.4		
Nickel	D-5185	PPM	0.0		
Silver	D-5185	PPM	0.0		
Molybdenum	D-5185	PPM	0.0		
Titanium	D-5185	PPM	0.0		
PQ Index	D-8184	Index			
Oil Condition					RO / L-Warning / L-Caution / U-Caution / U-Warning
Viscosity @ 40 °C	D-445	cSt	3.5		
Viscosity @ 100 °C	D-445	cSt			
Oxidation	D-7414	Abs			
Nitration	D-7624	Abs/cm			
Acid Number	D-974	mg KOH/g			
Contamination					RO / U-Caution / U-Warning
Water	D-63DM	% (Wt.)			
Sodium	D-5185	PPM	0		
Silicon	D-5185	PPM	0.3		
Additive Element					RO
Boron	D-5185	PPM	0		
Magnesium	D-5185	PPM	0		
Calcium	D-5185	PPM	0		
Barium	D-5185	PPM	0		
Phosphorus	D-5185	PPM	4		
Zinc	D-5185	PPM	0		
Additional Test					RO / L-Caution / L-Warning / U-Caution / U-Warning
Flash Point	D-3828	°C			
Viscosity Index	D-2270				
Flash Point	D-93	°C	93		

Note: Alarm Limits are variable and dependent upon dataset size and to be used as general guideline.
No Sign or N : NORMAL , C or C : CAUTION [first level warning limit] , W or W : Warning [second level warning limit]
Accuracy of interpretation and recommendation are based on representative sample and information supplied. No warranty is expressed or implied for this report.
Focuslab Ltd. Bangkok Thailand www.focuslab.co.th focuslab@focuslab.co.th FL-6.8

B-4: elemental compositions of premium diesel.

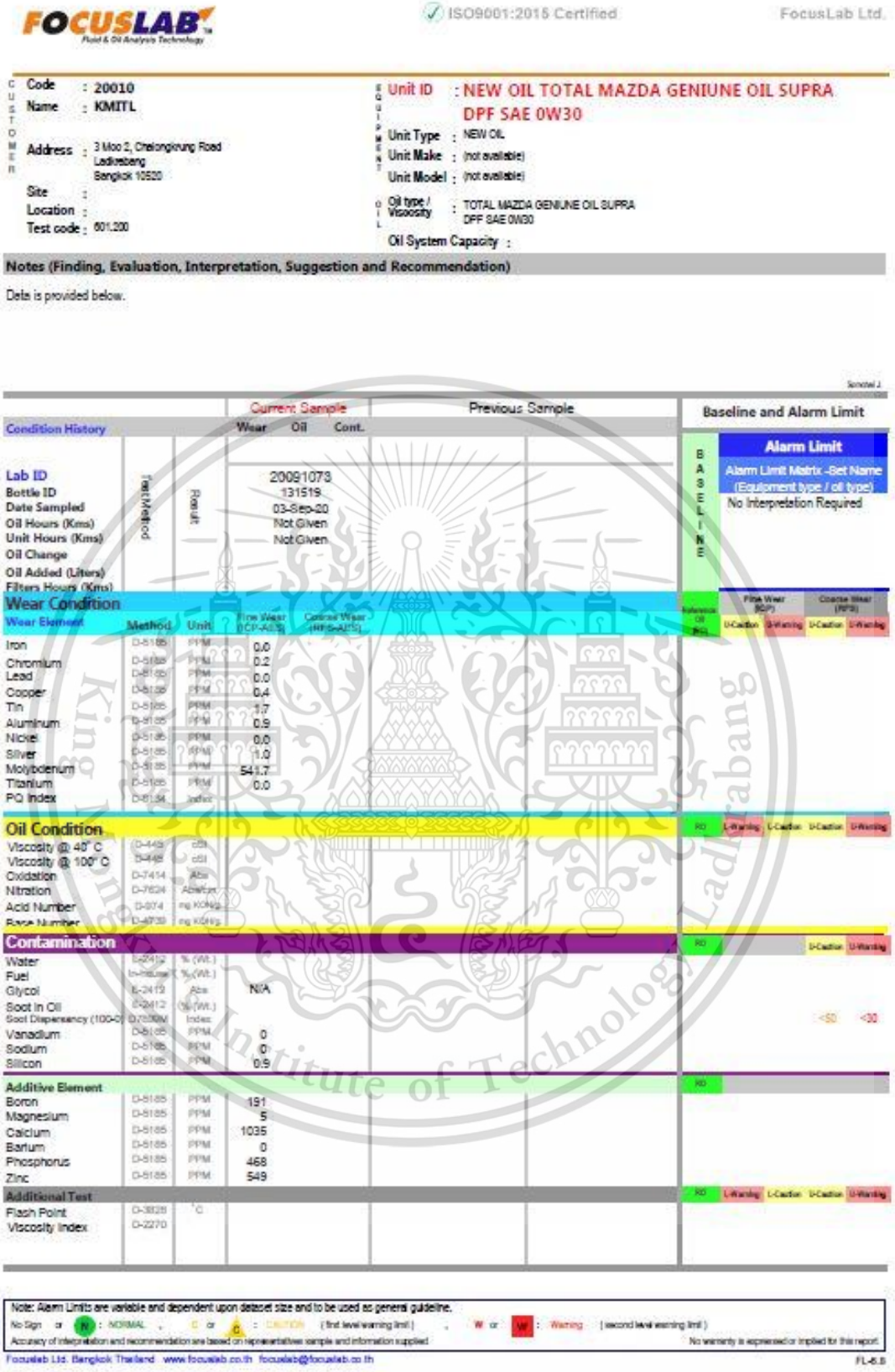

FOCUSLAB Fluid & Oil Analysis Technology

ISO9001:2015 Certified

FocusLab Ltd.

CUSTOMER
Code : 20010
Name : KMITL
Address : 3 Moo 2, Chalongkrung Road Ladkrabang Bangkok 10520
Site :
Location :
Test code : 601.200

EQUIPMENT
Unit ID : NEW OIL TOTAL MAZDA GENIUNE OIL SUPRA DPF SAE 0W30
Unit Type : NEW OIL
Unit Make : (not available)
Unit Model : (not available)

OIL
Oil type / Viscosity : TOTAL MAZDA GENIUNE OIL SUPRA DPF SAE 0W30
Oil System Capacity :

Notes (Finding, Evaluation, Interpretation, Suggestion and Recommendation)

Data is provided below.

Condition History	Test Method	Result	Current Sample Wear Oil Cont.	Previous Sample	Baseline and Alarm Limit
Lab ID			20091073		Alarm Limit
Bottle ID			131519		Alarm Limit Matrix -Set Name (Equipment type / oil type)
Date Sampled			03-Sep-20		No Interpretation Required
Oil Hours (Kms)			Not Given		
Unit Hours (Kms)			Not Given		
Oil Change					
Oil Added (Liters)					
Filters Hours (Kms)					
Wear Condition					
Wear Element	Method	Unit	Fine Wear (ICP-AES) / Coarse Wear (RPT-AES)		Reference Oil (RO) / Fine Wear (ICP) U-Caution U-Warning / Coarse Wear (RPT) U-Caution U-Warning
Iron	D-5185	PPM	0.0		
Chromium	D-5185	PPM	0.2		
Lead	D-5185	PPM	0.0		
Copper	D-5185	PPM	0.4		
Tin	D-5185	PPM	1.7		
Aluminum	D-5185	PPM	0.9		
Nickel	D-5185	PPM	0.0		
Silver	D-5185	PPM	1.0		
Molybdenum	D-5185	PPM	541.7		
Titanium	D-5185	PPM	0.0		
PQ Index	D-8184	Index			
Oil Condition					RO U-Caution U-Warning U-Caution U-Warning
Viscosity @ 40° C	D-445	cSt			
Viscosity @ 100° C	D-445	cSt			
Oxidation	D-7414	Abs			
Nitration	D-7624	Abs/cm			
Acid Number	D-974	mg KOH/g			
Base Number	D-4739	mg KOH/g			
Contamination					RO U-Caution U-Warning
Water	D-2412	% (Wt.)			
Fuel	In-House	% (Wt.)			
Glycol	D-2412	Abs	N/A		
Soot in Oil	D-2412	% (Wt.)			
Soot Dispersancy (100-0)	D-7686M	Index			<50 <30
Vanadium	D-5185	PPM	0		
Sodium	D-5185	PPM	0		
Silicon	D-5185	PPM	0.9		
Additive Element					RO
Boron	D-5185	PPM	191		
Magnesium	D-5185	PPM	5		
Calcium	D-5185	PPM	1035		
Barium	D-5185	PPM	0		
Phosphorus	D-5185	PPM	468		
Zinc	D-5185	PPM	549		
Additional Test					RO U-Caution U-Warning U-Caution U-Warning
Flash Point	D-3828	°C			
Viscosity Index	D-2270				

Note: Alarm Limits are variable and dependent upon dataset size and to be used as general guideline.
No Sign or (N) : NORMAL , C or (C) : CAUTION (first level warning limit) , W or (W) : Warning (second level warning limit)
Accuracy of interpretation and recommendation are based on representatives sample and information supplied. No warranty is expressed or implied for this report.
Focuslab Ltd. Bangkok Thailand www.focuslab.co.th focuslab@focuslab.co.th FL-6.8

B-5: elemental compositions of new MAZDA lubricating oil.

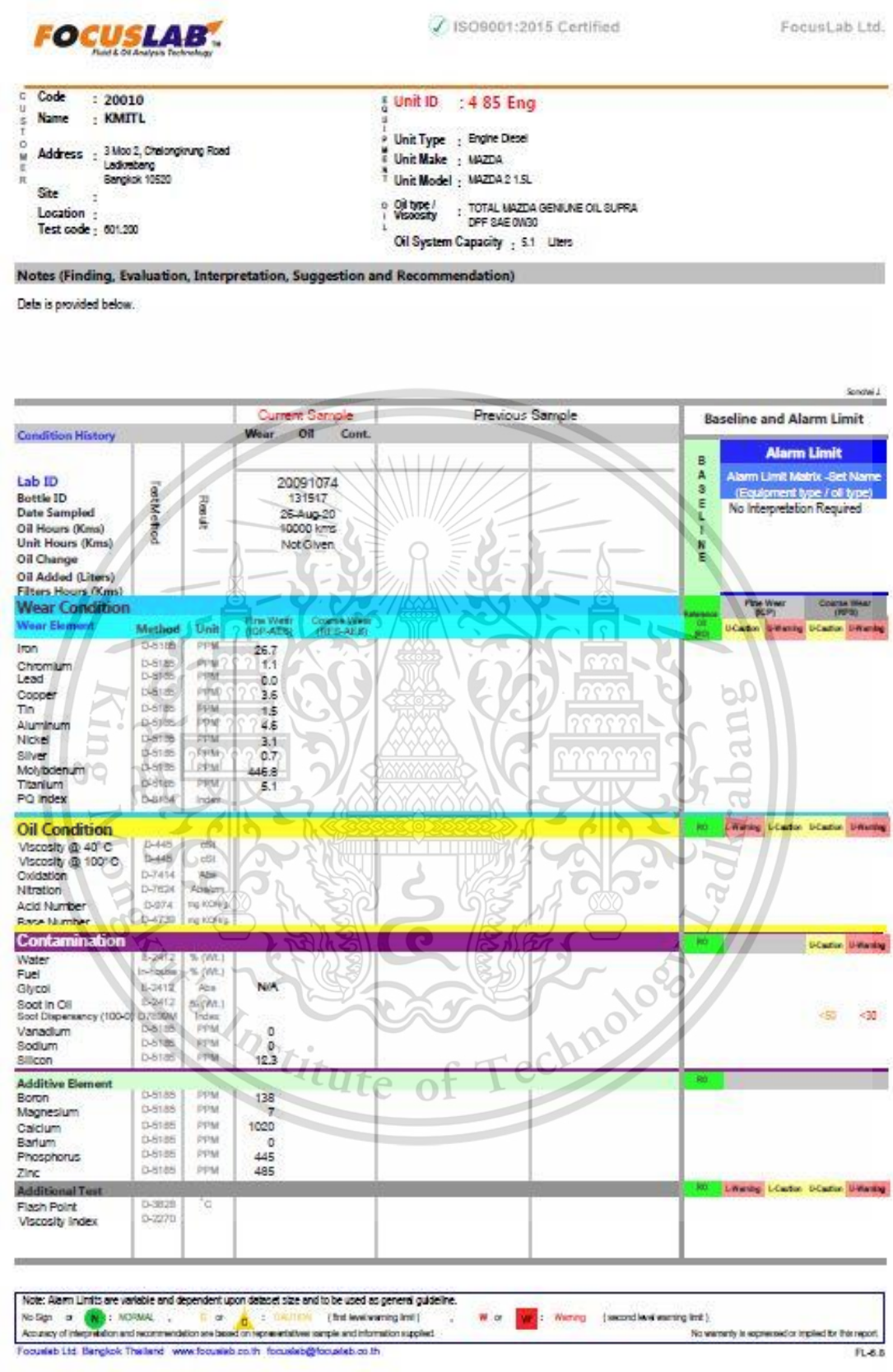

FOCUSLAB Fluid & Oil Analysis Technology — ISO9001:2015 Certified — FocusLab Ltd.

CUSTOMER
Code : 20010
Name : KMITL
Address : 3 Moo 2, Chalongkrung Road Ladkrabang Bangkok 10520
Site :
Location :
Test code : 601.200

EQUIPMENT
Unit ID : 4 85 Eng
Unit Type : Engine Diesel
Unit Make : MAZDA
Unit Model : MAZDA 2 1.5L

OIL
Oil type / Viscosity : TOTAL MAZDA GENUINE OIL SUPRA DPF SAE 0W30
Oil System Capacity : 5.1 Liters

Notes (Finding, Evaluation, Interpretation, Suggestion and Recommendation)

Data is provided below.

Condition History	Test Method	Result	Current Sample: Wear Oil Cont.	Previous Sample	Baseline and Alarm Limit
Lab ID			20091074		Alarm Limit
Bottle ID			131517		Alarm Limit Matrix -Set Name (Equipment type / oil type)
Date Sampled			25-Aug-20		No Interpretation Required
Oil Hours (Kms)			10000 kms		
Unit Hours (Kms)			Not Given		
Oil Change					
Oil Added (Liters)					
Filters Hours (Kms)					
Wear Condition					
Wear Element	Method	Unit			
Iron	D-5185	PPM	26.7		
Chromium	D-5185	PPM	1.1		
Lead	D-5185	PPM	0.0		
Copper	D-5185	PPM	3.6		
Tin	D-5185	PPM	1.5		
Aluminum	D-5185	PPM	4.6		
Nickel	D-5185	PPM	3.1		
Silver	D-5185	PPM	0.7		
Molybdenum	D-5185	PPM	446.8		
Titanium	D-5185	PPM	5.1		
PQ Index	D-8184	Index			
Oil Condition					
Viscosity @ 40° C	D-445	cSt			
Viscosity @ 100°C	D-445	cSt			
Oxidation	D-7414	Abs/cm			
Nitration	D-7624	Abs/cm			
Acid Number	D-974	mg KOH/g			
Base Number	D-4739	mg KOH/g			
Contamination					
Water	D-2412	% (Vol.)			
Fuel	In-House	% (Vol.)			
Glycol	D-2412	Abs	N/A		
Soot in Oil	D-2412	% (Vol.)			
Soot Dispersancy (100-0)	D-7593M	Index			<50 <30
Vanadium	D-5185	PPM	0		
Sodium	D-5185	PPM	0		
Silicon	D-5185	PPM	12.3		
Additive Element					
Boron	D-5185	PPM	138		
Magnesium	D-5185	PPM	7		
Calcium	D-5185	PPM	1020		
Barium	D-5185	PPM	0		
Phosphorus	D-5185	PPM	445		
Zinc	D-5185	PPM	485		
Additional Test					
Flash Point	D-3828	°C			
Viscosity Index	D-2270				

Note: Alarm Limits are variable and dependent upon dataset size and to be used as general guideline.
No Sign or N : NORMAL , I or Q : CAUTION (first level warning limit) , W or WF : Warning (second level warning limit)
Accuracy of interpretation and recommendation are based on representative sample and information supplied. No warranty is expressed or implied for this report.
Focuslab Ltd. Bangkok Thailand www.focuslab.co.th focuslab@focuslab.co.th FL-6.6

B-6: elemental compositions of used MAZDA lubricating oil sample 1.

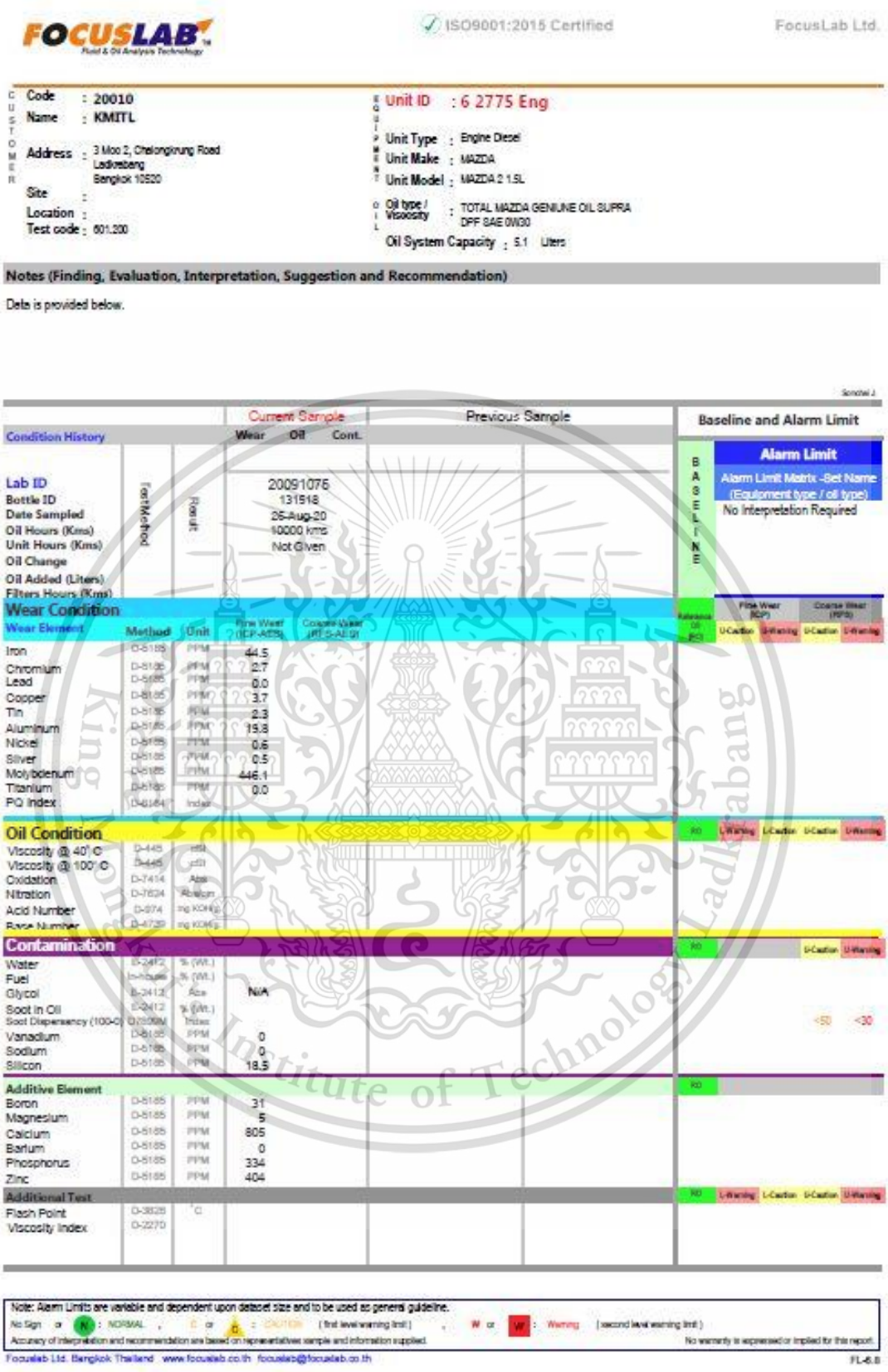

FOCUSLAB Fluid & Oil Analysis Technology — ISO9001:2015 Certified — FocusLab Ltd.

CUSTOMER
Code : 20010
Name : KMITL
Address : 3 Moo 2, Chalongkrung Road Ladkrabang Bangkok 10520
Site :
Location :
Test code : 601.200

EQUIPMENT
Unit ID : 6 2775 Eng
Unit Type : Engine Diesel
Unit Make : MAZDA
Unit Model : MAZDA 2 1.5L

OIL
Oil type / Viscosity : TOTAL MAZDA GENUINE OIL SUPRA DPF SAE 0W30
Oil System Capacity : 5.1 Liters

Notes (Finding, Evaluation, Interpretation, Suggestion and Recommendation)

Data is provided below.

Condition History	Method	Unit	Current Sample Wear Oil Cont.	Previous Sample	Baseline and Alarm Limit
Lab ID			20091076		Alarm Limit
Bottle ID			131918		Alarm Limit Matrix -Set Name (Equipment type / oil type)
Date Sampled			26-Aug-20		No Interpretation Required
Oil Hours (Kms)			10000 kms		
Unit Hours (Kms)			Not Given		
Oil Change					
Oil Added (Liters)					
Filters Hours (Kms)					
Wear Condition					
Wear Element	Method	Unit	Fine Wear (ICP-AES) / Coarse Wear (RT,S-AES)		Abnormal Oil (PC) / Fine Wear (ICP) / Coarse Wear (RPS)
Iron	D-5185	PPM	44.5		
Chromium	D-5185	PPM	2.7		
Lead	D-5185	PPM	0.0		
Copper	D-5185	PPM	3.7		
Tin	D-5185	PPM	2.3		
Aluminum	D-5185	PPM	19.8		
Nickel	D-5185	PPM	0.6		
Silver	D-5185	PPM	0.5		
Molybdenum	D-5185	PPM	446.1		
Titanium	D-5185	PPM	0.0		
PQ Index	D-8184	Index			
Oil Condition					KO / U-Warning / U-Caution / U-Caution / U-Warning
Viscosity @ 40° C	D-445	cSt			
Viscosity @ 100° C	D-445	cSt			
Oxidation	D-7414	Abs			
Nitration	D-7624	Abs/cm			
Acid Number	D-974	mg KOH/g			
Base Number	D-4739	mg KOH/g			
Contamination					KO / U-Caution / U-Warning
Water	D-2412	% (Wt.)			
Fuel	D-3524	% (Wt.)			
Glycol	D-2412	Abs	N/A		
Soot in Oil	D-2412	% (Wt.)			
Soot Dispersancy (100-C)	D7500M	Index			<50 / <30
Vanadium	D-5185	PPM	0		
Sodium	D-5185	PPM	0		
Silicon	D-5185	PPM	18.5		
Additive Element					KO
Boron	D-5185	PPM	31		
Magnesium	D-5185	PPM	5		
Calcium	D-5185	PPM	805		
Barium	D-5185	PPM	0		
Phosphorus	D-5185	PPM	334		
Zinc	D-5185	PPM	404		
Additional Test					KO / L-Warning / L-Caution / U-Caution / U-Warning
Flash Point	D-3828	°C			
Viscosity Index	D-2270				

Note: Alarm Limits are variable and dependent upon dataset size and to be used as general guideline.
No Sign or N : NORMAL , C or C : CAUTION (first level warning limit) , W or W : Warning (second level warning limit)
Accuracy of interpretation and recommendation are based on representative sample and information supplied. No warranty is expressed or implied for this report.
Focuslab Ltd. Bangkok Thailand www.focuslab.co.th focuslab@focuslab.co.th FL-6.8

B-7: elemental compositions of used MAZDA lubricating oil sample 2.

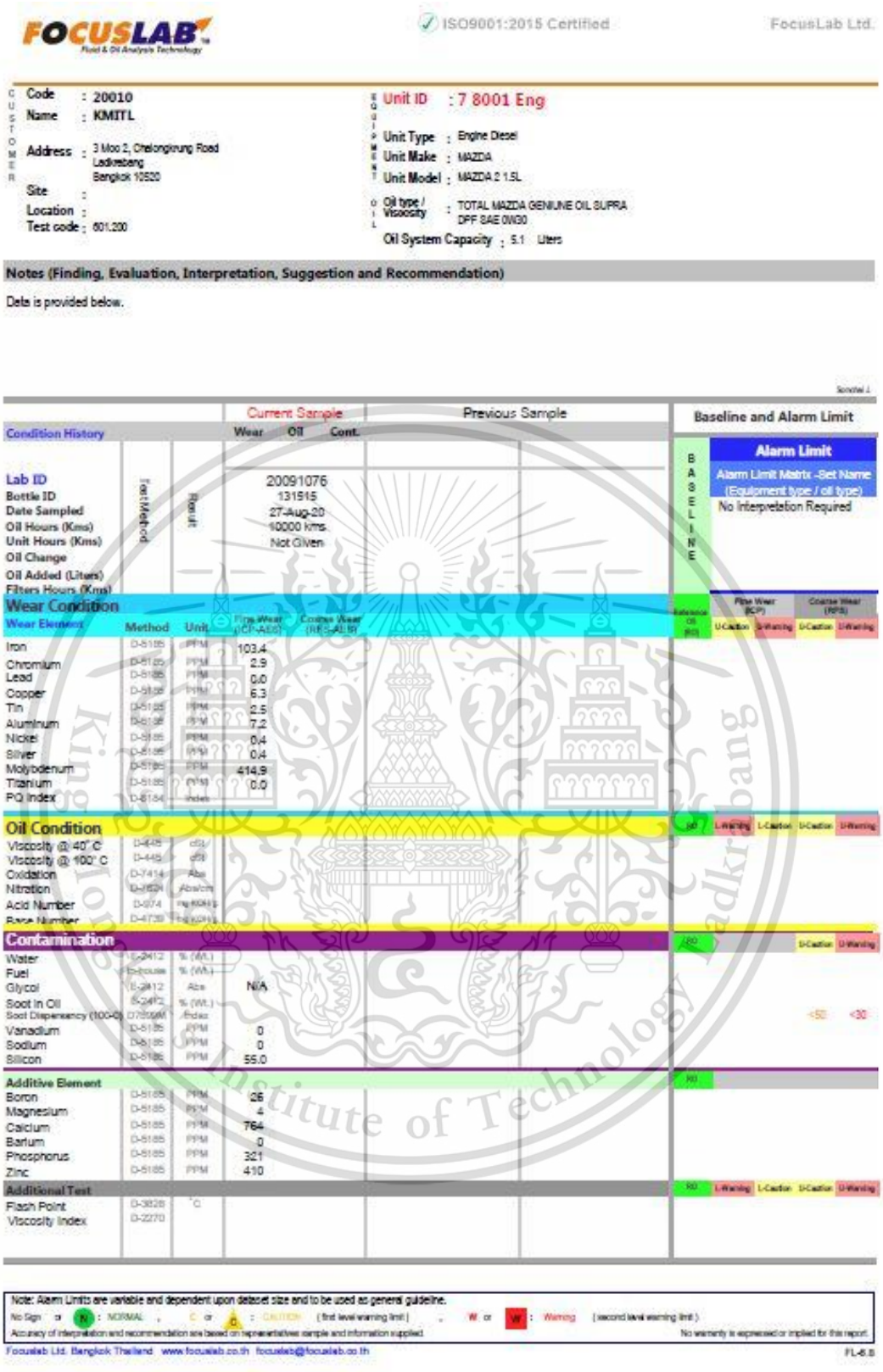

FOCUSLAB Fluid & Oil Analysis Technology

ISO9001:2015 Certified — FocusLab Ltd.

CUSTOMER
Code : 20010
Name : KMITL
Address : 3 Moo 2, Chalongkrung Road Ladkrabang Bangkok 10520
Site :
Location :
Test code : 601.200

EQUIPMENT
Unit ID : 7 8001 Eng
Unit Type : Engine Diesel
Unit Make : MAZDA
Unit Model : MAZDA 2 1.5L

OIL
Oil type / Viscosity : TOTAL MAZDA GENUINE OIL SUPRA DPF SAE 0W30
Oil System Capacity : 5.1 Liters

Notes (Finding, Evaluation, Interpretation, Suggestion and Recommendation)

Data is provided below.

Condition History	Test Method	Result	Current Sample: Wear Oil Cont.	Previous Sample	Baseline and Alarm Limit
Lab ID			20091076		BASELINE: Alarm Limit
Bottle ID			131515		Alarm Limit Matrix -Set Name (Equipment type / oil type)
Date Sampled			27-Aug-20		No Interpretation Required
Oil Hours (Kms)			10000 kms		
Unit Hours (Kms)			Not Given		
Oil Change					
Oil Added (Liters)					
Filters Hours (Kms)					
Wear Condition					Fine Wear (FCP) / Coarse Wear (RFS)
Wear Element	Method	Unit	Fine Wear (CF-AES) / Coarse Wear (RFS-AES)		Reference Oil (RO) / L-Caution / L-Warning / U-Caution / U-Warning
Iron	D-5185	PPM	103.4		
Chromium	D-5185	PPM	2.9		
Lead	D-5185	PPM	0.0		
Copper	D-5185	PPM	6.3		
Tin	D-5185	PPM	2.5		
Aluminum	D-5185	PPM	7.2		
Nickel	D-5185	PPM	0.4		
Silver	D-5185	PPM	0.4		
Molybdenum	D-5185	PPM	414.9		
Titanium	D-5185	PPM	0.0		
PQ Index	D-8184	Index			
Oil Condition					RO / L-Warning / L-Caution / U-Caution / U-Warning
Viscosity @ 40° C	D-445	cSt			
Viscosity @ 100° C	D-445	cSt			
Oxidation	D-7414	Abs			
Nitration	D-7624	Abs/cm			
Acid Number	D-974	mg KOH/g			
Base Number	D-4739	mg KOH/g			
Contamination					RO / U-Caution / U-Warning
Water	D-2412	% (Wt.)			
Fuel	D-Fouse	% (Wt.)			
Glycol	D-2412	Abs	N/A		
Soot in Oil	D-2412	% (Wt.)			
Soot Dispersancy (100-0)	D7208M	Index			<50 <30
Vanadium	D-5185	PPM	0		
Sodium	D-5185	PPM	0		
Silicon	D-5185	PPM	55.0		
Additive Element					RO
Boron	D-5185	PPM	26		
Magnesium	D-5185	PPM	4		
Calcium	D-5185	PPM	764		
Barium	D-5185	PPM	0		
Phosphorus	D-5185	PPM	321		
Zinc	D-5185	PPM	410		
Additional Test					RO / L-Warning / L-Caution / U-Caution / U-Warning
Flash Point	D-3828	°C			
Viscosity Index	D-2270				

Note: Alarm Limits are variable and dependent upon dataset size and to be used as general guideline.
No Sign or N : NORMAL , C or Δ : CAUTION (first level warning limit) , W or W : Warning (second level warning limit)
Accuracy of interpretation and recommendation are based on representatives sample and information supplied. No warranty is expressed or implied for this report.
Focuslab Ltd. Bangkok Thailand www.focuslab.co.th focuslab@focuslab.co.th FL-6.8

B-8: elemental compositions of used MAZDA lubricating oil sample 3.

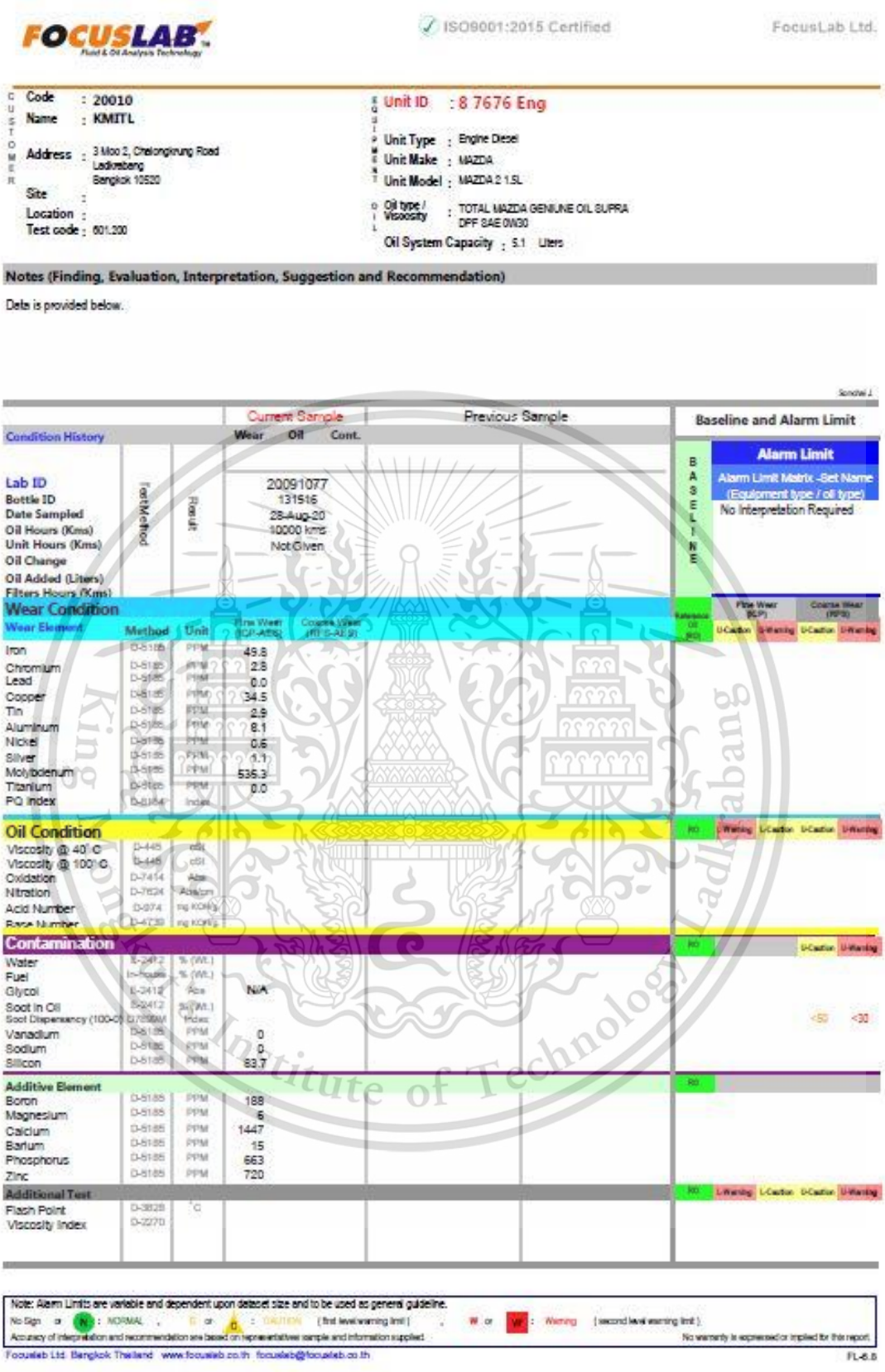

FOCUSLAB Fluid & Oil Analysis Technology — ISO9001:2015 Certified — FocusLab Ltd.

CUSTOMER
Code : 20010
Name : KMITL
Address : 3 Moo 2, Chalongkrung Road Ladkrabang Bangkok 10520
Site :
Location :
Test code : 601.200

EQUIPMENT
Unit ID : 8 7676 Eng
Unit Type : Engine Diesel
Unit Make : MAZDA
Unit Model : MAZDA 2 1.5L

OIL
Oil type / Viscosity : TOTAL MAZDA GENUINE OIL SUPRA DPF SAE 0W30
Oil System Capacity : 5.1 Liters

Notes (Finding, Evaluation, Interpretation, Suggestion and Recommendation)

Data is provided below.

Condition History	Test/Method	Result	Current Sample Wear Oil Cont.	Previous Sample	Baseline and Alarm Limit
Lab ID			20091077		Alarm Limit
Bottle ID			131516		Alarm Limit Matrix -Set Name (Equipment type / oil type)
Date Sampled			28-Aug-20		No Interpretation Required
Oil Hours (Kms)			10000 kms		
Unit Hours (Kms)			Not Given		
Oil Change					
Oil Added (Liters)					
Filters Hours (Kms)					
Wear Condition					
Wear Element	Method	Unit	Fine Wear (ICP-AES) / Coarse Wear (FTIR-ALS)		Reference Oil (RO) / Fine Wear (ICP) / Coarse Wear (FTIR)
Iron	D-5185	PPM	49.6		
Chromium	D-5185	PPM	2.8		
Lead	D-5185	PPM	0.0		
Copper	D-5185	PPM	34.5		
Tin	D-5185	PPM	2.9		
Aluminum	D-5185	PPM	8.1		
Nickel	D-5185	PPM	0.6		
Silver	D-5185	PPM	1.1		
Molybdenum	D-5185	PPM	535.3		
Titanium	D-5185	PPM	0.0		
PQ Index	D-8184	Index			
Oil Condition					RO / L-Warning / L-Caution / U-Caution / U-Warning
Viscosity @ 40°C	D-445	cSt			
Viscosity @ 100°C	D-445	cSt			
Oxidation	D-7414	Abs			
Nitration	D-7624	Abs/cm			
Acid Number	D-974	mg KOH/g			
Base Number	D-4739	mg KOH/g			
Contamination					RO / U-Caution / U-Warning
Water	E-2412	% (Wt.)			
Fuel	In-House	% (Wt.)			
Glycol	E-2412	Abs	N/A		
Soot in Oil	E-2412	% (Wt.)			
Soot Dispersancy (100-0)	D7686M	Index			<50 <30
Vanadium	D-5185	PPM	0		
Sodium	D-5185	PPM	0		
Silicon	D-5185	PPM	83.7		
Additive Element					RO
Boron	D-5185	PPM	188		
Magnesium	D-5185	PPM	6		
Calcium	D-5185	PPM	1447		
Barium	D-5185	PPM	15		
Phosphorus	D-5185	PPM	663		
Zinc	D-5185	PPM	720		
Additional Test					RO / L-Warning / L-Caution / U-Caution / U-Warning
Flash Point	D-3828	°C			
Viscosity Index	D-2270				

Note: Alarm Limits are variable and dependent upon dataset size and to be used as general guideline.
No Sign or N : NORMAL , C or A : CAUTION (first level warning limit) , W or WF : Warning (second level warning limit).
Accuracy of interpretation and recommendation are based on representative sample and information supplied. No warranty is expressed or implied for this report.
Focuslab Ltd. Bangkok Thailand www.focuslab.co.th focuslab@focuslab.co.th FL-6.5

B-9: elemental compositions of used MAZDA lubricating oil sample 4.

APPENDIX C

THERMOGRAVIMETRIC ANALYSIS REPORT

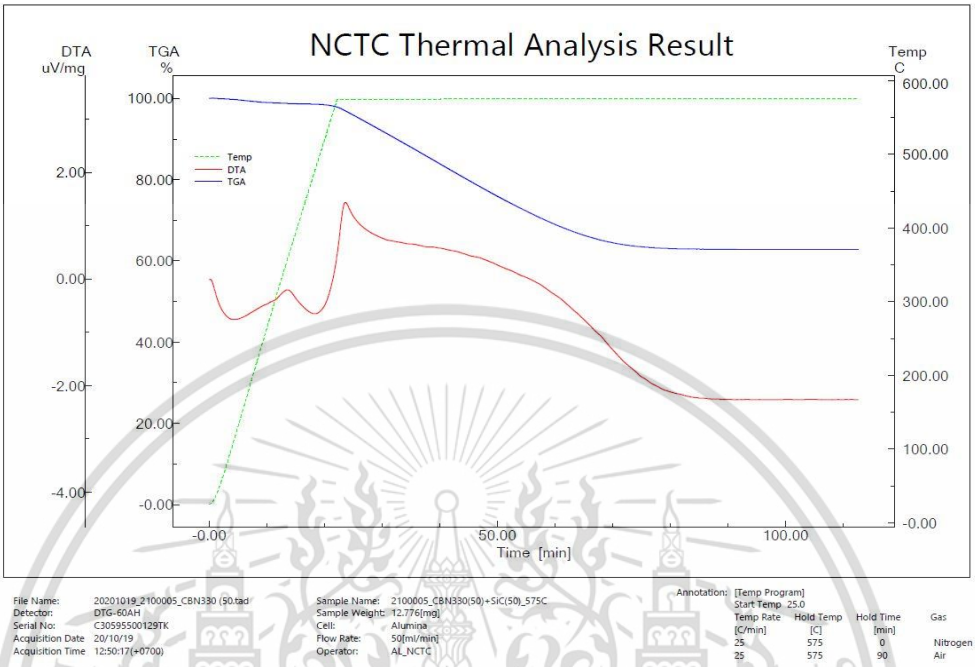

C-1: Thermogravimetric analysis report of CBN330 (50%) + SiC (50%) using isothermal method under 575°C with pure air atmospheric condition.

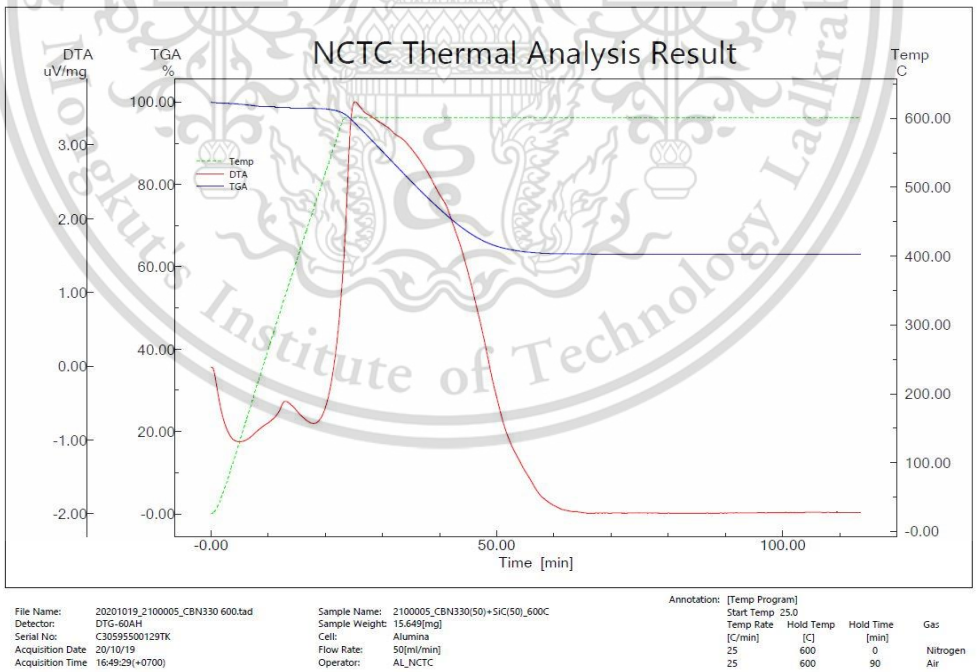

C-2: Thermogravimetric analysis report of CBN330 (50%) + SiC (50%) using isothermal method under 600°C with pure air atmospheric condition.

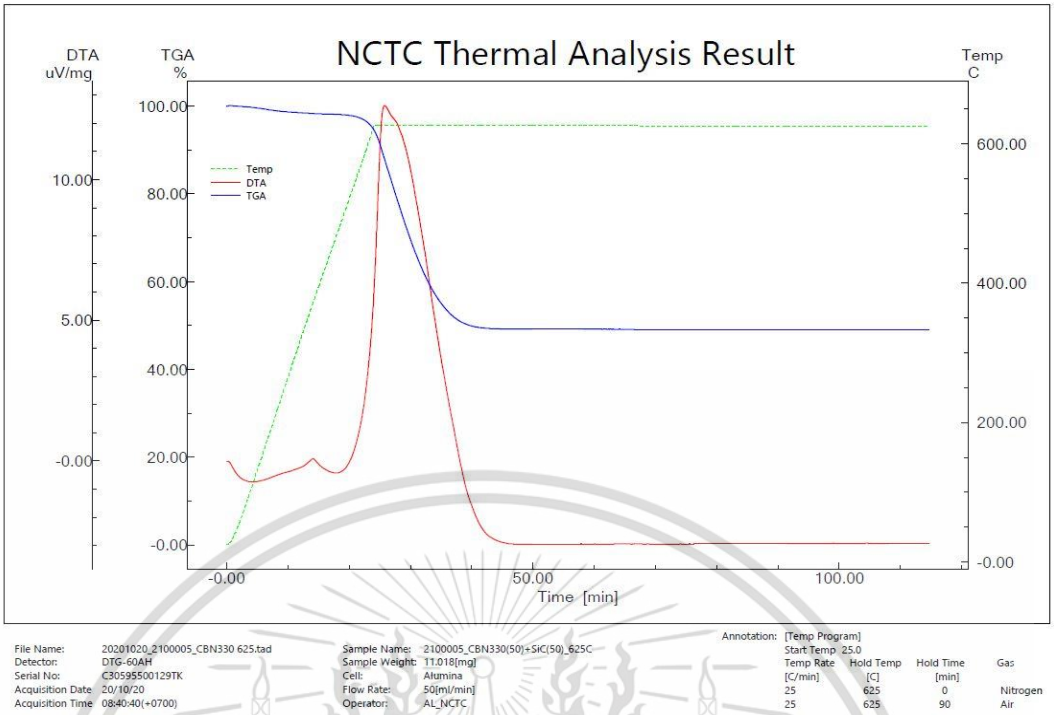

C-3: Thermogravimetric analysis report of CBN330 (50%) + SiC (50%) using isothermal method under 625°C with pure air atmospheric condition.

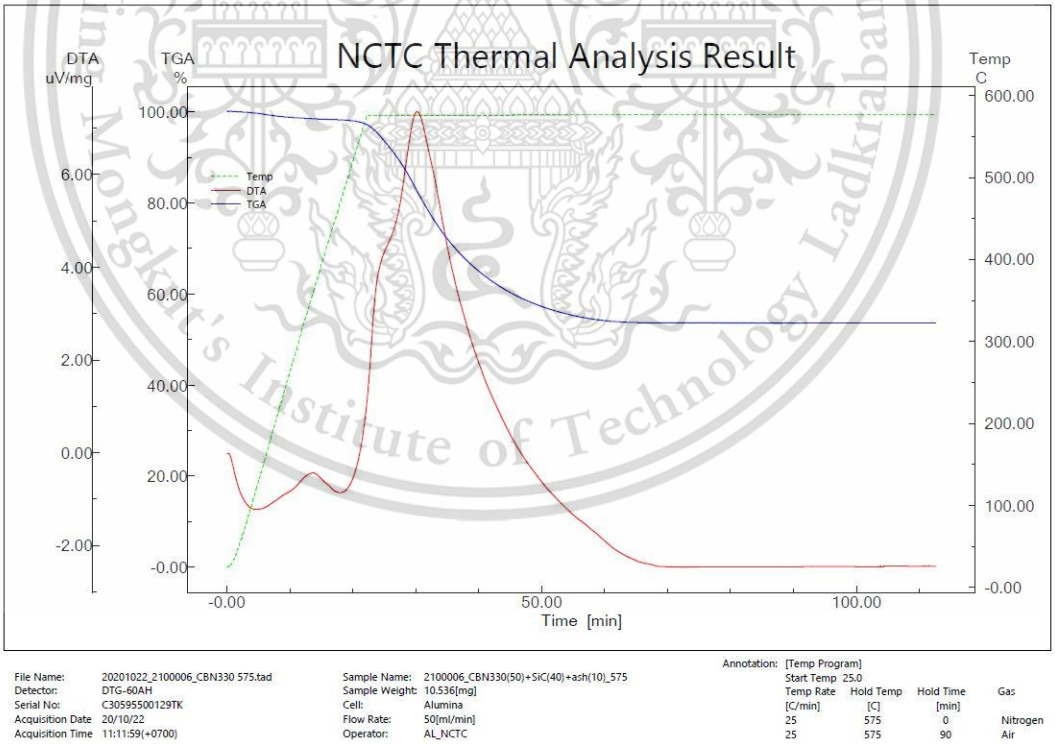

C-4: Thermogravimetric analysis report of CBN330 (50%) + SiC (50%) + Ash (10%) using isothermal method under 575°C with pure air atmospheric condition.

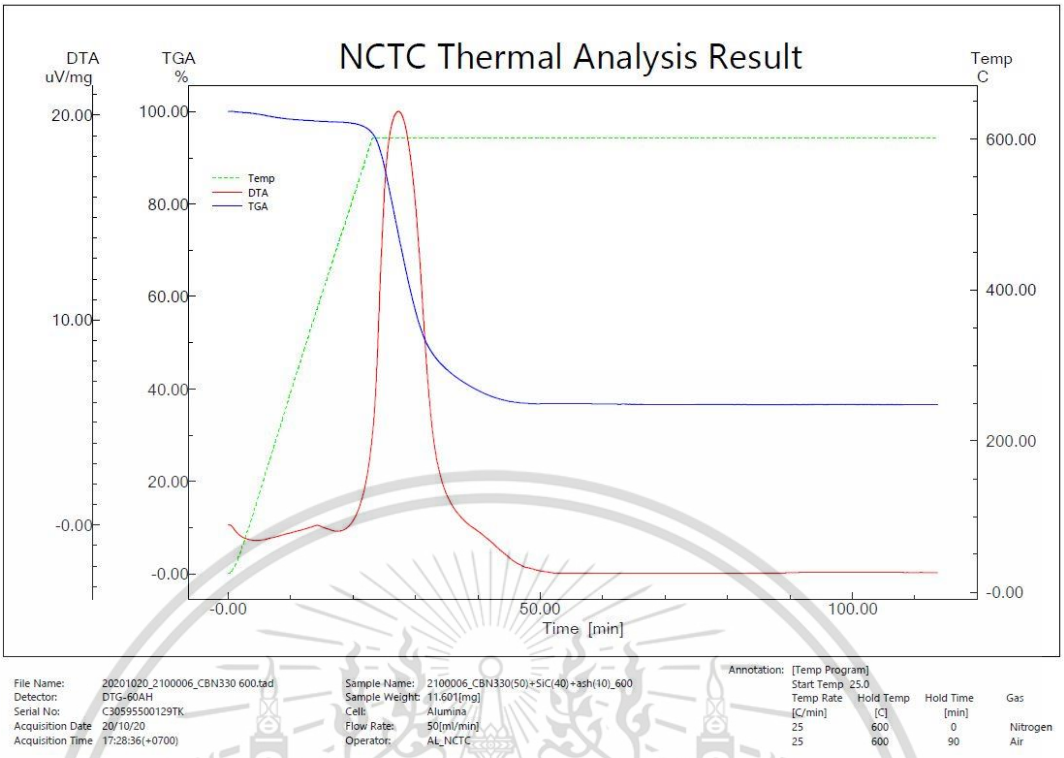

C-5: Thermogravimetric analysis report of CBN330 (50%) + SiC (50%) + Ash (10%) using isothermal method under 600°C with pure air atmospheric condition.

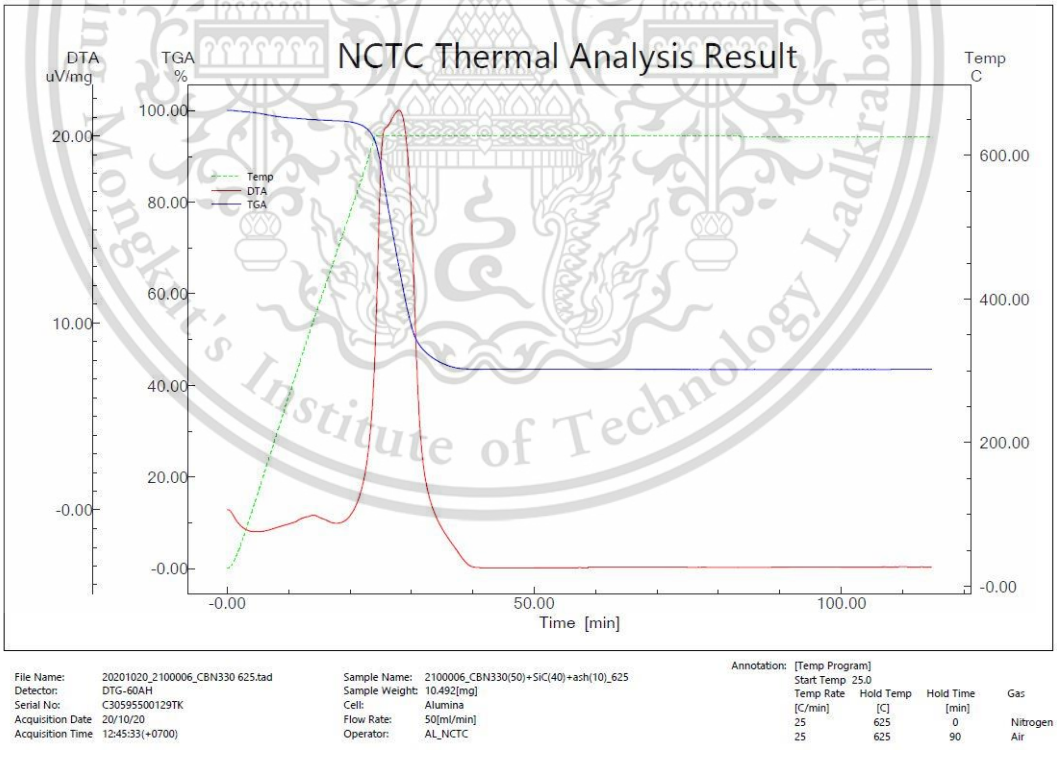

C-6: Thermogravimetric analysis report of CBN330 (50%) + SiC (50%) + Ash (10%) using isothermal method under 625°C with pure air atmospheric condition.

APPENDIX D

PUBBLICATIONS

The 11th TSME International Conference on Mechanical Engineering
1st – 4th December 2020
Ubon Ratchathani, Thailand

TSME ICOME 2020
Challenging Trends in Mechanical Engineering

AME0007

Characterization of metal oxide ashes in diesel particulate filter utilizing electron microscopy

Sattatad Rodvanna[1,*], Preechar Karin [1,*], Nuwong Chollacoop[2] and Katsunori Hanamura[3]

[1]Faculty of Engineering, King Mongkut's Institute of Technology Ladkrabang, Bangkok 10520, Thailand
[2]National Metal and Materials Technology Center, National Science and Technology Development Agency, Pathumthani 12120, Thailand
[3]School of Engineering, Tokyo Institute of Technology, Tokyo 152-8552, Japan

* Corresponding Author: ton230937@gmail.com

Abstract. Physicochemical characteristics of metal oxide ashes derived from the actual passenger cars' diesel particulate filter (DPF) were investigated utilizing an electron microscopy, energy dispersive spectroscopy, X-Ray Fluorescence, and X-Ray Diffractometer. A deposition of ash particles mainly took place at the end plug with various deposited length depending on channels. The majority of ash components, derived from lubricant additives, consisted of Fe, Si, Ca, Cu, S, P, Zn, Al and minor Cr, Ni, Mn. These ash components resulting in a clogging which is the main concern of a diesel vehicle equipped with DPF.

Keywords: Diesel engine; Particulate filter; Metal oxide ash; Fuel additives; Engine wear

1. Introduction

Nowadays, automotive trends are focusing to the future of the vehicles, for example, autonomous vehicle, Plug-in Hybrid Electric Vehicle (PHEV), and the most popular one Electric vehicles (EV). These future developments require a revolutionized of the infrastructure in which only a few countries are well-prepared. Therefore, internal combustion engines will continue to be used as a main power source for transportation. Among the engines, diesel engine is widely used [1] due to its highest thermal efficiency among others [2]. However, the diesel exhaust gas contains high amount of particulate matter (PM), which is harmful for our body and environment. A solid fraction of diesel PM composed of soot formed by an incomplete combustion, and ash which mainly derived from fuel or engine oil additives [3]. Diesel Particulate Filter (DPF) was introduced as the most effective way to mitigate this emission because the PM removal efficiency is more than 98% [4]. As PM continuously trapped in DPF, the filter back pressure is increased resulting in a reduction of engine efficiency. As a result, DPF need to be regenerated by oxidizing of trapped PM. Unlike to soot particles, an incombustible metal oxide ash cannot be removed from DPF by burning and will deposit in it. There are two types of ash deposition: wall ash [5] and plug ash [6]. Wall ash covers the DPF wall and performs as a membrane

filter resulting in a high filtration efficiency, but too much deposition can restrict the channel diameter. On the other hand, plug ash completely fills the channel and reduces the effective length of the filter [7].

Previous research [8], suggested that the mechanism of ash distribution process depended on the DPF regenerative way. By using active regeneration ash tends to accumulate at the end of the channel as plug ash, while wall ash was formed by the passive regeneration. In addition, the ash formation can be influenced by the attractive forces between particles. Based on the previous results of in-situ optical system [9], revealed that wall ash can be removed and accumulated at the end plug as the plug ash through the process of soot oxidizing at 600°C. This process can occur even in the absence of any flow through the channel due to the presence of substantial cohesive. Although the different mechanisms of the ash distribution process were proposed, the debate about the complex ash formation, accumulation, as well as fundamental mechanisms of ash property, are still ongoing without firm evidence. Therefore, the investigations on the ash physico-chemical property and the ash formation process by using advanced analytical tools will be helpful to solve the abovementioned issues.

In this study, the actual DPF was disassembled and accumulated ashes were investigated their distribution pattern. Furthermore, morphological, nanostructures and chemical composition characteristics of ash particles were investigated utilizing electron microscopy techniques.

2. Experiments

2.1 Investigated DPF system

Figure 1. Passenger cars' DPF assembly (A), DPF with honey-comb structure (B), 16 segments of DPF after it was disassembled (C), a removed top wall DPF (D).

Figures 1(A) presents DPF assembly obtained from a diesel passenger car which was used in this experiment. The investigated DPF had 'honey-comb' structures (figure 1B) and consists of different 'segments', there were disassembled in their segment constituents as shown in figure 1(C). Then, the horizon top wall of each segment was removed layer by layer utilizing abrasive papers and grinding machine (figure 1D). The macroscale analysis data of ash accumulation length, as well as distribution patterns in each layer were collected, as trapped within the filter channels. In order to confirm the reproducibility of data, several DPF from the same car manufactures were investigated in this experiment.

In addition, a mechanical removal of ash from the filter also performed as the microscale analysis. Characterization and chemical components analysis of ash particles were carried out by X-Ray Fluorescence (XRF), and X-Ray Diffractometer (XRD) at NSTDA Characterization and Testing Service Center (NCTC). For the microscopic investigations, a field emission scanning electron microscope (FE-SEM), and a transmission electron microscope (TEM) analytical facility were used at the National Nanotechnology Center (NANOTEC). The FE-SEM instrument was Hitachi SU5000 combined with an energy dispersive X-Ray spectroscopy (EDX) for qualitative chemical analysis. The majority of TEM study was made by using a transmission electron microscope (JEOL model JEM 2100) also equipped with an energy dispersive X-Ray spectroscopy (EDX), this instrument was operated at 200kV acceleration voltage.

3. Results and Discussion

3.1 The macroscale analysis of plug ash in DPF

3.1.1. Ash accumulation in DPF

Figure 2 (A) presents the twelfth DPF segment in which the horizontal top wall has already removed. This segment has the total of 9 inflow channels, as indicated on the right-hand side of figure 2 (A). Ash in DPFs tends to loosely accumulate, as a brown brittle powdery, and entirely filled up at the end of inflow channels (plug ash). The asymmetrical can be observed in this sample as the plug ash lengths are varied depending on channels. Channel 1 has about 18 mm. which is a highest compare to others. The plug ash length drastically reduced to about 6.5 mm. in channel 7, however, the length gradually increased again to 7 and 7.3 mm. in channel 8 and 9, respectively. The amount of ash diminishing distinctively toward the inflow. The channels area without plug ash had a very thin ash layer (wall ash) attached on the channel wall, as well as deposited deep inside the surface pore along the filter length (figure 2 B). The mechanisms that altered ash particles from the channel walls to the end plug consists of flow-induced transport and regeneration-reduced transport [6]. Flow induced transport is a detachment and transport of ash particles by a shear force from the exhaust that can overcome the force of adhesion between the particle and filter wall (or neighboring particles).

Figures 2. Accumulation of plug ash inside the DPF.

During the regeneration process, soot cake continuously oxidized from the bottom [10]. The adhesive force between soot and ash, as well as DPF substrate are reduced. As a result, ash particles detach from DPF surface and subsequent transport to the end plug. The term "regeneration-reduced transport" can be used to describe this phenomenon.

3.1.2. Ash distribution in DPF

Figure 3 presents plug ash length distribution in 16 segments of the DPFs. The horizontal axis represents "Segments number "in which each segment consists of 6-9 channels, depending on locations. The vertical axis represents plug ash length in millimeter (mm.). From this figure, deposited ash length fluctuates between 2-21 mm. with the average of 4.7 mm. from the 125 mm. long filter channel. Ash distribution in most of segments were corresponding to the asymmetrical parabolic flow profile. At the filter center, ash length is varied between 2 to 8 mm., no significance difference of ash deposition in the same DPF segment. However, there were some significant increase of ash deposited length at the outer channel in the segments numbers 8,12 and 16 which are close to filter periphery. The maximum length is up to 21 mm. which is almost 5 times more than the average. Previous study [11] on morphology and size of ash PM from the light truck DPF, found such a contradict result that the center part contained higher amounts of ash deposited than the periphery. One Possibility is the unique design of DPF inlet pipeline which is a characteristic of each vehicle. Thus, resulting in the difference inflow pattern inside the DPF.

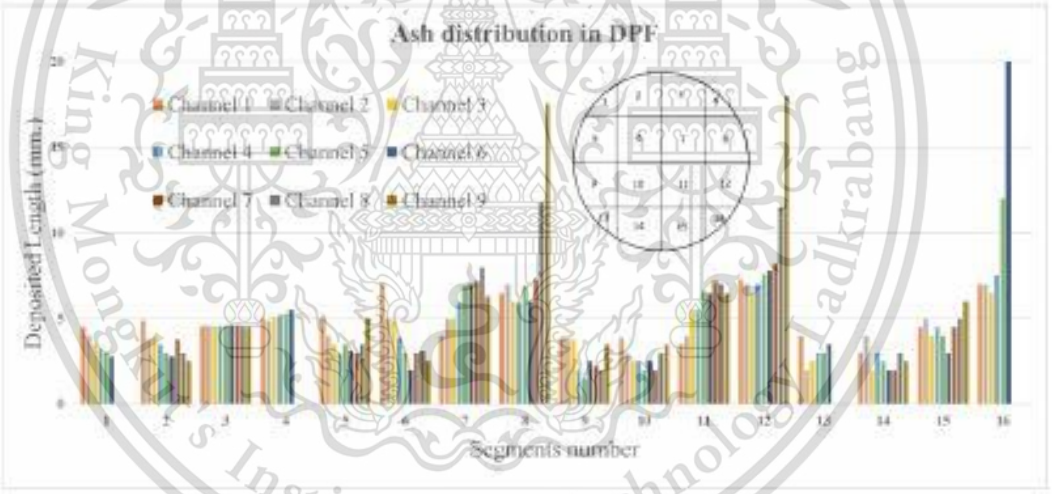

Figure 3. Ash distribution and deposited length inside the DPF.

3.2 The microscale analysis of ash powder

3.2.1 XRD analysis of DPF material

Before further investigation on ash elemental composition, the material analysis of DPF need to be conducted. Thus, a small piece of DPF was cut and made approximately 2 g. into a powder for XRD analysis. The main composition of this DPF is SiC as shown in XRD spectra figure 4. There is no signal of catalyst materials such as Pt, Pd, therefore, it can be concluded that the investigated DPF in this experiment is a non-coated type.

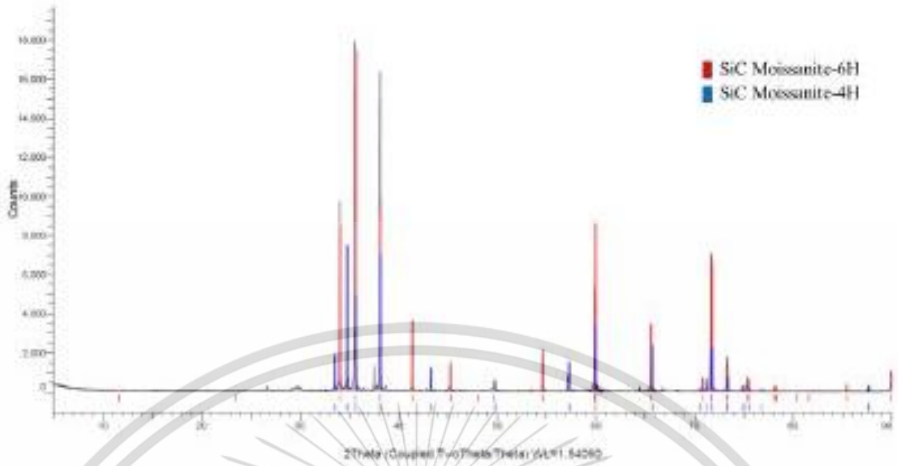

Figure 4. XRD spectra analysis of DPF material.

3.2.2 XRF and XRD analysis of ash components

Table 1 presents XRF analysis of elemental contained (wt.%) in ash sample. From the XRF result, the large proportion elements constitution of ash are Fe, Si, Ca, Cu, S, P, Zn, and Al which often presents in forms of $Cu_{0.5}Zn_{0.5}Cr_{1.1}Fe_{0.9}O_4$, $Ca(SO_4)$, Fe_2O_3 and $Ca_{10}Cu_2(PO_4)_{14}$, as shown in XRD spectra result (figure 5). It is well-known that metal oxide ashes mainly derived from metal in the diesel fuel, engine wear, and lubricating oil. Sine Fe is the main constituent of ash, it is expected that a majority of Fe might produce from the fuel-borne additive (ferrocene) which is the Fe-based catalyst used to reduce the soot ignition and burning temperature. Another possibility is that Fe with minor Ni and Cr may originate from the engine wear which blended in lubricating oil [12].

Table 1. XRF elemental analysis of ash powder.

Elements	Wt%	Elements	Wt%
Fe	30.88	Zn	7.46
Si	16.18	Al	4.78
Ca	10.88	K	1.17
Cu	9.47	Ni	0.99
S	9.16	Cr	0.71
P	7.92	Mn	0.41

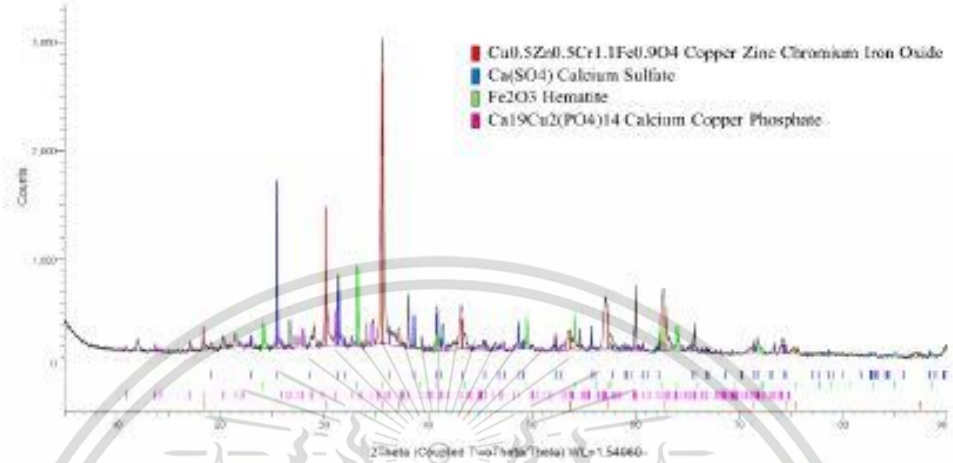

Figure 5. XRD spectra analysis of elements contained in deposited ash.

3.3.3 SEM-EDS imaging of ash particles

Figure 6 presents SEM image (A) and EDS elemental analysis (B) of Fe-oxide ash particle. This nearly spherical particle, with approximately 5 microns. in diameter, is a common type ash found in this sample. The elemental analysis revealed that Fe and O are the major elements included in this particle while Cu, Si, Zn, Al, P, Ca also found as minor components. This particle generated during the melting of iron at 1538°C in cylinder. A surface tension draws the molten material into is spherical shape and rapidly solidified [11]. As a result, this particle has a cubic aggregation on its surface. Subsequently, transported by the exhaust gas and deposited in DPF as shown.

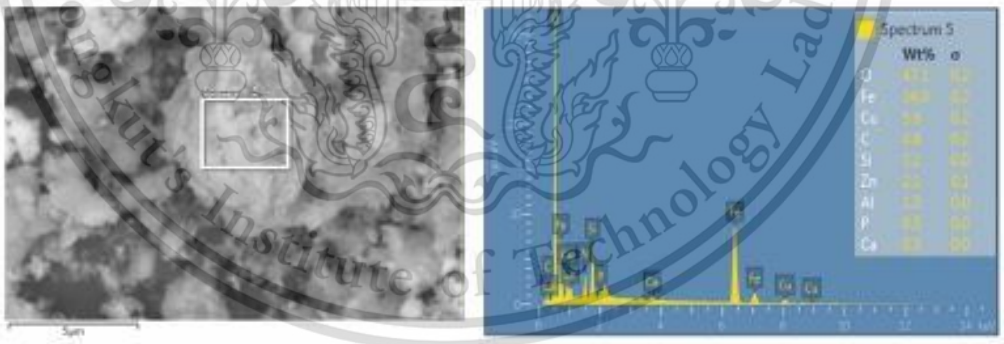

A B

Figure 6. SEM image (A) and EDS elemental analysis of ash particle (B).

3.3.4 TEM imaging

The bright field TEM image in figure 7 presents an agglomeration of ash particles with irregular round outlines shapes. Previous study suggested that this round ash particles derived from a condensation of hot combustion vapors from S which is a volatile species [13]. The right image (B) presents a higher magnification image of finer individual particle with approximately 25 nm. in diameter. A parallel straight-line hatch patterns can be clearly observed, indicated a crystalline structure which is similar to a nanostructure of metals. This particle has a strong tendency to form an aggregation, and resulting in a densification of ash particle caused by repeated regenerations.

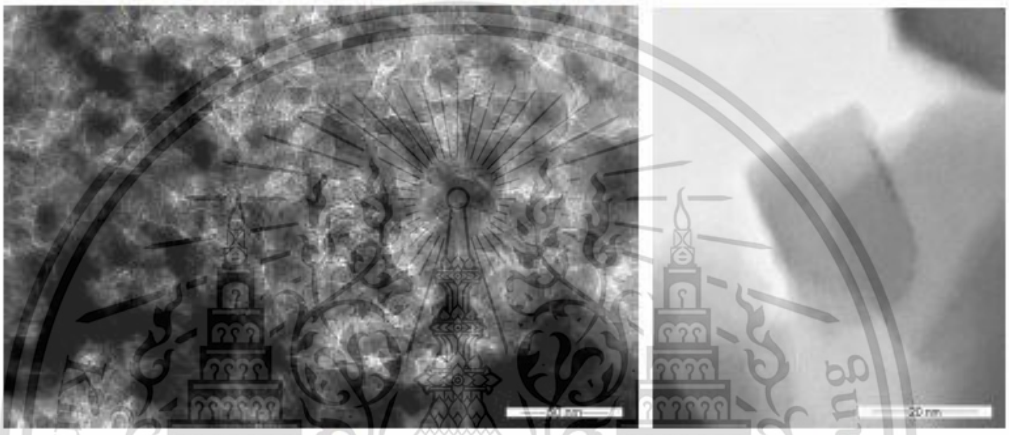

A B

Figure 7. Bright field TEM image of various agglomerated ash particles (A), and bright field TEM presents nanostructure of metal oxide ash (B).

The top left figure 8 presents bright field TEM image of ash agglomeration, the EDS elemental mappings also shown. The agglomerates usually have round outlines with irregular shape, as shown in the bright field TEM image. EDS spectra mappings show an inhomogeneous of elemental distribution. Elements of Fe, O, Zn, Al, Ni, Cr and S are found in greater amounts, while Ca and P show some local concentrated. The presence of Ca, S, P, Fe, Zn and O are usually in form of $CaSO_4$, $Zn_3(PO_4)_2$, $FePO_4$ and $Ca_3(PO_4)_2$ which are a common diesel ash [14]. The EDS spectra mappings reveal some interesting information of element distribution. P, S, Ca and O showed similar pattern, thus, formed compounds such as -O, -SO4 and -PO4 of Ca. Additionally, oxides of Fe, Al, Zn and minor Cr, Ni are considered to be the majority of ash compounds found within this sample. These compounds might be abrasion products of engine wear formed during movement of pistons. This inference is in compliance with previous XRD, XRF analysis of ash powder which also show the presence of anhydrite ($CaSO_4$), hematite (Fe_2O_3), as well as minor fragment of Ni and Cr.

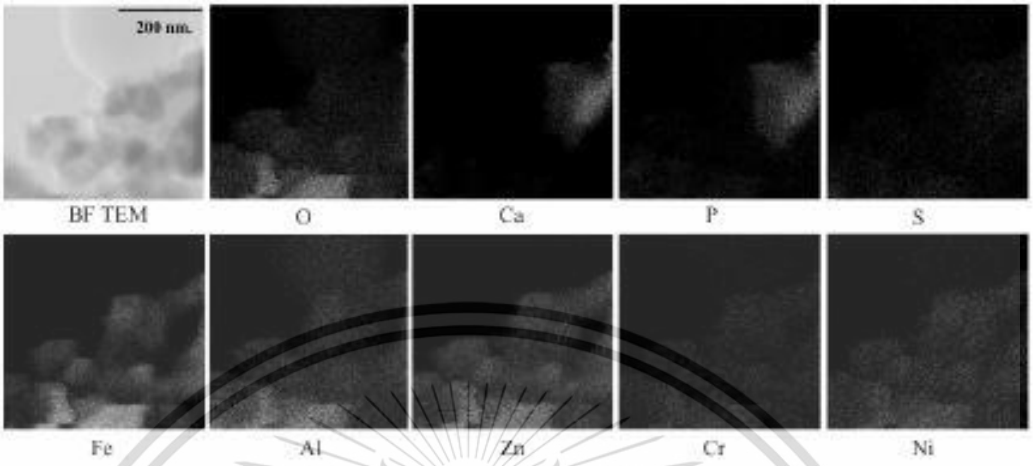

Figure 8. Bright field TEM image (Top-left) and EDS elemental distribution mappings.

4. Conclusion

The actual DPFs acquired from a diesel passenger car was disassembled for an investigation of macro/microscale analysis of metal oxide ashes. The macroscale analysis results found that ash entirely filled up the end plug of channels and distribution in most segments were corresponding to the asymmetrical parabolic flow profile. Much amounts of ash were deposited at the filter periphery with the maximum length of 21 mm. due to the unique design of DPF inlet pipeline. The XRF microscale analysis revealed that Fe is the main component of deposited ash on the SiC non-coated DPF, while XRD analysis confirmed the presence of $Cu_{0.5}Zn_{0.5}Cr_{1.1}Fe_{0.9}O_4$, $Ca(SO_4)$, Fe_2O_3 and $Ca_{19}Cu_2(PO_4)_{14}$. The TEM results confirmed that the agglomerated ashes are mostly round and consist chemically of Fe, O, Zn, Al, Ni, Cr, S and minor Ca and P in form of sulfates, phosphates and oxides. It was clarified that majority of ash components found within DPFs samples are oxides of Fe, Al, Zn and minor Cr, Ni. These components originated from engine wear metal, exhaust corrosion products, as well as fuel and lubricant additives. In the future, the further investigation on additive elements of fuel and lubricant oil will be helpful to precisely confirm sources of this deposited ash in DPF.

5. Acknowledgements

The authors would like to express their sincere appreciation for financial support from National Research Council of Thailand (Diesel Engine's Particulate Matters Reduction using Ethanol-Biodiesel-Diesel Blends and Particulate Filter 398/2563), technical support from King Mongkut's Institute of Technology Ladkrabang (KMITL) and National Science and Technology Development Agency.

6. References

[1] Plotkin, S. and Ribeiro, S. K. Energy Efficiency Technologies for Road Vehicles 2009; 2:125-137

[2] Heywood, J. B. Internal Combustion Engine Fundamentals. McGraw-Hill. Singapore; 1988.

[3] Bagi, S., R. Bowker, and R. Andrew. 2016. Understanding chemical composition and phase transitions of ash from field returned DPF units and their correlation with filter operating conditions. SAE International Journal of Fuels and Lubricants 9:239–59. doi:10.4271/2016-01-0898.

[4] Gao, J., C. Ma, S. Xing, L. Sun, and L. Huang. 2018. A review of fundamental factors affecting diesel pm oxidation behaviors. Science China-Technological Sciences 61:330–45. doi:10.1007/s11431-016-9117-x.

[5] Viswanathan, S., Rakovec, N., and Foster, D. : Microscale Study of Ash Accumulation Process in DPF Walls Using the Diesel Exhaust Filtration Analysis (DEFA) System, ASME, ICEF 2012-92104, (2012)

[6] Sappok, A., Wang, Y. et al. : Theoretical and Experimental Analysis of Ash Accumulation and Mobility in Ceramic Exhaust Particulate Filters and Potential for Improved Ash Management, SAE Technical paper, 2014-01-1517, (2014)

[7] Sappok, A. : The Nature of Lubricant-Derived Ash-Related Emissions and Their Impact on Diesel Aftertreatment System Performance, PhD Thesis, Massachusetts Institute of Technology, 2009.

[8] Ishizawa, T., H. Yamane, H. Satoh, K. Sekiguchi, M. Arai, N. Yoshimoto, and T. Inoue. 2009. Investigation into ash loading and its relationship to DPF regeneration method. SAE International Journal of Commercial Vehicles 2:164–75. doi:10.4271/2009-01-2882.

[9] Sappok, A., I. Govani, C. Kamp, Y. Wang, and V. Wong. 2013. In-situ optical analysis of ash formation and transport in diesel particulate filters during active and passive DPF regeneration processes. SAE International Journal of Fuels and Lubricants 6:336–49. doi:10.4271/2013-01-0519.

[10] Rodvanna, S., Srilomsak, M., Mitsuhiro S., and Katsunori H.: Scanning electron microscopic time-lapse visualization of ash movement during regeneration of Diesel Particulate Filters, International Journal of Automotive Engineering, Vol. 11,No.2(2020).

[11] Liati, A., P. Dimopoulos Eggenschwiler, E. Müller Gubler, D. Schreiber, and M. Aguirre. 2012a. Investigation of diesel ash particulate matter: A scanning electron microscope and transmission electron microscope study. Atmospheric Environment 49:391–402. doi:10.1016/j.atmosenv.2011.10.035.

[12] Sappok, A., Wong, V., 2007. Detailed Chemical and Physical Characterization of Ash Species in Diesel Exhaust Entering Aftertreatment Systems SAE Technical Paper,2007-01-0318.

[13] Buhre, B.J.P., Hinkley, J.T., Gupta, R.P., Wall, T.F., Nelson, P.F., 2005. Submicron ash formation from coal combustion. Fuel 84, 1206e1214.

[14] Nemoto, S., Kishi, Y., Matsuura, K., Miura, M., Togawa, S., Ishikawa, T., Hashimoto, T., Yamazaki, T., 2004. Impact of Oil-derived Ash on Continuous Regeneration-type Diesel Particulate Filter- JCAPII Oil WG Report JCAPII Oil WG Report SAE Technical Paper 2004-01-1887.

AUTHOR BIOGRAPHY

Author: Mr. Sattatad Rodvanna

Degree: Master of Engineering

Date of Graduation: 31th July 2021

Date of Birth: 23th September 1994

Place of Birth: Bangkok, Thailand

Undergraduate and Graduate Education:

Master of Engineering in Automotive Engineering,
King Mongkut's Institute of Technology Ladkrabang, Bangkok, 2021

Bachelor degree in Mechanical Engineering,
International Undergraduate Program, Bangkok, 2017

Major: Automotive Engineering

Presentations and Publications:

[1] Sattatad Rodvanna, Preechar Karin, Nuwong Chollacoop and Katsunori Hanamura " Characterization of metal oxide ashes in diesel particulate filter utilizing electron microscopy", 2020, The 11th TSME International Conference on Mechanical Engineering, 1st – 4th December 2020 Ubon Ratchathani, Thailand

[2] Rodvanna, S., Srilomsak, M., Mitsuhiro, S., and Katsunori, H.: Scanning electron microscopic time-lapse visualization of ash movement during regeneration of Diesel Particulate Filters, International Journal of Automotive Engineering, Vol. 11, No.2(2020).

[3] Rodvanna, S., Srilomsak, M., Mitsuhiro S., and Katsunori H.: Time-lapse Visualization of agglomeration and growth of ash during regeneration of Diesel Particulate Filter, JSAE proceedings Number: 20195139 May, 2019 Issued No.29-19